Biochemical characterization of disease-related alleles of human Telomerase RNA (hTR)

Dissertation

Zur Erlangung des Grades

Doktor der Naturwissenschaften

Am Fachbereich Biologie

Der Johannes Gutenberg-Universität Mainz

Alex Orioli

geb. am 15.05.1992 in Forlì, Italien

Mainz, 11 Dezember 2023

Index

Zusammenfassung

Telomere sind die Endbereiche von Chromosomen, die sie vor einem Verfall sowie der Verschmelzung mit anderen Chromosomen schützen. Sie bestehen aus dem sich wiederholenden DNA-Hexamer 5'-GGTTAG-3', dessen Länge beim Menschen 10 bis 15 kbp beträgt, mit 100 bis 200 bps einzelsträngigem 3'-Überhang. Die wichtigste Strategie, um der Telomerverkürzung entgegenzuwirken, die sowohl von Stammzellen als auch von den meisten Tumoren genutzt wird, ist die Aktivität der Telomerase. Die Kernkomponenten der menschlichen Telomerase sind die katalytische Proteinuntereinheit Telomerase Reverse Transcriptase (TERT) und die menschliche Telomerase-RNA (hTR). hTERT ist in der Lage, die endständigen DNA-Sequenzen, die bei der DNA-Replikation während der Zellteilung verloren gehen, durch wiederholte reverse Transkription der in hTR enthaltenen Template-Region auf die Chromosomenenden zu ergänzen.

Mutationen in verschiedenen Komponenten der Telomerase, sowie in Faktoren, die an ihrer Biogenese beteiligt sind, wurden bei Patienten mit Telomerbiologie-Störungen (TBDs) festgestellt. Durch die Beeinträchtigung der Telomerasefunktion beschleunigen diese Mutationen die Verkürzung der Telomere, was zu einer Reduktion der Stammzellen in verschiedenen Geweben führt.

Das Ziel dieser Arbeit ist es, zu verstehen, wie verschiedene Regionen der hTR die Telomerase-Biogenese und -Aktivität beeinflussen. Zunächst konzentrierte ich mich auf die Untersuchung der 5'-terminalen Region von hTR, die G-reich ist und bekanntermaßen G-Quadruplex-Strukturen (G4) bildet, sowie mit der Helikase DHX36 und den heterogenen nuklearen Ribonukleoproteinen hnRNP H/F interagiert. Unter Ausnutzung von zwei bekannten krankheitsbezogenen Mutationen von hTR in dieser Region, insbesondere der Transversion G>C an Position 2 (G2C) und G>T an Position 11 (G11T), habe ich hauptsächlich die Ansätze der qPCR und der direkten Telomerase-Aktivitäts-Assays (DTAAs) verwendet, um die Bedeutung dieser Region für die hTR-Expression und Telomerase-Aktivität zu testen. Darüber hinaus untersuchte ich die Beteiligung von DHX36 und hnRNP H1 (eines der hnRNP H/F-Proteine, die mit hTR interagieren) an denselben Prozessen durch Depletion und Überexpression dieser Proteine in Zellen, die entweder Wildtyp (WT) oder mutierte hTR exprimieren. Insgesamt konnte ich zeigen, dass beide hTR-Mutationen die Telomerase-Aktivität verringern, ohne die Telomerase-Prozessivität zu beeinträchtigen, und dass sie im Vergleich zu WT-hTR auf einem ähnlichen Niveau exprimiert werden. Auch die Deletion von DHX36 selbst senkt die Telomeraseaktivität und zeigt eine additive Wirkung auf die Expression beider hTR-Mutanten. Umgekehrt erhöht die Reduktion/Depletion von hnRNP H1 die Telomeraseaktivität, während seine Überexpression die mit DTAA nachgewiesene Produktakkumulation verringert. Im zweiten Teil meiner Dissertation charakterisierte ich zwei Mutationen in der hTR-Template-Region, die Substitutionen A>G an Position 48 (A48G) und C>A an Position 50 (C50A) unter Verwendung der zuvor erwähnten Ansätze. Beide Mutanten zeigen eine stark verringerte Prozessivität der Telomerase, werden aber im Vergleich zu WT-hTR in ähnlichem Maße exprimiert. Nach weiterer Charakterisierung der C50A-hTR-Mutante zeigen meine Ergebnisse, dass die Template-Mutationen die Telomererhaltung auf verschiedene Weise beeinflussen. Erstens verursachen sie im mutierten Enzym eine Verschiebung von Translokation zu Dissoziation. Zweitens ist die Verlängerungsaktivität der WT-Telomerase beeinträchtigt, sobald mutierte Wiederholungen am Ende eines Telomers vorhanden sind. Drittens ist es wahrscheinlich, dass der Einbau der mutierten Wiederholungen in die Telomere die Wechselwirkungen mit Telomer-bindenden Proteinen und dadurch die Schutzfunktion von Shelterin beeinträchtigt. Abschließend begann ich mit der Charakterisierung von Fibroblastenzellen, die von einem Patienten mit Dyskeratosis Congenita isoliert wurden, der die Mutation C50A-hTR und eine weitere Miss-Sense-Mutation im RTEL1-Gen (ebenfalls an der Telomererhaltung beteiligt) in Heterozygotie trägt. Ich konnte zeigen, dass die Fibroblasten des Patienten ein beeinträchtigtes Zellwachstum aufweisen, was eher auf eine beschleunigte Seneszenz der Zellen als auf einen erhöhten Zelltod zurückzuführen ist.

Abstract

Telomeres are the terminal regions of chromosomes that protect chromosome ends from deterioration and fusion with other chromosomes. They are composed of the repetitive DNA hexamer 5'-GGTTAG-3', with a length that in human spans from 10 to 15 kbp, with 100 to 200 bps of single-stranded 3' overhang.

The main strategy to counteract telomere shortening used by both stem cells and the majority of tumors, is through the activity of telomerase. The core components of human telomerase are the catalytic protein subunit Telomerase Reverse Transcriptase (TERT) and the human Telomerase RNA (hTR). hTERT is able to replenish the terminal DNA sequences lost upon DNA replication during cell division, by repeatedly reverse transcribing the template region contained in hTR onto the chromosome ends.

Mutations in different components of telomerase as well as in factors participating in its biogenesis have been identified in patients affected by Telomere Biology Disorders (TBDs). By interfering with telomerase function, these mutations accelerate telomere shortening leading to the depletion of stem cells in various tissues.

The aim of this thesis is to understand how different regions of hTR affect telomerase biogenesis and activity. At first, I focused on studying the very 5' terminal region of hTR, which is G-rich, known to form G-quadruplex structures (G4), and to interact with the helicase DHX36 and the heterogeneous nuclear ribonucleoproteins hnRNP H/F. Taking advantage of two reported disease-related mutations of hTR within this region, specifically the transversion G>C at position 2 (G2C) and G>T at position 11 (G11T), I mainly used the approaches of qPCR and Direct Telomerase Activity Assays (DTAAs) to test the relevance of this region to hTR expression and telomerase activity. Additionally, I studied the involvement of DHX36 and hnRNP H1 (one of the hnRNP H/F proteins interacting with hTR) to the same processes thanks to depletion and overexpression of those proteins in cells expressing either wild-type (WT) or mutant hTR. Altogether, I showed that both mutations of hTR reduce telomerase activity without affecting telomerase processivity, and are expressed at a similar level compared to WT-hTR. Similarly, DHX36 depletion by itself lowers telomerase activity and displays an additive effect upon either mutant hTR expression. Conversely, hnRNP H1 depletion increases telomerase activity, while its overexpression reduces the product accumulation detected by DTAA.

In the second part of my thesis, I characterized two mutations within the template region of hTR, namely the substitutions A>G at position 48 (A48G) and C>A at position 50 (C50A), using the same approaches applied previously. Both mutants display a severe reduction in processivity of telomerase, besides being expressed at a similar level compared to WT-hTR. After further characterization of the mutant C50A-hTR, my results reveal that template mutations affect telomere maintenance in multiple ways. Firstly, they cause a shift from translocation to dissociation in the mutant enzyme. Secondly, once mutant telomeric repeats are present at the terminus of a telomere, elongation activity of WT telomerase is impaired. Thirdly, it is likely that incorporating mutant repeats into the telomeres affects the interactions with telomere binding proteins thereby compromising the protective function of shelterin. Finally, I began the characterization of fibroblasts cells isolated from a patient affected by Dyskeratosis Congenita who is carrying the mutation C50A-hTR and another miss-sense mutation in the RTEL1 gene (also involved in telomere maintenance), both in heterozygosis. I could show that the patient fibroblasts display impaired cell growth, which is due to accelerated senescence of the cells rather than increased cell death.

Introduction

Telomeres through history

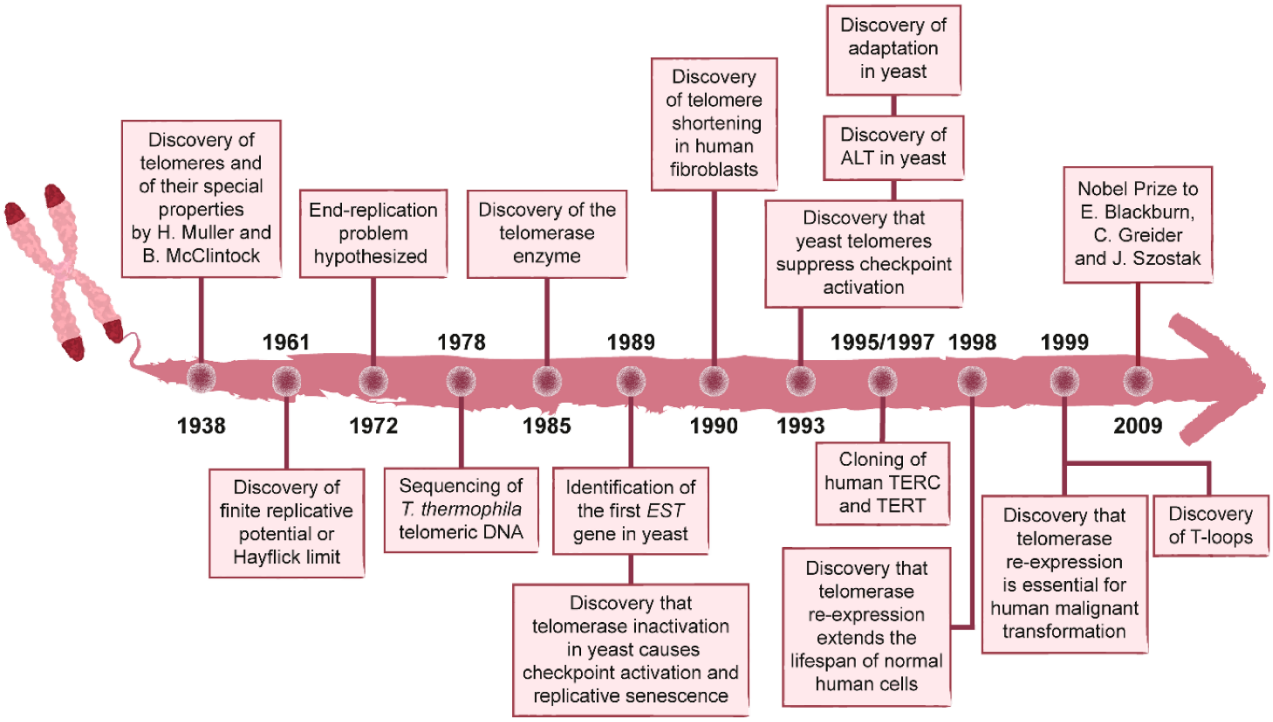

Figure 1: Timeline of the major discoveries in the telomere field. Figure taken from Casari et al. 2022 [1].

The history of the telomere field begun in the first half of the twentieth century (Figure 1). The idea of telomeres rose in 1938, when Hermann J. Muller was working with the fruit fly *Drosophila melanogaster*. He found that X-rays could generate brakes into the chromosomes, making them able to fuse to each other leading to deletions, inversions and/or translocations. Interestingly, these structural alterations never involved the chromosome termini. These findings guided him to propose the existence of a “terminal gene” that “must have a special function, that of sealing the ends of the chromosome, so to speak, and that for some reason, a chromosome cannot persist indefinitely without having its ends thus sealed”. H.J. Muller named this gene “telomere”, from the Greek telos “end” and meros “part” [2]. In the same year, through her cytological studies on irradiated maize chromosomes, Barbara McClintock confirmed the concept that telomeres gave identity to the natural ends of a chromosome, so that a cell could distinguish them from the intra-chromosomal ends generated by the occurrence of a Double Strand Break (DSB). She discovered that broken chromosomes frequently fuse with other broken ends, producing dicentric chromosomes that would break in the following mitosis, when the two centromeres would be pulled apart toward the opposite poles of the mitotic spindle. These newly generated broken ends can fuse with other broken ends, starting the so-called “breakage-fusion-bridge cycle”. Notably, she never detected fusions involving telomeres, giving the first evidence that one function of telomeres must be to protect the natural chromosome ends from fusing to each other [3]. In 1961, Hayflick and Moorhead demonstrated that human fetal cells possessed a finite replicative potential of 50 to 60 doublings, subsequently dubbed ‘‘Hayflick limit’’ or more generally, replicative senescence [4, 5]. In the early 1970s, both Watson in 1972 and Olovnikov in 1973 introduced the so-called ‘‘end replication problem’’, by observing the asymmetry in linear DNA replication. They predicted that after each cell division there would be a loss of chromosomal DNA from the terminus of the lagging strand due to removal of the terminal RNA primer, resulting in progressive chromosomal shortening [6, 7].

The ciliated protozoan *Tetrahymena thermophila* was the first eukaryotic organism to have its telomeric DNA sequence identified. Blackburn and Gall found that the ends of the macronuclear ribosomal DNA (rDNA) molecules in this organism consisted of a variable number of 5′-CCCCAA-3′ repeats [8]. Thanks to the sequencing of the telomeric DNA from other eukaryotic organisms, it was discovered that as in *T. thermophila*, the ends of chromosomes were composed of tandemly repeated sequences, whose sequence, length and number varied depending on the organism. Additionally, the composition of telomeric DNA was asymmetric, with the DNA strand running in the 5′ to 3′ direction being guanine-rich and exhibiting a 3’ overhang compared to the complementary strand [9]. Telomeres from the same organism were found to differ in lengths, suggesting that telomeric DNA was not templated by the parental chromosome. Supporting this idea, Szostak and Blackburn ligated *T. thermophila* rDNA telomeres onto both ends of a linear yeast plasmid and transformed it into yeast [10]. The transformed yeast cells were capable to maintain the plasmid as a linear molecule, and interestingly, the cells even added the yeast C1–3A telomeric repeats to the tips of *T. thermophila* rDNA telomeres [11]. These results argued that the structural features required for telomere replication must be evolutionary conserved. Because telomere elongation could be entirely attributable to an increase in the number of tandemly repeated sequences, Blackburn and Szostak proposed the existence of a terminal transferase enzymatic activity that was able to add telomeric repeats onto chromosomes ends. Furthermore, only *T. thermophila* chromosomes’ end sequence, but not random sequences, could be recognized as substrate by the putative “DNA addition enzyme” [11]. Taking advantage of cell-free extracts made from *T. thermophila*, Greider and Blackburn were the firsts to discover the existence of this terminal transferase enzymatic activity that was capable of adding telomeric DNA repeats to the chromosome ends [12]. They were able to purify this enzyme, which was named telomerase, and showed that it was a ribonucleoprotein (RNP) complex, where both the protein and the RNA components were essential for its activity [13]. After cloning and analyzing the RNA moiety of telomerase, it was found to include a short sequence that could act as a template for the addition of telomeric repeats [14]. Mutation within this short sequence of the RNA were able to introduce *in vivo* the corresponding mutated telomeric repeats, proving that telomerase used its integral RNA component as a template for addition of new telomeric repeats to telomeres [15]. At the same time, Lundblad and Szostak were pursuing the search of the *S. cerevisiae* telomerase enzyme by utilizing different mutants that were not able to convert a circular plasmid containing inverted telomeric repeat sequence of *T. thermophila* into a stable linear form. They discovered the first gene encoding for one of the subunits of the budding yeast telomerase RNP complex, which was named *EST1* because of the so-called “ever shorter telomere” (est) phenotype showed by mutation in this gene, caused by progressive loss of telomeric DNA. Interestingly, *est1* mutants also showed a gradual decrease in cell viability, giving the first experimental evidence that loss of telomeric DNA limits cellular proliferation [16]. Seven years later, three additional *EST* genes (*EST2*, the actual budding yeast reverse transcriptase, *EST3*, and *EST4*, now called *CDC13*) were discovered in a screen for mutants that exhibited increased defects in plasmid linearization in combination with chromosome instability [17]. In 1990, Harley et al. demonstrated that telomere attrition occurred in parallel with the decline in replicative lifespan of human primary cells in culture, establishing that the triggers of the Hayflick limit are short telomeres [18]. Continuing the characterization of the telomeres’ properties, Sandell and Zakian performed a critical experiment in the budding yeast *Saccharomyces cerevisiae*, where they placed the recognition site of the HO endonuclease 20 kb away from the dispensable left telomere of chromosome VII, so that the telomere will be chopped off upon HO expression. After loss of the telomeric DNA, they discovered that cells underwent a cell-cycle arrest due to DNA damage checkpoint activation, suggesting that telomeres must be essential to prevent the natural chromosome ends from being recognized as DSBs by the checkpoint-associated proteins [19]. Singer and Gottschling were able to identify the gene encoding for the budding yeast RNA carrying the template sequence required for telomeres elongation, which they named *TLC1* (telomerase component 1), by looking for a gene that when overexpressed was capable of counteracting the ability of telomeres to silence transcription [20].

Thanks to the purification of the catalytic protein subunit of telomerase from a ciliated protozoan, J. Lingner et al. were able to demonstrate that reverse transcriptase motifs were essential for telomeric DNA synthesis both *in vivo* and *in vitro* [21]. This discovery was followed by that of the human telomerase RNA component (TERC, hTR) [22] and that of the human catalytic protein telomerase reverse transcriptase (TERT) [23]. Since the end of the twentieth century, it is known that vertebrate telomeres consist of several kilobases of double stranded DNA containing the repetitive sequence GGTTAG, which terminate with a 100 – 200 bases of single-stranded GGTTAG at the 3′ end, the so-called G-rich 3′ overhang [24, 25]. Specifically, mammalian telomeres contain anywhere from <1 to >50 kb of telomeric DNA, depending on the species, cell type and genetic background. Laboratory mice (*Mus musculus*) for example have telomeres that frequently exceed 30 kb in length, while in human, where telomeres represent about ≈0.04% of the genome, their length spans between 10 and 15 kb in the germline, but somewhat shorter in somatic cells and often much shorter in cancer cells [26-30].

Shelterin

Already from the early work from H.J. Muller [2] and B. McClintock [3], it was evident that telomeres show the ability to avoid the DNA damage response (DDR) that is triggered when other DNA ends are generated across the chromosomes upon Double Strand Breaks (DSBs). Several data from the literature, nicely summarized in a review from Titia de Lange about Shelterin-mediated telomere protection [31], indicate that at least seven distinct DDR pathways (Figure 2A) threaten telomeres integrity.

A

DDR pathway	Shelterin subunit(s)	Mechanism	General repressor
ATM kinase	TRF2 (TIN2)	t-loop	None
ATR kinase	POT1a (POT1b)	RPA exclusion	None
PARP1	TRF2, TIN2	Branched-DNA binding, ?	Ku70/80
c-NHEJ	TRF2	t-loop (iDDR, Rap1)	CYREN (S/G2)
alt-NHEJ	TRF2 (TIN2, POT1a/b)	t-loop, PARP1 repression, ?	Ku70/80
HDR	POT1a or POT1b + Rap1	?, ?	Ku70/80
Hyper-resection	POT1a/b, TRF2	Repression of ATM/ATR	53BP1/Rif1/Rev7

B

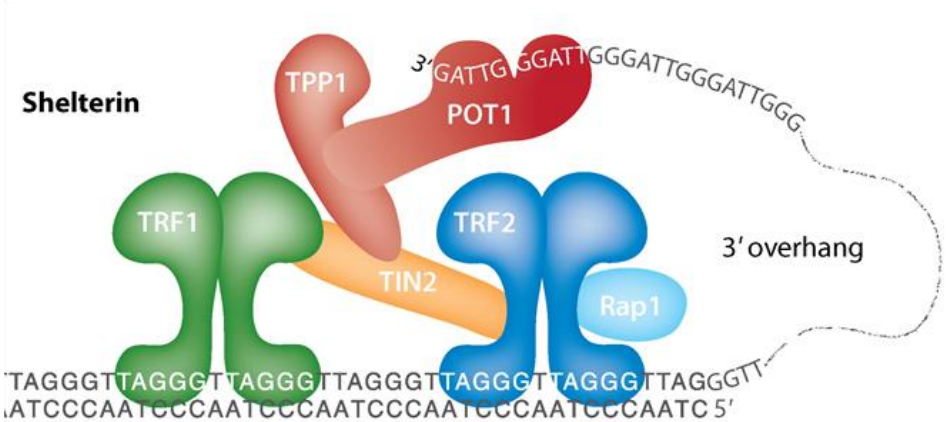

Figure 2: (**A**) Summary of DDR pathways that are repressed by shelterin, the subunits dedicated to each pathway, and their proposed mechanism of action. For several pathways, general repressors are listed. In the repression of c-NHEJ, it is speculated that Rap1 and the iDDR domain in TRF2 contribute to preventing c-NHEJ when telomeres are in a linear state. (**B**) Depiction of the six-subunit human shelterin complex associated with the double-stranded and single-stranded telomeric DNA. Figure edited from T. de Lange 2018 [31].

Protecting telomere ends is therefore a complicated task, but remarkably, all the necessary activities to block the DDR are performed by a single telomeric protein complex called Shelterin (Figure 2B). A summary of which shelterin component is mainly responsible to silence a specific DDR pathway is shown in Figure 2A. Shelterin has evolved to specifically recognize the sequence and structure of mammalian telomeres, being capable of interacting with both double stranded (ds) and single stranded (ss) telomeric DNA and sufficiently abundant to bind all telomeric DNA (Figure 2B) [32].

Six distinct proteins form the human shelterin complex: TRF1 and TRF2, two homodimer that bind dsDNA; Rap1; TIN2; TPP1; and POT1, a ssDNA-binder protein (Figure 2B) [33]. Thanks to different experimental approaches like yeast two-hybrid analysis, co-immunoprecipitation and structural studies, the main interactions between the different shelterin subunits have been established. In a work from F. Erdel et al., they showed that TRF1 and TRF2 bind to TIN2 using distinct interaction surfaces. TIN2 also binds to TPP1, which in turn binds to POT1. Finally, Rap1 binds TRF2, completing the six-subunit complex. Despite the numerous reported modifications for each of the Shelterin subunits, the interaction interfaces between them do not seems to involve post-translational modifications. Additionally, the assembly of Shelterin does not require interactions with DNA [34]. The nanomolar affinity of TRF1 and TRF2 binding to duplex telomeric DNA is dependent on the formation of homodimers mediated by the TRFH domain possessed by both proteins [35, 36]. Together, the TRF1 and TRF2 homodimers provide four ds 5'-TAGGGTT-3' recognition modules to shelterin [36, 37].

POT1 binds to ss telomeric DNA with two N-terminal oligonucleotide / oligosaccharide binding (OB) folds [38, 39]. By *in vitro* analysis, POT1 was shown to bind ss 5'-TTAGGGTTAG-3' sites with sub-nanomolar affinity, either at a 3' end or (with slightly lower affinity) when at an internal position [39, 40]. Besides Rap1 and TPP1 having a putative nucleic acid binding domain, respectively a Myb-like domain and an OB-fold, both proteins do not interact directly with telomeric DNA [41-43]. The shelterin components that bind to DNA do not show cooperativity when analyzed individually *in vitro* [34-36, 40], suggesting that shelterin components may bind to the telomeric DNA as independent units. Thanks to *in vitro* experiments, it has been hypothesized that shelterin can find its binding sites through a diffusive 3D search as well as a 2D search along the DNA [34]. Interestingly, Rap1 has a subtle influence on TRF2, diminishing its affinity for branched DNA [44, 45] and preventing it to engage in sequence-independent interactions, thereby increasing the specificity of TRF2 for GGTTAG repeats [46]. The *in vivo* stoichiometry of the shelterin complex is still unclear. In human and mouse cells, TRF1, TRF2, TIN2, and Rap1 are about 10 times more abundant than the other two proteins, TPP1 and POT1 [32]. The core complex of shelterin is therefore likely to be composed of the four most abundant subunits, with a fraction of the complexes also containing TPP1 and POT1. The core of shelterin is sufficiently abundant within a cell, so that is able to bind all ds GGTTAG repeats. Additionally, there is a tenfold excess of TPP1/POT1 over its ss GGTTAG binding sites, suggesting that the majority of the telomeric DNA must be associated with shelterin proteins [32].

T-loops

In addition to binding the shelterin proteins, in many organisms, including mammals, telomeres form large lariat structures called T-loops [33]. These T-loops are generates through the invasion of the G-rich 3' overhang into the ds telomeric DNA (Figure 3) [47]. The current knowledge in the field, suggests that the G-rich 3' overhang pairs with the C-rich strand of telomeric DNA and displaces the G-rich strand into a D-loop [48]. Structurally, T-loops can have large loops and short tails or vice versa, suggesting that there is not a specified position where the 3' overhang invades the dsDNA [48].

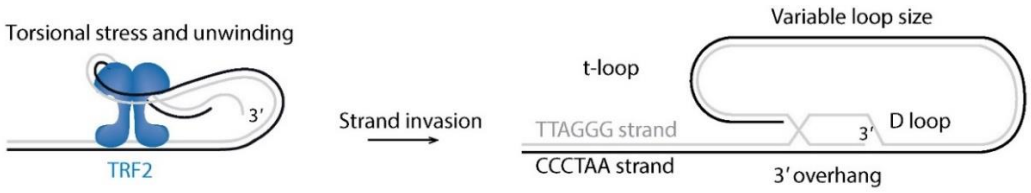

Figure 3: Model for TRF2-mediated T-loop formation. Figure edited from T. de Lange 2018 [31].

To be able to form T-loops, after DNA replication, telomeres need to regenerate a 3' overhang of the correct length, which is critical for telomere protection. Additionally, post-replicative processing of telomere ends dictates the telomere shortening rate during cell proliferation [49]. In mouse, the shelterin co-factors Apollo, CST, and Polα/primase are responsible for proper 3' overhang formation and are likely to perform a similar function also at human telomeres [50-56]. Nevertheless, the precise mechanism by which shelterin regulates 3' overhang formation in human telomeres is not yet completely understood. The formation of the G-rich 3' overhang at mouse telomeres involves the nucleolytic attack by Apollo and Exonuclease 1 (Exo1), followed by fill-in DNA synthesis performed by CST and Polα/primase. Due to their distinct structures upon DNA replication, the processing of the two sister telomere ends slightly differs. Presumably, leading-end telomeres are initially blunt, and the TRF2-mediated recruitment of Apollo is needed to initiate the nuclease attack on the leading-end telomeres. In a similar fashion to DSBs repair, such ends require an initial cleavage before further nucleolytic attacks can occur [57-59]. Likewise, at leading-end telomeres Apollo seems to prepare the substrate for subsequent Exo1 exonucleolitic activity. After DNA replication, lagging-end telomeres already possess a 5' recessed end, making them able to be immediately processed by Exo1. This is supported by the dispensability of Apollo for 3' overhang formation at lagging-end telomeres [57-59].

For both sister telomere ends, setting the length of the 3' overhang is mainly achieved through the CST-mediated fill-in activity of Polα/primase. Once the formation of the G-rich 3' overhang at each telomere end is completed, and shelterin proteins have found and bound the telomeric DNA within the nucleus, T-loop formation can take place [49, 60]. TRF2 is both necessary and sufficient for t-loop formation (Figure 3) [61]. At least *in vitro*, TRF2 is capable to remodel telomeric substrates into structures similar to t-loops [47, 62]. This feature of TRF2 can be explained by the ability of its TRFH domain to wrap DNA around itself without sequence specificity [63]. This is a low-affinity interaction of TRF2 with the telomeric DNA that is likely to induce local unwinding, promoting invasion by the 3' overhang [63]. Notably, POT1 is not required for T-loop formation, besides its potential ability to engage the D-loop with their OB folds and possible binding of the three-way junction with their Holliday junction resolvase-like domain [61]. Ultimately, because the exact structure at the base of the T-loop has not been established yet, neither the minimal length of telomeres required for t-loop formation, multiple questions about T-loops are still open. Additionally, it is not known what percentage of telomeres are actually engaged in this structure.

TElomeric Repeat-containing RNA (TERRA)

Due to their generally heterochromatic state, telomeres were historically viewed as transcriptionally inactive [64]. In 1989, Rudenko and Van der Ploeg identified a heterogeneous population of RNA transcripts containing telomeric repeats in the protozoa *Trypanosoma brucei* [65]. It took almost twenty years to obtain evidence of telomeric transcription in other species, with Azzalin et al. in 2007 discovering TElomeric Repeat-containing RNA (TERRA) molecules in a human cervical cancer cell line (HeLa cells) [66], shortly followed by the discovery of TERRA molecules in *S. cerevisiae* by Luke et al. in 2008 [67]. Both telomeric and subtelomeric regions are actively transcribed into TERRA molecules, which are composed of subtelomeric-derived RNA sequence and GGUUAG repeats [66]. In 2008, Schoeftner and Blasco characterized TERRA as a novel structural component of telomeric chromatin, with the ability to regulate telomerase activity [68]. Additionally, TERRA transcripts have been shown to promote Shelterin assembly at telomeres, therefore preserving genomic integrity [69].

TERRA is classified as long non-coding (lnc) RNA, being transcribed by RNA polymerase II starting in the subtelomeric region and terminating within the telomeric repeats, utilizing the telomeric C-rich strand as a template [70]. TERRA molecules display heterogeneity in their length, which spans from 100 bases up to 10 kilobases [71, 72]. Interestingly, the majority of TERRA molecules contains a tract with an average length of 200 bases of GGUUAG telomeric repeats, suggesting that the length heterogeneity of TERRA is probably due to the subtelomeric-derived sequence [70]. Multiple studies using specific primers in PCR- and qPCR-based methods to analyze the subtelomeres, reported that TERRA is expressed from several chromosome ends in human cells [73-76]. Furthermore, several studies suggested that TERRA promoters are located within the subtelomeres on at least two-thirds of chromosome ends [77, 78]. TERRA promoter regions include CpG islands, as well as binding sites for the CCCTC-binding factor (CTCF), which, together with Rad21 (member of the cohesin complex), regulate TERRA expression through the binding of its promoter in multiple human chromosomes [78-80]. CTCF and Rad21 promote the recruitment of RNA Pol II to TERRA promoters inducing transcription [78]. Depletion of either CTCF or Rad21 decreases TERRA levels and increases DDR activation at chromosome ends [78, 80]. The majority of TERRA molecules in human cells, possess a 7-mono-methylguanosine (m7G) cap structure at their 5′-ends, with a small fraction of molecules containing also a poly(A) tail at their 3′-end, contributing to RNA stability [66, 70]. Moreover, TERRA expression was reported to vary in a cell-cycle-dependent manner, with highest levels detected in G1 phase and gradually decreasing to the lowest levels detected during S phase. Notably, increased expression is observed again at the very end of mitosis [70].

Telomerase-negative tumor cells that rely on the recombination-base Alternative Lengthening of Telomeres (ALT) pathway (explained in more detail in the next chapter) express the highest levels of TERRA [81]. This is probably due to the open chromatin conformation at subtelomeres and to the abnormally long telomeres resulting from adaptive responses to mutations in ATRX or DAXX genes, both considered chromatin remodeling factors [82]. Furthermore, it was then established that TERRA expression is dependent on telomere length, such that short telomeres display increased transcription of TERRA, correlating with a decrease in repressive histone marks in telomeric repeats [83].

TERRA transcripts can function as essential regulators of telomeres in *cis* and as epigenomic modulators in *trans*, therefore indirectly controlling DDR by regulating gene expression [84]. Notably, TERRA molecules have been shown to base pair with the telomeric C-rich strand, displacing the complementary G-rich ssDNA strand, and forming DNA-RNA hybrids structures called R-loops [81, 85]. Formation of R-loops at telomeres can affect telomere maintenance and genome stability in multiple ways, by creating a permissive environment that promote telomeric DNA replication as well as homologous recombination between telomeres, favoring ALT mechanisms [81, 85-89].

In vitro studies suggested that TERRA molecules play a role at the ends of chromosomes in switching between the DNA-binding protein RPA, required for the activation of the ATR checkpoint, and the shelterin component POT1, which acts as a telomeric repressor of the ATR-mediated DDR in telomeres [90, 91]. This function is mediated by the direct interaction between TERRA and the RNA-binding protein hnRNPA1, which belongs to the hnRNPs family and which can regulate the abundance and localization of TERRA in telomeres [92]. The alteration of TERRA levels in either direction, through silencing or overexpression, activates the DDR pathway at chromosome ends, resulting in an increase of telomere dysfunction-Induced Foci (TIFs) observed by microscopy, in addition to aberrations in metaphase telomeres [75, 93].

ALT pathways

Embryonic and adult stem cells, as well as the vast majority of cancer cells, elongate their telomeres by activating the telomerase holoenzyme. However, approximately 10 to 15% of human tumors preferentially maintain telomeres through the Alternative Lengthening of Telomeres (ALT) pathway [94, 95]. ALT pathway is a form of telomere maintenance that rely on telomere sequence-specific homologous recombination (HR) [96]. ALT cells lengthen their telomeres by recombination-mediated synthesis, using the DNA sequence of other telomeres as a template, therefore counteracting the telomere shortening caused by continuous cell division as well as other stress sources [97]. ALT activation is usually associated with characteristic phenotypes, like heterogeneous telomere length, abundant extrachromosomal telomeric repeats (ECTRs), nuclei containing ALT pathway-associated promyelocytic leukemia (PML) bodies (APBs) and telomeric sister chromatid exchanges (T-SCEs) [95]. A recent and in depth description of the ALT-related phenotype can be found in a recent review from K. Hou et al. 2022 [98].

Telomerase Reverse Transcriptase (TERT)

The human catalytic protein telomerase reverse transcriptase hTERT contains three main structural elements: a long N-terminal extension (NTE) that contains conserved DNA and RNA binding domains; a central catalytic domain responsible for the reverse transcriptase activity (RT); a short C-terminal extension (CTE) [99]. The linear organization of hTERT domains is illustrated in Figure 4. This organization defines most of TERT proteins within eukaryotes, but there are at least three notable exceptions. Firstly, certain insect and nematode TERT proteins display a truncated N-terminus that does not contain the telomerase essential N-terminal (TEN) domain [100, 101]. Secondly, the C-terminal region is completely absent in *Giardia lamblia* and nematodes' TERT proteins [101]. Thirdly, *Plasmodium falciparum* TERT is at least three times larger than all other TERT proteins and contains several hypervariable insertions between the conserved domains [102]. The biological significance of this divergent architecture between those species is still not well understood, and it remains to be determined if other uncharacterized TERT domains and/or species-specific accessory proteins compensate for the missing domains.

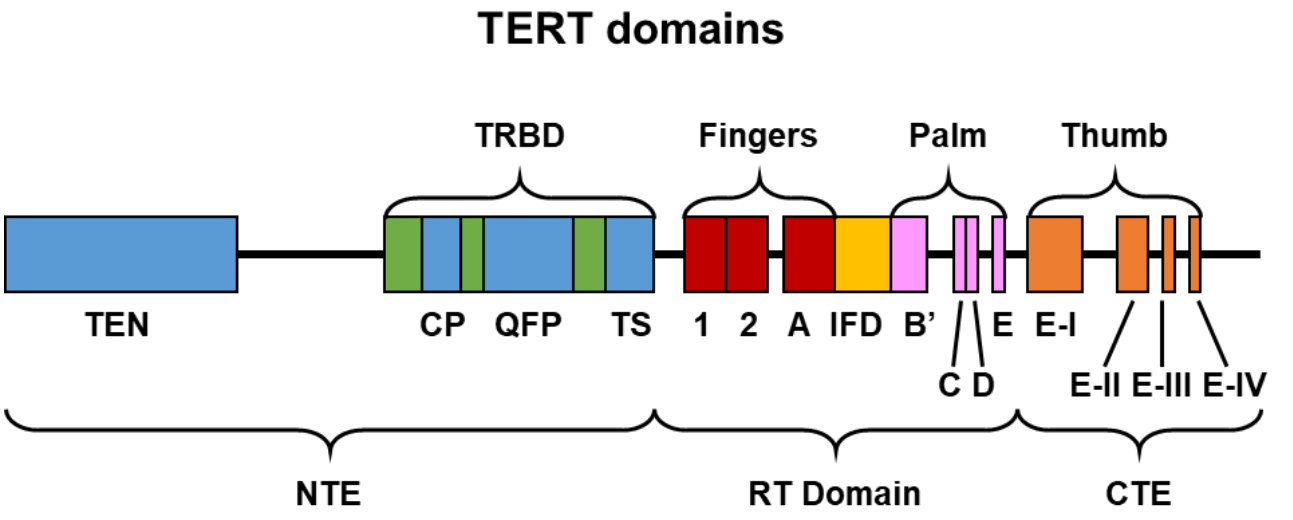

Figure 4: Predicted linear architecture of hTERT. In most organisms, TERT contains a long N-terminal extension (NTE), a central catalytic RT domain and a short C-terminal extension (CTE). Blue boxes indicate the predicted locations of the telomerase essential N-terminal (TEN) domain and the telomerase-specific motifs CP, QFP and TS. Green boxes indicate the TRBD, containing the CP motif, QFP motif and part of the TS motif. An unstructured linker region connects the TEN domain and TRBD. Red and pink boxes represent the seven evolutionarily conserved motifs in the RT domain (1, 2, A, B′, C, D, E) and a yellow box illustrates the telomerase-specific IFD. The CTE contains four blocks of conserved amino acids, which are shown as orange boxes (E-I, E-II, E-III, E-IV).

The NTE of most TERT proteins contains two conserved domains, the TEN domain and the telomerase RNA-binding domain (TRBD) (Figure 4). The TEN domain shows binding affinity for single-stranded telomeric DNA and interacts directly with TPP1/TIN2, allowing the shelterin-mediated recruitment of the holoenzyme to telomeres. The TEN domain is linked to the TRBD by a relatively long and unstructured linker region that may be important for conformational flexibility. The TRBD has been shown to interact with the CR4/5 region of hTR, mediating the assembly of the two core components of the holoenzyme [103, 104]. Within the TRBD several conserved telomerase-specific motifs are distinguishable, including the CP, QFP and TS motifs (Figure 4) [105, 106]. These regions are important for hTERT-hTR binding interactions and the rate of template copying during telomere synthesis [105, 107-117].

The catalytic RT domain of TERT is the most characterized region of the protein and contains seven evolutionarily conserved RT motifs that are essential for its enzymatic activity [21, 107, 118-124]. The RT domain is organized into two subdomains that resemble the ‘fingers’ and ‘palm’ subdomains of prototypical RT enzymes (Figure 4) [21, 119, 125].

These regions are linked by a loop that harbors the conserved region called ‘primer grip’ of motif E [126]. Molecular models predict that this loop makes direct contacts with the RNA–DNA hybrid and the 3′-end of the telomeric ssDNA, suggesting that the primer grip region is involved in positioning the 3′-end within the active site of the enzyme [126]. A unique structural feature of the telomerase RT domain is a large insertion between motifs A and B′, called the ‘insertion in fingers’ domain (IFD) (Figure 4) [21, 119]. The IFD consists of two antiparallel α-helices sandwiched between the fingers and palm subdomains [126]. Crystal structure information reveal that the IFD is engaged in intramolecular protein-protein interactions that organize and stabilize this region of the RT domain [126]. Notably, the IFD also makes extensive contacts with an α-helix that is involved in directly contacting the backbone of the incoming DNA sequence [126]. In the active site of TERT there are three invariant aspartic acid amino acids, one of which resides in motif A and the other two within motif C [21, 119]. These residues are conserved between different RT domains and form a catalytic triad that is directly involved in nucleotide addition via a two-metal cation mechanism [21, 119]. The substitution of these amino acids with Alanine completely abrogates telomerase activity [107, 112, 120, 122, 123]. In the interface between the palm and fingers subdomains, the nucleotide-binding pocket is formed by conserved residues from motifs 1, 2, A, B′, C and D [126]. Two conserved surface-exposed amino acids from motifs A and C (tyrosine and valine, respectively) form a hydrophobic patch that is predicted to bind the base of the nucleotide substrate. This interaction would promote nucleotide positioning within the active site of the enzyme, by coordination with a metal cation and the 3′-end of the DNA sequence [126]. Sequence alignment of the RT domain between TERT enzymes of different species, revealed a novel telomerase-specific motif, dubbed motif 3, between the motifs 2 and A [127, 128]. Notably, despite the predicted secondary-structure of motif 3 being evolutionarily conserved, the primary sequence is only conserved between vertebrate and ciliate telomerases, suggesting that motif 3 may regulate species-specific aspects of telomerase function [128].

The CTE of hTERT shows only weak sequence conservation compared to the NTE and RT domains, suggesting that it may have species-specific functions or that different amino acid sequences have evolved independently to fold into similar structural domains. The CTE adopts a novel protein fold, although by structural comparison with the closely related HIV-RT enzyme indicates that this region represents the thumb domain of telomerase [126]. This domain is a helical bundle that contains several surface-exposed loops that are likely to contribute to the formation and stabilization of the RNA–DNA hetero-duplex between hTR and the telomeric DNA within the enzyme active site [126, 129]. Additionally, it has been shown that addition of an epitope tag to the C-terminus of hTERT abolishes telomere elongation *in vivo*, suggesting that this region’s conformation is important for telomerase function [130].

Notably, the CTE is essential for telomerase activity in human and *T. thermophila*, but is dispensable for telomerase activity in budding yeast [105, 110, 111, 113] and even completely absent in other organisms [101], further suggesting that this domain has species-specific roles. Globally, TERT forms a ring-like structure in which the TRBD and the CTE come spatially close to each other forming a channel, which constitutes the catalytic pocket [126]. Notably, crystal structure information reveal the details of DNA substrate binding by the thumb domain in the CTE, and the RNA template region of hTR binding by the finger and palm domains in the RT, thus positioning the 3′ end of the G-overhang at the active site for nucleotide addition [131].

Mechanistically, telomerase adds new telomeric DNA repeats into the telomeres by iteratively copying the template sequence harbored by hTR. The relatively short template region within the whole hTR sequence is specifically defined to prevent incorporation of non-telomeric nucleotides from the template-flanking region, which could compromise the binding of shelterin hindering the protective function of the complex and culminating in genome instability [132-135]. Brown and colleagues characterized an intrinsic sequence-defined pausing mechanism of human telomerase that provides insights into the template boundary definition for vertebrate telomerases. They showed that the sequence-defined pause signal acts synergistically with the P1-helix physical boundary function during the telomerase catalytic cycle. After processive addition of six nucleotides to a DNA primer, the first rA:dT base pair formed in the duplex signals a pause in DNA synthesis, which coincides with the P1-defined boundary [136]. The authors proposed that this pausing event allows duplex dissociation from the active site, which is followed either by product release or template translocation. Furthermore, this sequence-defined mechanism stimulates high nucleotide addition processivity before reaching the pause site, the loss of which results in a multitude of weaker pause sites throughout the template and products that display heterogeneous terminal registers. In conclusion, Brown and colleagues suggest that such sequence-defined pausing mechanism is critical for generating 6-nt DNA repeats with identical GGTTAG terminal sequences [136].

human Telomerase RNA (hTR, TERC)

Telomerase RNAs between different species are highly variable in both sequence and structure. Where yeast telomerase RNA resembles small nuclear RNA (snRNA) [137-139], vertebrate telomerase RNAs are structurally more similar to small nucleolar RNA (snoRNA) and small Cajal Body RNA (scaRNA), which guide the pseudouridylation of respectively ribosomal RNA and snRNA [140]. The mature human telomerase RNA (hTR) is 451 nucleotides in length. The 5' half of hTR harbors a core domain, constitutes by the template region, a pseudoknot secondary structure and a Template Boundary Element (TBE), the latter embedded in the so-called P1-helix (Figure 5) [141, 142]. Furthermore, at its very 5' end, hTR contains multiple guanines stretches, some of which are involved into the formation of an rG-quadruplex (rG4) structure that protects hTR from degradation during the initial stage of transcription (Figure 5) [143]. In their 3' terminal region, vertebrate telomerase RNAs possess the H/ACA domain, which is formed by a 5' hairpin followed by the H-box comprising the consensus sequence 5'-ANANNA-3' (where N is any nucleotide), a 3' hairpin, and the trinucleotide ACA (Figure 5) [144]. The apical region of the 5' hairpin is known as conserved region 4/5 (CR4/5), and contains the P6b and P6.1 loops, which are absent in other H/ACA sno and scaRNAs [145]. The apical loop of the 3' hairpin contains a Cajal body box (CAB box), with the consensus sequence UGAG, and a biogenesis promoting box (BIO box), a unique feature of hTR, which are respectively required for localization and accumulation of hTR (Figure 5) [146, 147].

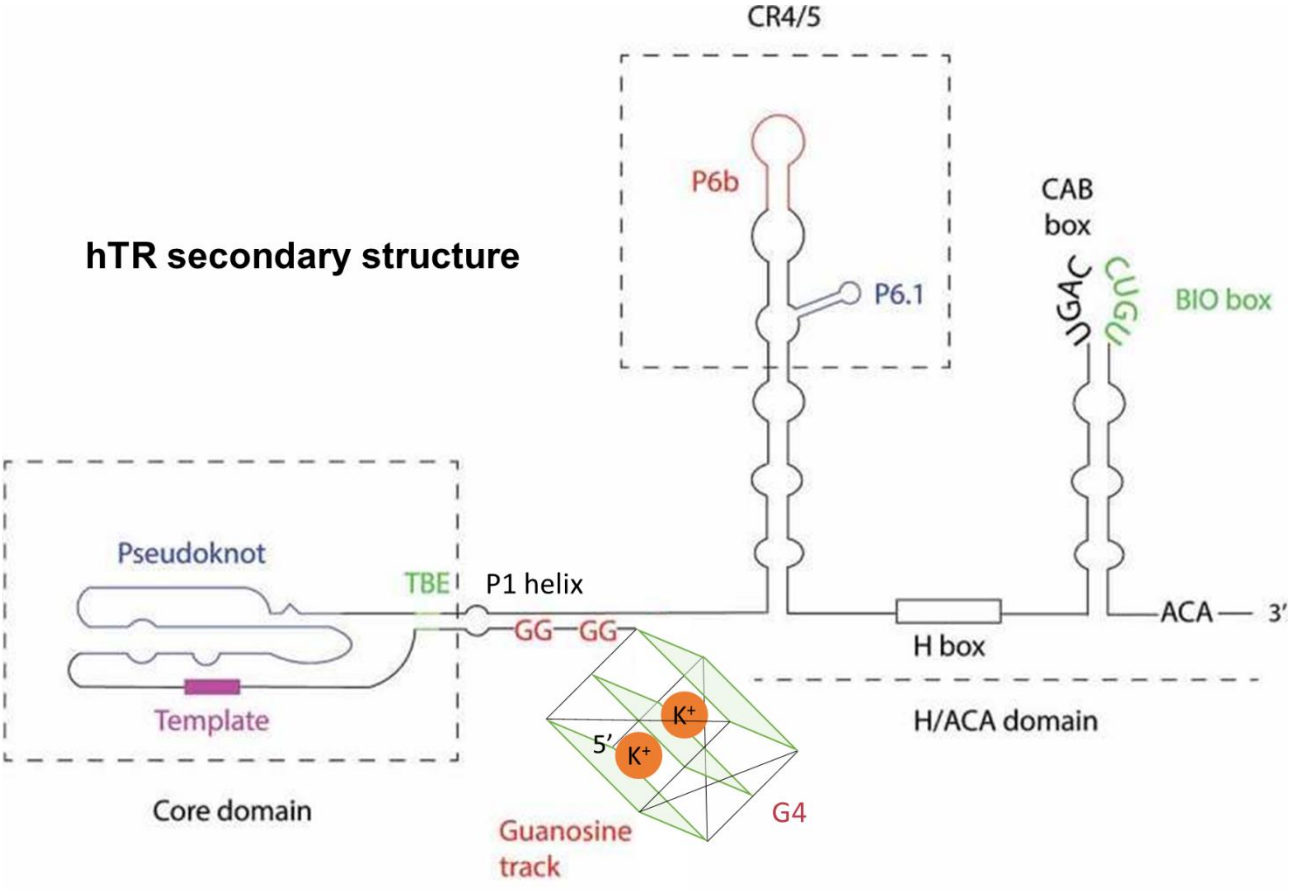

Figure 5: Secondary structure schematics of hTR, adapted from Qin & Autexier 2021 [148]. The 5' guanosine track forms a G-quadruplex structure at the early stage of hTR biogenesis. The core domain of hTR includes the pseudoknot secondary structure that interacts with hTERT, the template region, and TBE, the latter incorporated within the P1 helix. The H/ACA domain comprises two hairpins, each bound by a set of the H/ACA complex. The apical region of the 5' hairpin, termed conserved region (CR) 4/5, also interacts with hTERT. The apical loop of the 3' hairpin contains the CAB box that interacts with TCAB1 and regulates hTR localization, and the BIO box that facilitates recruitment of the H/ACA complex to hTR

Differently to most of the human H/ACA box snoRNAs and scaRNAs, which are embedded in introns, hTR is transcribed individually under the control of its own promoter [22] by RNA Polymerase II (Pol II), like yeast and other vertebrate telomerase RNAs. In ciliates, it is RNA Polymerase III (Pol III) that transcribes telomerase RNAs [149]. Pol II is capable of cooperating with the mediator and integrator complexes to execute transcription. Mediator is a multi-subunit scaffolding complex that regulates transcription of most mRNAs. It connects general transcription factors with Pol II and is required for transcription pre-initiation complex formation [150]. The integrator complex has been implicated with transcription termination of snRNAs and of replication-dependent histone mRNAs [151]. Recently, hTR promoter has been shown to be involved in hTR transcription termination by recruiting the integrator complex [152].

Like for other H/ACA RNAs [153], an important event that is critical for the accumulation of the mature form of hTR, is the co-transcriptional recruitment on its H/ACA box of the pre-H/ACA complex, which if formed by NAF1, NOP10, NHP2 and the pseudouridine synthase dyskerin (Figure 6) [154-158]. Specifically for hTR, this interaction with the pre-H/ACA complex is stimulated by the BIO box sequence [147]. At a later stage, NAF1 is then replaced by GAR1 during the conversion from a pre-H/ACA to a mature H/ACA RNP [159]. For a long time, it has been known that in active telomerase there are two sets of mature H/ACA complexes bound to hTR (Figure 6) [147, 160, 161].

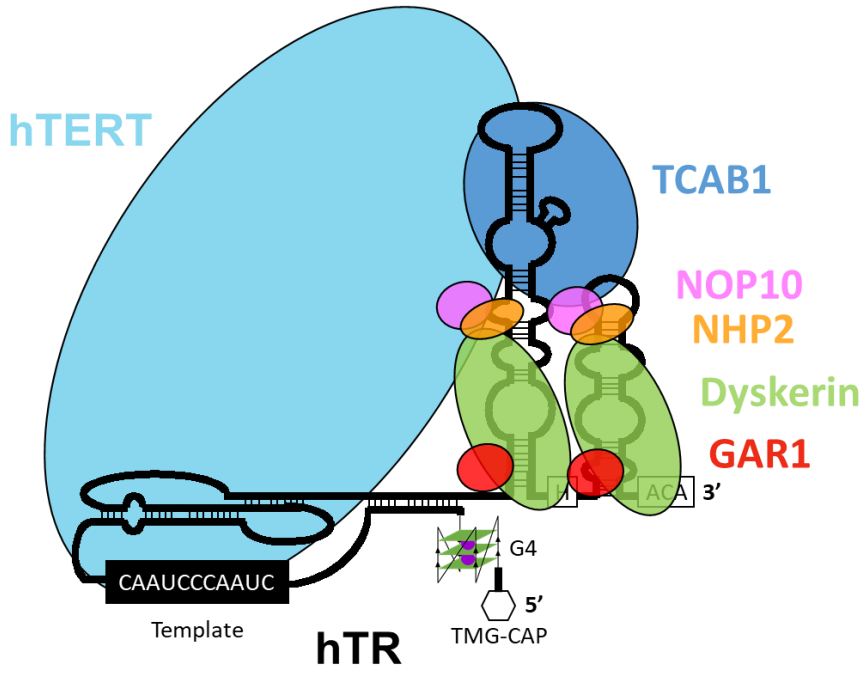

Figure 6: Schematic of hTR assembled into the human telomerase holoenzyme. hTERT interacts with the pseudoknot and the CR4/5. TCAB1 binds to the apexes of both the 3' stem-loops. Two sets of H/ACA complexes (NOP10, NHP2, Dyskerin, GAR1) recognize the H/ACA domain at the 3' end of hTR.

In cells, it has been detected a subpopulation of the total hTR which is 3'-extended with genomic encoded nucleotides, possibly due to read-through of Pol II past the mature end of hTR. At steady state levels, between 70% to 80% of total hTR exists in the mature form [162-165]. Intriguingly, from 72% to 75% of the nascent hTR produced within 4h is 3' extended, as analyzed by selective purification of nascent RNA transcripts [164]. These data suggest that hTR is primarily transcribed as a longer precursor, which is either processed into the mature form or degraded. The involvement of the nuclear exosome complex in hTR biogenesis was first shown by Northern blot, where depletion of the exosome core component RRP40 or the nuclease RRP6 led to increased accumulation of mature hTR or short extended precursors of hTR [163, 166, 167]. Generally, the exosome is recruited to different RNA species by at least three distinct adaptors: NEXT, TRAMP, and PAXT complexes [168, 169]. Additionally, in the nucleolus the microRNA biogenesis factor DGCR8 has been shown to facilitate exosome recruitment to hTR [170].

NEXT is a nucleoplasmic exosome complex formed by the scaffolding protein ZCCHC8, the RNA-binding protein RBM7 and the RNA helicase MTR4 [169].This complex preferentially targets the exosome to degrade non-adenylated RNAs [171], like 3' extended snRNA, PROMoter uPstream Transcripts (PROMPTs) and enhancer RNA [172-174]. Depletion of NEXT subunits RBM7 or ZCCHC8 increases the levels of long hTR precursors carrying at least a 50 nt extension past the mature 3' end as measured by qPCR, while there is no change on the levels of mature or short extended precursors of hTR by Northern blot analysis [163]. These results suggest that NEXT may primarily favor the degradation of long hTR precursors that are not processed into the 451 nt-long mature form (Figure 7A). Notably, the production of these long precursors of hTR must be a rare event, given that the majority of nascent hTR transcripts are not longer than 461 nt and are likely to be processed into the mature form, since the levels of nascent hTR only change mildly during the course of maturation [164].

More critical for hTR maturation is the antagonistic roles of the poly(A)-specific ribonuclease PARN and the TRAMP complex, which are also implicated in the maturation pathway of other H/ACA snoRNAs [175]. The TRAMP complex is an exosome adaptor specific to the nucleoli, which is formed by the RNA-binding protein ZCCHC7, the non-canonical poly(A) polymerase PAPD5 and once again the RNA helicase MTR4 [169]. On one hand, the polyadenylation of hTR precursors by the TRAMP complex (Figure 7B) can promote their degradation by the exosome (Figure 7C) [163, 164, 166]. On the other hand, PARN is able to deadenylate hTR precursors to prevent their degradation (Figure 7D) [163, 166, 167] and it also exhibits 3' trimming activity, which could complete the processing of hTR to the mature form (Figure 7E) [162]. Recombinant PARN process preferentially hTR precursors that are not longer than 455 nt, displaying reduced activity towards precursors that are 460 nt in length or longer due to the attenuation of PARN activity by the CGC trinucleotide from position 456 to 458 [162, 176-178]. Therefore, the initial processing of these longer precursors requires the exosome core nuclease RRP6, albeit is speculated that RRP6 may act in an exosome-independent manner [162]. Because RRP6 is found in both the nucleolus and nucleoplasm [179-181], while PARN localizes specifically in the nucleolus and in Cajal Bodies (CBs), which are membrane-less nuclear compartments enriched for splicing factors [175], it has been hypothesized that the replacement of RRP6 with PARN is likely to take place in the nucleolus (Figure 7E) [148]. Nevertheless, it is still possible that RRP6 processes directly long precursors into mature hTR (Figure 7F). Despite previous data showing that hTR biogenesis does not require nuclear export [182], unexpected aberrant localization of hTR to the cytoplasm has been reported after accumulation of hTR and/or processing defects induced by depletion of PARN or dyskerin [167].

Recently, the formation of a triple helix structure has been reported *in vitro*, formed by the tertiary interactions between the H-box, 5' hairpin and the 459-UUU-461 trinucleotide downstream the 3' of the mature hTR end [162]. This triple helix structure inhibits RRP6 activity and results in degradation of hTR precursors. The binding of the H/ACA complex to the H/ACA box of hTR is suggested to disrupt the triple helix, therefore allowing the initial processing of hTR precursors longer than 455 nt by RRP6 instead of degradation [162]. Additionally, it has been proposed that the H/ACA complex is defining the 3' end of mature hTR at position 451 by attenuating excessive hTR processing [162].

A parallel maturation pathway of hTR, independent of PAPD5 and PARN functions, has been recently proposed after analyzing data produced by 3' Rapid Amplification of cDNA End (3'-RACE) sequencing of purified nascent transcripts at different time points. One possible candidate responsible for this alternative pathway is TOE1, which is enriched at CBs and has been shown to share some deadenylation target RNAs with PARN, including scaRNA, snoRNA and hTR. Specifically, TOE1 shows deadenylation and 3' end processing activities towards hTR both *in vitro* and *in vivo*, acting mainly on short hTR precursors not longer than 455 nt (Figure 7G) [183, 184]. Notably, depletion of TOE1 does not significantly affect total hTR levels, unlike PARN deficiency. Furthermore, a decrease in telomerase activity upon TOE1 depletion in cells normally expressing PARN suggests that TOE1 possesses its unique function in telomerase regulation independently of PARN [183]. Nevertheless, other still unknown factors might be responsible for hTR precursors' maturation in the nucleoplasm or in the nucleolus in PAPD5/PARN double knockout cells [183].

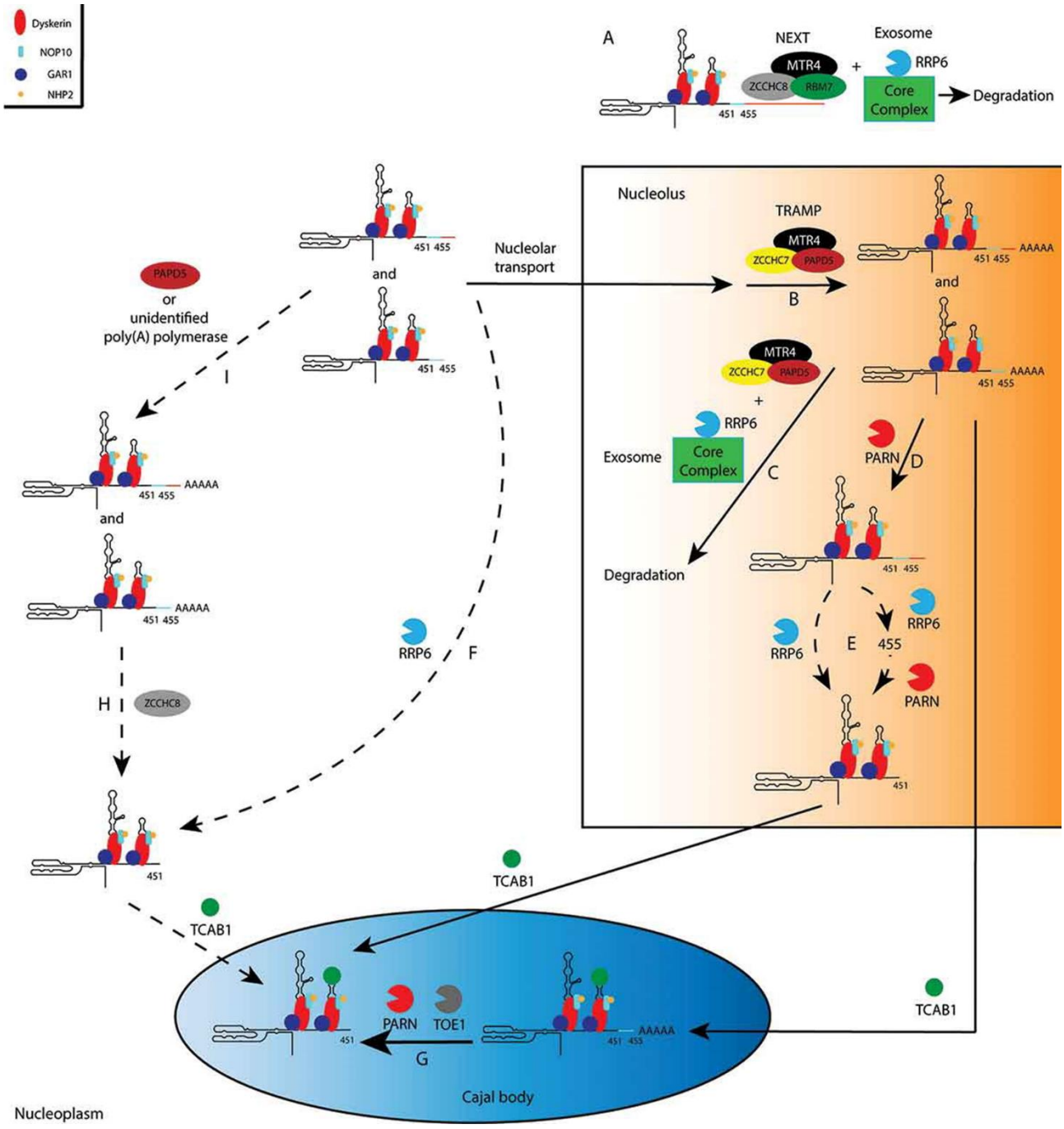

Figure 7: Comprehensive model of hTR 3' processing taken from Qin & Autexier 2020 [148]. Dashed arrows indicate speculated pathways that requires further investigation. For clarity, the steps prior the binding of the H/ACA complex, the cap hypermethylation and the assembly of hTR with hTERT are omitted. All the exosome components other than RRP6, including RRP40, are together referred to as the core complex. (A) In the nucleoplasm, long hTR precursors are degraded through NEXT-dependent recruitment of the exosome. (**B**, **C**) In the nucleolus, polyadenylation of hTR precursors by the TRAMP complex leads to degradation by the exosome. (**D**) PARN mediates deadenylation of hTR precursors. (**E**) Deadenylated hTR precursors from 456 to 461 nt in length are either directly processed into the mature form by RRP6, or first processed to 455 nt by RRP6, followed by subsequent trimming by PARN. (**F**) Nucleoplasmic RRP6 might also directly process non-adenylated hTR precursors into the mature form. (**G**) Residual poly(A) tail and 3' extension are removed by TOE1 and/or PARN in the Cajal body to complete hTR maturation. (**H**) ZCCHC8 might be involved in deadenylation and 3' processing of short hTR precursors no longer than 461 nt in the nucleoplasm. (**I**) Polyadenyation of nucleoplasmic hTR precursors by PAPD5 or an unidentified poly(A) polymerase. Either mature hTR resides in the nucleoplasm, or it is translocated to the Cajal body by TCAB1.

The nuclear poly(A) binding protein PABPN1 has already been shown to bind and promote degradation of polyadenylated RNA by recruiting the exosome [185-187]. Additionally, PABPN1 is part of the PAXT complex, formed by the stably interacting proteins MTR4 and the RNA-binding protein ZFC3H1, and the transiently interacting PABPN1 itself [168]. PABPN1 binds hTR species with longer poly(A) tails compared to those associated with hTERT or dyskerin [166]. Interestingly, PABPN1 depletion results in a reduction of total hTR levels and an increased amount of 3' extended precursors, suggesting that in the context of hTR biogenesis, PABPN1 promote hTR maturation instead of the exosome-mediated degradation of hTR precursors [166]. Because PABPN1 interacts with PARN in a RNA-independent manner, one possibility that explains the promoting role PABPN1 in hTR biogenesis is through its ability to recruit PARN to polyadenylated hTR precursors [166]. It has been speculated that a long poly(A) tail on hTR acts as a sensor towards degradation, and PABPN1 is preferentially recruited to hTR precursors with longer poly(A) tail to shift their fate towards maturation [148]. Nevertheless, due to the different localization of PABPN1, enriched in nuclear speckles [188], and PARN, predominantly localized in the nucleolus and CBs [175], it is still unclear in which nuclear compartment take places the PABPN1-mediated recruitment of PARN to hTR precursors.

Concerning hTR localization, fluorescence *in situ* hybridization (FISH) experiments show that hTR resides in CBs throughout most of the cell cycle [189, 190], which is in line with the CBs facilitating the recruitment of telomerase to telomeres [191, 192]. The binding of TCAB1 to the evolutionarily conserved CAB box sequence in the 3' hairpin loop of hTR (Figure 5 and Figure 6), which is also present in other H/ACA scaRNAs, is necessary for the localization of hTR to CBs [146, 190, 193]. Depletion of TCAB1 abolishes the localization of hTR in CBs without affecting hTR levels or telomerase assembly [193-195]. A recent study challenges this idea that hTR is predominantly localized in CBs taking advantage of hTR live cell imaging, which shows that only 5% to 10% of hTR is found in CBs in asynchronous cells [196]. Furthermore, the authors show that hTR is also transiently present in the nucleolus, which they interpret as processing of hTR precursors. The differences between the live cell imaging/high-sensitivity FISH they used, and conventional FISH methods could be a result of the extended residence time of hTR in CBs or the detection limits of conventional FISH [196]. The frequency of hTR and hTERT localization at telomeres peaks in mid-S-phase, indicative of telomerase recruitment to the telomeres. Previously, CBs have been found adjacent to hTR-containing telomere foci but not hTR-free telomeres, suggesting that CBs may be involved in transporting telomerase proximal to telomeres [192, 197]. Notably, hTR live cell-imaging shows that the recruitment of hTR to telomeres is not exclusively restricted to CBs, and the overexpression of hTERT further reduces the fraction of hTR in CBs [196]. Furthermore, the disruption of CBs formation through depletion of the structural protein Coilin, does not impair the telomere localization of hTR, supporting the non-essential role of CBs in transporting telomerase to telomeres [198].

Initially, it has been proposed that telomerase assembly took place in the nucleolus, facilitated by the peak in early S phase of both hTR and hTERT localization in this nuclear compartment [199]. In an alternative model, it is suggested that hTR assembles with hTERT in CBs [196, 197]. However, because TCAB1 depletion prevents hTR localization to CBs, but does not affect telomerase assembly, a CBs-independent pathway may take place [193, 194]. Two regions in hTR independently mediate the interaction with hTERT: the pseudoknot and the CR4/5 (Figure 6) [110, 200]. Both of them are required for maintaining telomerase activity [200], as well as the template region of hTR, which is required for synthesizing telomeric DNA repeats by reverse transcription.

Precursor snRNAs possess a 7-mono-methylguanosine (MMG) cap that recruits the cap-binding complex (CBC), the adaptor protein PHAX and the nuclear export factor CRM1 to facilitate translocation to the cytoplasm [201-203]. The CBC recruits the exosome to target RNAs through its interaction with the NEXT and PAXT complexes [168, 174]. Depletion of CBC components increases the percentage of mature hTR while decreasing the fraction of polyadenylated hTR [163]. These results can be explained by the ability CBC to inhibit PARN activity, similar to what was shown for mRNAs [204], towards polyadenylated hTR precursors [163]. During maturation, the MMG cap of snRNAs is hypermethylated by the full-length trimethylguanosine synthase 1 (TGS1) to a [2, 2, 7]-trimethylguanosine (TMG) cap, which promotes reimport of the snRNP into the nucleus [205].

Unlike snRNAs, PHAX directs MMG-capped C/D box snoRNA precursors into CBs, where their MMG cap is hypermethylated to TMG cap to mediate a CBC-independent recruitment of CRM1 to these C/D box snoRNAs. Those are then sequestered in CBs by TGS1, while CRM1 dissociates TGS1 and allows translocation of the RNPs into the nucleolus [182, 206]. In human, the interaction between nuclear transport/export and cap hypermethylation of H/ACA snoRNAs and scaRNAs, including hTR, is less clear compared to that of C/D box snoRNAs. Recently, it has been reported that TGS1 hypermethylates the cap of hTR [207]. Depletion of TGS1 results in accumulation of hTR into the cytosol. Nonetheless, the inhibition of CRM1 does not alter hTR distribution between the nucleus and the cytoplasm in both control cells and TGS1-depletead cells [207]; hence, the factors regulating hTR nuclear export upon TGS1 depletion remain unknown. Besides the aberrant localization phenotype upon TGS1 depletion, the total levels of hTR are increased, without altering the ratios of 3' extended and oligoadenylated hTR species. This is likely due to the separation of cytoplasmic hTR from the nuclear RNA deadenylation/processing and degradation machineries. The inhibition of CRM1 increases total hTR levels in control cells, but not in TGS1 depleted cells, suggesting that these two proteins act epistatically in regulating hTR levels through the intranuclear transport pathway [207]. Compared to control cells, TGS1 depleted cells show increased telomere length and increased detected telomerase activity. Additionally, because the majority of hTR molecules associated with hTERT do not contain the TMG cap, it is proposed that the hypermethylation of the hTR cap is dispensable for telomerase assembly and function [207].

Interestingly, a small RNA arising from nucleotide 425–447 of hTR, called hTR-sRNA, has been reported to associate with AGO2, one of the AGO proteins which is involved in microRNA-induced silencing of mRNAs [208]. hTR-sRNA can recruit AGO2 to hTR through base pairing, which is predicted to occur at two different locations, between positions 12–31 and positions 313–340 of hTR respectively. It has been shown that AGO2 enhances the hTR-hTERT interaction and increases telomerase activity without affecting hTR levels. Nevertheless, the biogenesis pathway of hTR-sRNA is still not well defined [209].

Besides its function in telomerase activity, two non-canonical roles of hTR have been identified. hTR has been found to translocate to the mitochondria, where it gets processed into a shorter form ranging from nucleotide 53 to nucleotide 247, and is subsequently exported to the cytoplasm, where it serves as an indicator of mitochondrial functions [210]. Additionally, an open reading frame (ORF) encoding for a small peptide is predicted to exist in vertebrate telomerase RNA, including hTR [211]. In human, the presence of this peptide, called hTERP, has been detected by Western blot, immunofluorescence and mass spectrometry in telomerase positive cells but not in the hTR-negative VA13 cells. Consistent with a reported telomerase-independent function of hTR that promotes cell survival [212], the overexpression of WT hTR confers resistance against drug-induced apoptosis, ability that is lost with overexpression of hTR mutants defective for hTERP production [211].

Telomere Biology Disorders (TBDs)

Critically short telomeres induce checkpoint activation, which leads to senescence or apoptosis. When these checkpoint responses are dysfunctional, telomeres shorten further and become unprotected. Unprotected telomeres induce the so-called “crisis” state, which is characterized by genome instability and have the potential to result in cell death or cellular transformation. In human cells, the progressive telomere shortening that occurs with each cell division contributes to aging and age-related ailments [213]. Germline defects that leads to accelerated telomere shortening and/or telomere instability can be the cause of a set of rare and heterogeneous Mendelian diseases called telomeropathies or Telomere Biology Disorders (TBDs). These diseases manifest with a broad array of clinical features that involve mainly high-proliferating tissues, such as the hematopoietic system and different epithelia, and generally sensitize other tissue, like liver and lungs, to environmental stress factors like smoking, high-fat diet and elevated alcohol consumption. TBDs include dyskeratosis congenita (DC), pulmonary fibrosis (PF), Høyeraal-Hreidarsson syndrome, Coats plus syndrome and Revesz syndrome [214, 215].

To date, there are seventeen genes recognized as causative of various TBDs in human, with many others proposed to be associated with TBDs, but whose link to them is not well understood [216]. Unsurprisingly, all these seventeen genes, summarized in Table 1, are involved in telomerase function and telomere maintenance. The first gene reported as genetic cause of a TBD was DKC1, which was identified in a patient affected by dyskeratosis congenita in 1998 [217]. The common feature shared between most of these different diseases is telomere shortening, which is used as a diagnostic marker thanks to telomere length measurement mainly performed by flow cytometry and fluorescence *in situ* hybridization (flow-FISH) analysis of blood leukocytes [218]. Adult-onset of TBDs is often associated with telomere length between the first to the tenth percentile range for age, while pediatric-onset presentation of TBDs are associated with telomeres well below the first percentile for age [219].

Gene	Function	Genetic status	Telomere length
TERT	Catalytic subunit of telomerase	Mono and Bi-allelic	Reduced
TERC (hTR)	Telomerase RNA providing the template	Mono and Bi-allelic	Reduced
DKC1 (Dyskerin)	hTR biogenesis	X-linked	Reduced
NOP10	hTR biogenesis	Mono and Bi-allelic	Reduced
NHP2	hTR biogenesis	Mono and Bi-allelic	Reduced
WRAP53 (TCAB1)	hTR biogenesis	Bi-allelic	Reduced
PARN	hTR biogenesis	Mono and Bi-allelic	Mostly Reduced
ZCCHC8	hTR biogenesis	Mono-allelic	Reduced
NAF1	hTR biogenesis	Mono-allelic	Reduced
TINF2 (TIN2)	Shelterin component	Mono-allelic (de novo)	Reduced
ACD (TPP1)	Shelterin component	Mono and Bi-allelic	Reduced
POT1	Shelterin component	Mono and Bi-allelic	Elongated (bi-allelic) and reduced (mono-allelic)
RTEL1	Accessory factor for telomeres’ replication	Mono and Bi-allelic	Not consistently reduced
RPA1	Accessory factor for telomeres’ replication	Mono-allelic	Reduced
DCLRE1B (Apollo)	Accessory factor for 3’ overhang regulation	Bi-allelic	Normal
CTC1	Accessory factor for 3’ overhang regulation	Bi-allelic	Not consistently reduced
STN1	Accessory factor for 3’ overhang regulation	Bi-allelic	Not consistently reduced

Table 1: Summary of the seventeen TBDs-causative genes, with indicated function in telomere biology, genetic status and global telomere length. Table adapted from P. Revy et al. 2022 [216].

TBDs display multiple models of genetic inheritance, as well as variable expressivity and incomplete penetrance [219]. Of the seventeen genes listed here, DKC1 is the only X-linked one that causes X-linked recessive diseases. Four of these genes show an autosomal recessive inheritance of TBDs: CTC1, STN1, WRAP53 and DCLREB1B. For those, carriers of mono-allelic variants are usually asymptomatic. TINF2 variants are mostly *de novo* mutation and strictly mono-allelic. The other eleven genes display autosomal dominant inheritance, where heterozygous pathogenic variants are able to cause manifestations of premature ageing. The presence of bi-allelic variants, as well as a combination of more than one distinct mono-allelic variant of these genes, results in early-onset and more severe TBDs symptoms [216]. Individuals carrying mutations in TBD-causing genes that affect telomere maintenance can transmit to their progeny not only the deleterious variant, but also short telomeres. This event can translate into progressive telomere shortening, earlier-onset and greater extent of clinical manifestations over successive generations, a phenomenon known as “genetic anticipation” [216]. Five of the seventeen genes reported in Table 1 shows genetic anticipation: TERC, TERT, PARN, RTEL1 and POT1 [220-226].

Thanks to seminal studies conducted in mice carrying the heterozygous Terc and Tert knockouts, it is known that short telomeres and the associated premature-ageing phenotypes are transmitted to the progeny even when those possess a wild-type genotype [227, 228]. The phenomenon where a phenotype, in this case short telomeres and/or premature ageing, dissociates from the genotype is called “phenocopy”. Phenocopying has been observed in families with TBDs, in which individuals having a wild-type genotype, inherited short telomeres from a parent and exhibited TBD-related symptoms [229-232]. Notably, in families with TBDs, telomeres recover to a normal length after two successive generations of individuals with wild-type genotypes [223].

It is well established that in humans somatic point mutations accumulate over time, with a frequency of ~20 mutations per cell per year, specifically in the hematopoietic compartment. This phenomenon give rise to the so-called age-related clonal hematopoiesis (ARCH) in healthy older individuals (also known as clonal hematopoiesis of indeterminate potential; CHIP) [233-235]. In the context of a Mendelian disease, a spontaneous genetic mutation can induce a ‘genetic rescue’. Somatic Genetic Rescue (SGR) is defined as a somatic genetic mutation that specifically counteracts the deleterious effects of a germline variant at the cellular level and confers a selective advantage over non-mutated cells, leading to somatic mosaicism due to expansion of the SGR-positive cells [236]. Recent studies suggest that SGR events are particularly frequent in the hematopoietic system of patients with a TBD [237-245]. Since somatic mutations and chromosomal alterations accumulate over time in hematopoietic cells of normal individuals, it is not surprising that SGR is more frequent in patients with TBDs that develop in adulthood (e.g. pulmonary fibrosis and liver diseases) than in young patients with early-onset of dyskeratosis congenita or Høyeraal–Hreidarsson syndrome [234, 235, 241]. Recently, longitudinal studies demonstrated that, at least in some cases, the SGR could be associated with delayed onset of clinical manifestations, blood count improvement, telomere length stabilization, and reduced frequency of both myelodysplastic syndrome and acute myeloid leukemia development, suggesting a protective potential for SGR events in these patients [239, 245]. Finally, since several organs are affected by TBDs, it is possible that SGR-positive cells could emerge also in tissues with high renewal potential other than the blood, such as liver, the skin and gut [216].

We refer to direct SGR when a somatic genetic event modifies the same germline-mutated gene. This includes either modifications that correct the germline mutation by uniparental isodisomy, replacing the mutated allele with another copy of the WT allele from the sister chromosome, or point mutations that revert the germline variant to the wild-type sequence (back mutation), which has been observed for loss-of-function variants of DKC1 and TERC [243, 244]. Alternatively, direct SGR can also occur by inactivation of a gain-of-function or dominant negative germline variant via different possible mechanisms [246].

Conversely, we refer to indirect SGR when the occurring somatic genetic event does not modify the germline-mutated gene itself, but rather a gene that participates in the same pathway affected by the germline mutation, providing a selective advantage to the mutated cells [246]. To date, indirect SGR has been identified only in a few Mendelian disorders [237, 241, 242, 245, 247, 248]. An example of indirect SGR in the context of TBDs corresponds to TERT-promoter activating-mutations in patients who carry pathogenic germline variants not in TERT but in TERC, NAF1, NHP2, PARN or CTC1 [237, 241, 242, 245].

G-quadruplexes (G4)

When a DNA or an RNA molecule possesses a minimum of four stretches containing at least three guanines each, it is prone to guanine quadruplex (G4) formation. Structurally, the base of a G-quadruplex is a planar tetrad in which four guanine bases interact through Hoogsteen base pairing, with a monovalent metal cation positioned at the center of the tetrad (Figure 8). The stacking of multiple tetrads on top of each other adds structural stability and results in the tri-dimensional structure that is referred to as G4 [249]. G4s can assume different structural topologies and mix with other nucleic acid structural elements like helices, loops and bulges [250, 251]. When all the guanines interacting in a G4 belong to a single strand, this structure is called “intramolecular” G4. Conversely, an “intermolecular” G4 is formed when two or more different strands are involved [252]. G4s are classified as “parallel” if the strands forming them are all oriented in the same direction (4↓ or ↑). On the opposite, “antiparallel” G4s derive from strands directed in different orientations (2↓ + 2↑). “Antiparallel” G4s can be arranged as a basket or chair-type configurations depending on the loops’ position. Furthermore, when the structure is formed by one antiparallel strand and three parallel strands, the G4 is defined as a “hybrid” (3↓ + 1↑ or 3↑ + 1↓) (Figure 8) [250-252].

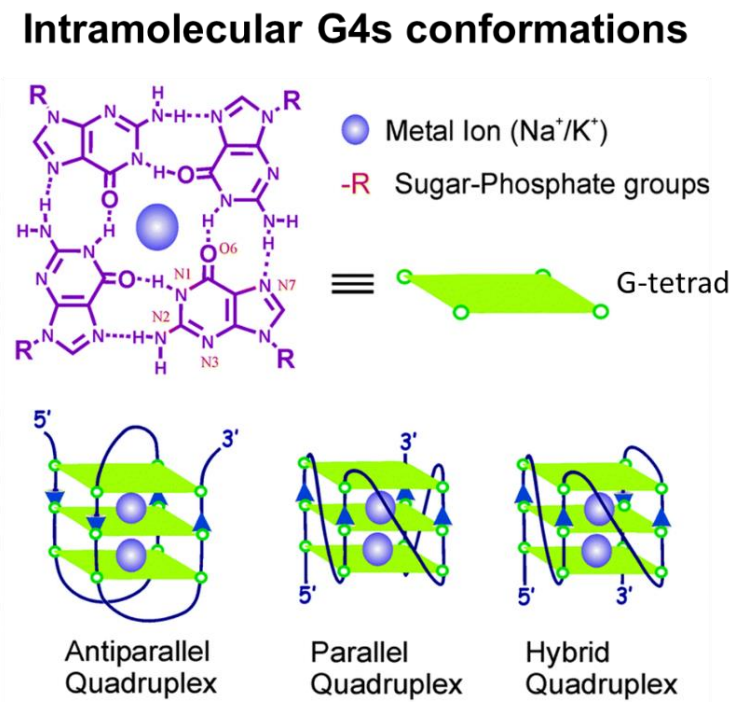

Figure 8: Schematic showing the structures of a G-tetrad and the three different folding topologies found in G-quadruplexes. Image adapted from Bhasikuttan and Mohanty 2015 [253].

By the end of the twentieth century, DNA G4s sequences were identified at gene promoter regions [254], and at telomeres in eukaryotic chromosomes [255]. The research on RNA G4s is more recent, but it is now well established that RNA G4s and G4s formed in the context of RNA-DNA hybrids are involved in regulating multiple chromosome functions [256-259]. Altogether, G4s have been shown to be involved in regulating transcription, translation and splicing of multiple genes, as well as gene product localization [260].

DHX36 (DDX36, RHAU, G4R1)

Human cells utilize multiple helicases to resolve the G4 structures in both DNA and RNA. The most characterized dual DNA/RNA G4 helicases are DHX36 (alias RHAU, G4R1), DDX21, and DHX9 [261-263]. RHAU was identified back in 2004 by the Nagamine's laboratory, when they characterized a new AU-Rich Element (ARE)-binding protein that was associated with the ARE fragment of the urokinase plasminogen activator mRNA [264]. The protein was named RNA Helicase associated with AU-rich elements (RHAU) and it was found to promote the degradation of mRNAs containing the ARE sequence [264]. Through careful analysis of the protein sequence of RHAU, it was found to possess identical amino acid composition with the ATP-dependent DEAD/DEAH-box helicase 36 (DDX36 or DHX36) [265]. In 2005, it was discovered that RHAU possessed DNA G4 resolving activity and was able to bind and unwind DNA G4 structure, granting it the additional name of G4 Resolvase 1 (G4R1) [266]. Few years later, the G4 resolvase activity of this helicase was extended to RNA molecule through *in vitro* biochemical analysis in HeLa cell lysates [263]. For consistency, from now on this protein is going to be referred to as DHX36 within this thesis. As already stated, DHX36 belongs to the DEAH-box helicase family. DEAH-box RNA helicases have a core component consisting of 2 RecA-like domains that are flanked by the N-terminal domain and the C-terminal domain (Figure 9A) [267, 268].

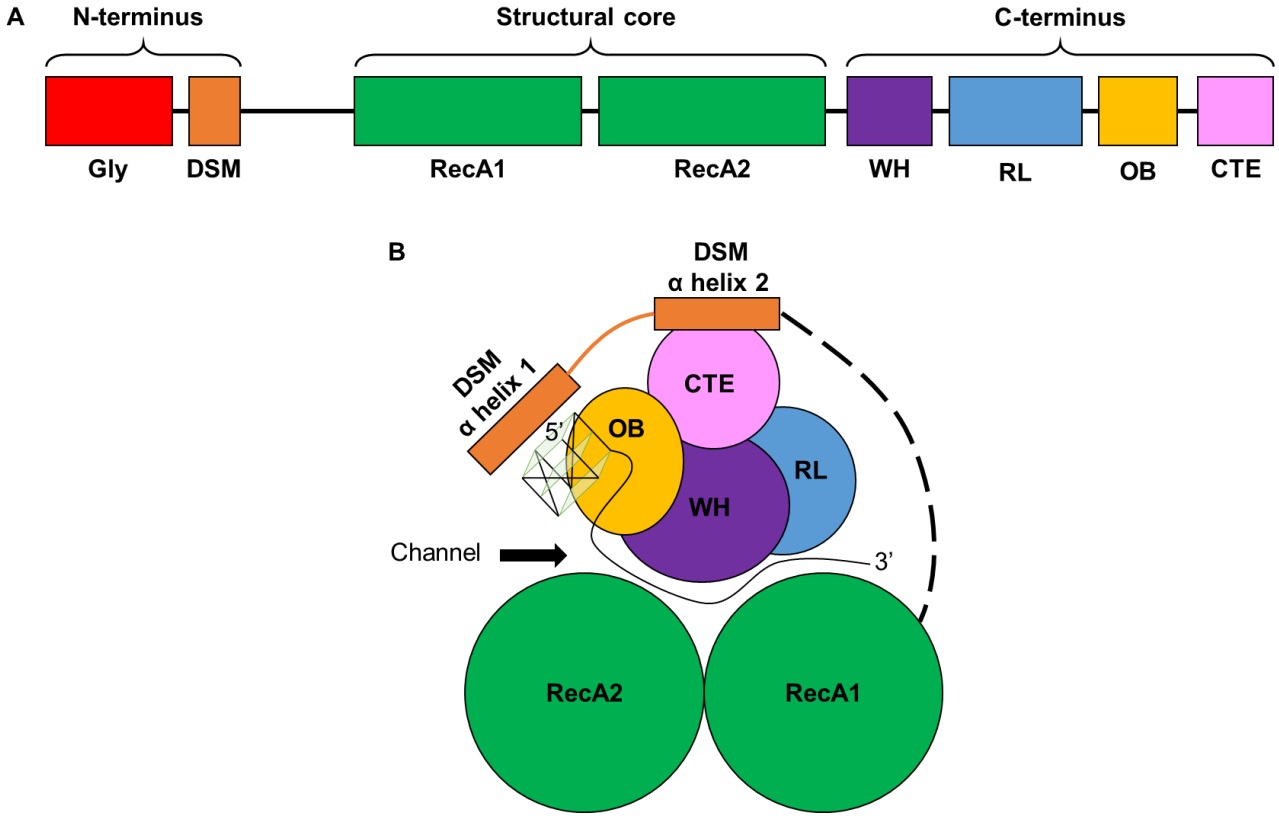

Figure 9: Schematic showing the domains and structural regions of DHX36. (**A**) The domains of DHX36: the N-terminal domain, structural core, and the C-terminal domain. (**B**) Geometric representation of the complex of RHAU bound to a single stranded nucleic acid molecule folded into a G4. CTE: constitutive transport element. OB: oligosaccharide-binding-fold-like. RL: ratchet-like. DSM: DHX36-specific motif. WH: degenerate-winged-helix.

RecA-like structural domains possess ATPase activity to move macromolecules or move along macromolecules, either peptides or nucleic acids [269]. Proteins carrying the RecA-like domains are thus called motor ATPase. At the N-terminus of DHX36, there is a glycine-rich element (Gly) followed by a DHX36-specific motif (DSM) [270]. More in detail, RSM contains two α-helixes that are essential for the G4s-binding of DHX36 [271] (Figure 9B). The C-terminal domain of DHX36 protein contains four subdomains: a degenerate-winged-helix (WH), a ratchet-like (RL), an oligonucleotide and oligosaccharide-binding-fold-like (OB) and a constitutive transport element (CTE) (Figure 9) [270].

As DHX36 binds to G4s, the RecA1, RecA2, and the C-terminal domains create a conformation known as a trefoil (Figure 9B). The two α-helixes of the DSM domain are connected to the RecA1 domain of the trefoil through a random sequence, and its N-terminal α-helix contacts the 5′ (top) face of the bound G4 [267]. The “trefoil” structure possesses a channel that facilitates the pass-through of the 3′-end single strand of G4 (Figure 9B) [267]. DHX36 unwinds G4 structures by pulling one by one the nucleotide residues towards the 3′ to 5′ direction through the aforementioned channel. Such activity is achieved by the C-terminal RecA-like domain via ATP hydrolysis [267, 272].

DHX36 interacts with a variety of DNA and RNA molecules primarily in a G4-dependent manner, regulating multiple biological processes. It has been shown that DHX36 is involved in the regulation of gene transcription, mRNAs translation, mRNA degradations, and complex interactions with noncoding RNAs [273]. DHX36 can regulates gene expression via its DNA-G4 resolvase activity on G4-prone gene promoters. One example is the gene Yin Yang 1 (YY1), which was found to form dG4s in its gene promoter region, as well as rG4s in the 5′-UTR of its own mRNA. These G4 structures modulated the expression of a chimeric YY1/luciferase construct. Further analysis showed that DHX36 can bind to the G4 sequence of the YY1 promoter *in vitro*, and overexpression of DHX36 increased endogenous YY1 levels [274].

DHX36 is also important for post-transcriptional regulation of mRNAs. Recently, more than 4500 mRNAs with G4-forming and G-rich sequences were shown to preferentially interact with DHX36 in human cell [275, 276]. Deletion of DHX36 caused a significant increase in target mRNAs level with reduced protein output, suggesting that DHX36 directed mRNA degradation and translation [277]. Those mRNAs harboring G4-forming sequences were found to be enriched in stress granules (SG), and DHX36 knockout (KO) resulted in increased stress granule formation and phosphorylation of the protein kinase R (PKR), a cellular stress response marker. DHX36 KO cells also displayed other cellular stress characteristic, such as morphological changes and reduced cell proliferation, suggesting that DHX36 is involved in the alleviation of G4-induced cell stress [278].

During DDR, like after UV treatment, pre-mRNA 3′-end processing and polyadenylation is usually inhibited, consequently impairing protein production [279]. DHX36 specifically recognizes and unwinds the rG4 in the p53 mRNA precursor, which is necessary to sustain its 3′-end processing. Mutations that prevents rG4 formation in the p53 mRNA precursor suppressed the ability of DHX36 to sustain pre-mRNA 3′-end processing. Therefore, it was proposed that DHX36 acts as a compensatory mechanism, safeguarding p53 mRNA precursor processing and its subsequent translation after UV damage [280].

DHX36 can also associate with non-coding RNA to regulate different biological processes [273]. Long non-coding RNAs (lncRNAs) are often dysregulated in multiple human cancers [281, 282]. For instance, the lncRNA FLJ39051, also known as G-quadruplex-forming SEquence Containing-lncRNA (GSEC), is a lncRNA upregulated in colorectal cancer that is bound by DHX36 through its G4 forming sequence. GSEC suppresses the resolvase activity of DHX36 by depleting the free pool of DHX36 within the cell. The downregulation of GSEC rescued DHX36 activity and showed reduced colon cancer cells migration [283].

Interestingly, DHX36 binding to RNAs is not exclusively G4-dependent. Recent studies have found that DHX36 is able to immunoprecipitate the noncoding RNA BC200 (BCYRN1) [284, 285]. Despite BC200 being unable to form G4, therefore also not interacting with the G4 binding motif of DHX36, it showed direct affinity for DHX36 *in vitro*. It was discovered that the adenosine-rich region at the 3′-end of BC200 binds to the C-terminal region of DHX36, while the cytosine-rich region at the 3′-end of BC200 is necessary for association with unwound G4-prone sequences. This study provides a possible regulatory pathway in which DHX36 utilizes BC200 to modulate G4-prone RNA or DNA sequences [286].

The RNA helicases DDX1, DDX21 and DHX36 can assemble into a complex that acts as viral sensor to detect the invasion of viruses in myeloid dendritic cells. Subsequently, the recruitment of the adaptor molecule TRIF triggers the type I interferon (IFN) and cytokine responses that suppress the viral infection [287, 288]. Additionally, it has been shown that DHX36 forms a complex with dsRNA-dependent protein kinase (PKR) that sense dsRNA in the cytoplasm. In such complex, DHX36 assists in dsRNA binding and PKR phosphorylation that activates RIG-I, triggering once again antiviral IFN responses. DHX36 KO reduced IFN secretion and abolished the ability to resist RNA virus infections [278].

As most relevant to the topics of this thesis, DHX36 binds through its RSM domain to the G4 structure at the 5′ terminal region of TERC [143, 289, 290] and associated with the telomerase holoenzyme [289]. It has been proposed that DHX36 could resolves these obstructive rG4s at the 5’ end of hTR, promoting the now untwisted sequence to form a stable P1 helix. Additionally, DHX36 KO resulted in a decrease in average telomere length [289].

hnRNP H1

Proteins that bind to mRNAs during their maturation are often involved in controlling the expression of such genes. The heterogeneous nuclear ribonucleoproteins (hnRNPs) are a group of pre-mRNA binding proteins where about 30 members have been identified [291]. The hnRNPs harbor multiples modular structure with RNA-binding motifs, named ‘‘RNA recognition motifs’’ (RRM) and auxiliary domains (AUX) containing an unusual distributions of amino acid [291]. The RRM domains bind RNA, while the auxiliary domains are predicted to possess various functions including annealing of RNA, RNA splicing, nuclear localization and protein–protein interactions [292].

A subgroup of hnRNPs includes hnRNP F [293], hnRNP H/HV [294] and the hnRNP 2H9 family, which in itself consist of at least six proteins formed by alternative splicing [295, 296]. These proteins are characterized by a special structure of the RRM domains that have been named quasi-RRM (qRRM) domains (Figure 10) [294]. These qRRM domains possess a special nucleotides binding preference biased towards the sequence GGGA, which can be found in exonic as well as intronic sequences in various pre-mRNAs. Furthermore, the intensive study of hnRNPs F and H/HV proteins revealed their fundamental role in controlling gene expression of specific genes [297-301]. Members of the hnRNP F/H subgroup comprises hnRNP F, H1, H2, H3, and G-rich sequence factor 1 (GRSF1). The amino acid sequence of hnRNP H1 is 96% and 68% identical to hnRNP H2 and hnRNP F, respectively (Figure 10) [302, 303].

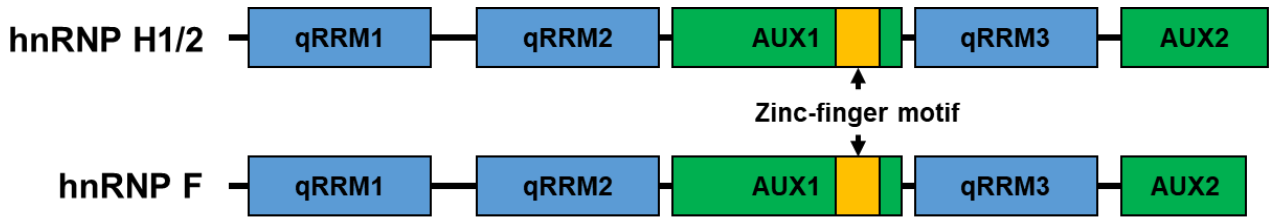

Figure 10: Simplified schematic showing the domains’ architecture of hnRNP H1/2 and hnRNP F.

As discussed above, these hnRNP F/H proteins bind specifically to G-rich RNA sequences, which are intrinsically prone to fold into rG4 structures. In 2011, A. Decorsière et al. demonstrated that hnRNP F/H binds a region in the 3′ end of p53 pre-mRNA that folds into an rG4. Furthermore, they showed that after DNA damage induction by UV treatment, as well as after ligand-mediated G4 stabilization, the interaction between p53 pre-mRNA and hnRNP F/H was increased. This interaction contributes to p53 protein accumulation after DNA damage, counteracting the global repression in mRNA synthesis [304].

Our interest in the hnRNP F/H proteins arose after the findings of C.Xu et al. in 2019, where they showed that hnRNP F/H can associate with hTR and telomerase holoenzyme, modulating telomerase function and promoting cell proliferation [305]. They identified three qRRM domains present in each member of the hnRNP F/H proteins (Figure 10), with the domain closest to the N-terminus of the protein (qRRM1) being the most critical for interaction with hTR [305]. Furthermore, they showed that the minimum 5' truncation of hTR able to bind hnRNP F/H includes the first three guanines stretches contained between position 1 and 18, and that the very first guanines stretch (position 1 to 3) is the most important for the interaction of hTR with hnRNP F/H [305]. Interestingly, conversely to what has been shown for p53 pre-mRNA [304], C.Xu et al. reported that hnRNP F/H preferentially bind the 5' end of hTR when it is in an unwound state, rather than folded into a rG4 structure. This led the authors to propose that the binding of hnRNP F/H prevents G4 formation and promotes formation of the P1 helix [305]. Taken together, these findings imply that the bias of hnRNP F/H towards binding a G-rich RNA folded into a rG4 structure rather than in a linear state, or vice-versa, may be a gene-specific feature.

Results

The aim of my thesis is unveiling the molecular mechanism underlying the telomere shortening observed in TBDs associated with mutations within hTR. Mutations across the whole length of hTR have been found in patients affected by different TBDs [306]. Mutations that interfere with the highly conserved structural folding of hTR are likely to affect the interaction with its binding partners, resulting in alteration of the stability of the RNA and/or functionality of the telomerase RNP complex. Mutations in the template region of hTR may lead to the incorporation of aberrant telomeric repeats into telomeres, which could affect Shelterin binding and lead to telomere de-protection. Interestingly, the 5'-terminal region of hTR is dispensable to reconstitute an active telomerase complex *in vitro* [307]. Furthermore, in mouse there are only few nucleotides past the template sequence [307], suggesting that this region is not critical for neither the stability, nor the activity of telomerase. Nevertheless, mutations in this region have been associated with TBDs [306]. In the last decades, different laboratories have identified multiple binding partners of hTR that interact with its 5'-terminal region. These interactions are mediated either through the cap structure of hTR, as in the case of CBC [163], or through interaction with the multiple G-stretches present in this region. Furthermore, a distinction can be made between proteins that bind when this region is folded into an rG4, like is the case for the helicase DHX36 [143, 289, 290], or when this region is unwound, like for the binding of hnRNPH/F proteins [305]. Interfering with the interaction between those proteins and hTR has showed a significant effect in both the stability of this RNA and the activity of telomerase [143, 289, 290, 305]. These findings suggest that, besides the initial observations, at least in human the 5'-terminal region of hTR constitute an additional layer of complexity in the already highly regulated processes of hTR stabilization and telomerase activity.

In my doctoral studies, I focused in examining the effect in stability and telomerase activity of specific mutations of hTR located either in the template region or in the rG4-prone 5' terminal region of this RNA, as well as the contribution of DHX36 and hnRNP H1 to telomerase activity.

Telomerase modulating activity of the 5'-end of hTR

In this first part of the Results section, the focus is the role of DHX36 and hnRNP H1 in hTR biogenesis and modulation of telomerase activity, as well as the characterization of two disease-related mutations, the transversions G2C and G11T [308, 309], which fall into the 5' terminal region of hTR.

Depletion of DHX36 decreases telomerase activity

To test if DHX36 was involved in hTR biogenesis, a DHX36 KO line of HEK-293T cells and its respective Parental line, both gifted to us by Kathrin Paeshke's laboratory, were used in the following experiments. Performing qPCR, we were able to distinguish between the signal of hTR precursor molecules from the total level of hTR, thanks to different primer pairs that fall respectively within the mature sequence of hTR (Total hTR) or flanking the mature end of hTR at position +451 nt (Precursor hTR). hTR levels for both Total hTR or Precursor hTR are only slightly increased (≈1,5 fold) in the absence of DHX36 (Figure 11), suggesting that DHX36 has only a minor role in either the biogenesis or the degradation pathway of hTR.

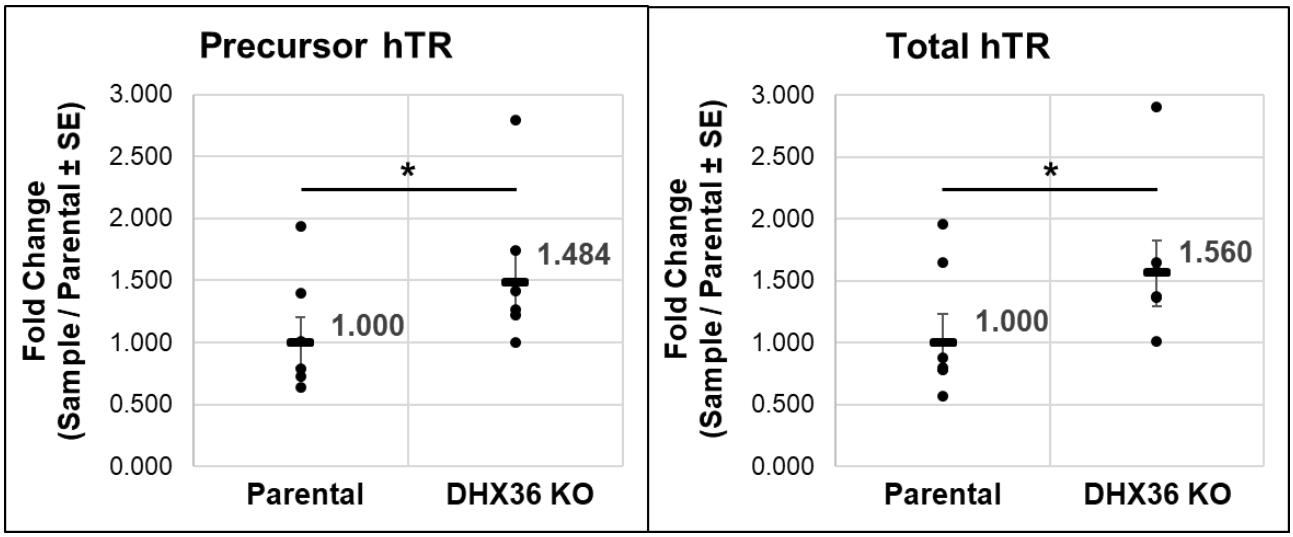

Figure 11: qPCR analysis of hTR levels in HEK-293T Parental or DHX36 KO cells. n = 6 biological replicates. Statistical analysis = T.test, *** =** p-value < 0.5

To understand whether DHX36 was required for telomerase function, DTAAs were done using whole cell extract made from HEK-293T cells, either parental or DHX36 KO, where TERT and hTR were transiently overexpressed. At first, a qPCR analysis was conducted to confirm a successful overexpression of both hTR and hTERT, which is necessary to perform DTAA. In Figure 12 is shown that both hTR and TERT mRNA levels are considerably increased after overexpression.

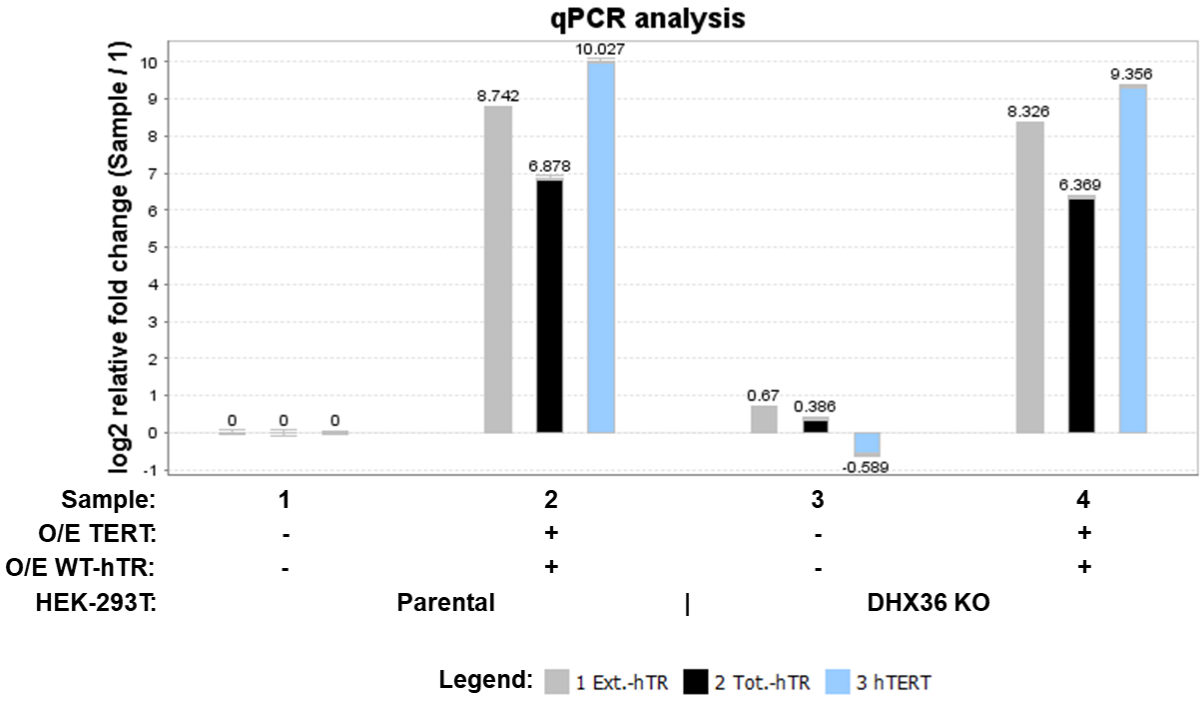

Figure 12: qPCR analysis showing the successful overexpression of hTR and TERT mRNA in both Parental and DHX36 KO cells. Error bars: standard deviation between 3 technical replicates.

As shown in Figure 13, the absence of DHX36 resulted in a decrease to about half of the activity, measured as total products accumulation, compared to the parental cells, suggesting that DHX36 is required to achieve optimal telomerase activity. As expected, an increase in the amount of extract used for the assay resulted in increased signal detected (Figure 13B), confirming the reliability of the assay. Interestingly, a doubling in the amount of extract did not resulted in a doubling of the signal.

A possible explanation for this is the proximity to saturation of the telomerase complex within the reaction, where the amount of active telomerase present in the less concentrated samples is sufficient to carry out the majority of the repeat additions. Another possibility is the oversaturation of the more intense bands on the gels, which can result in an imperfect quantification of the signal.

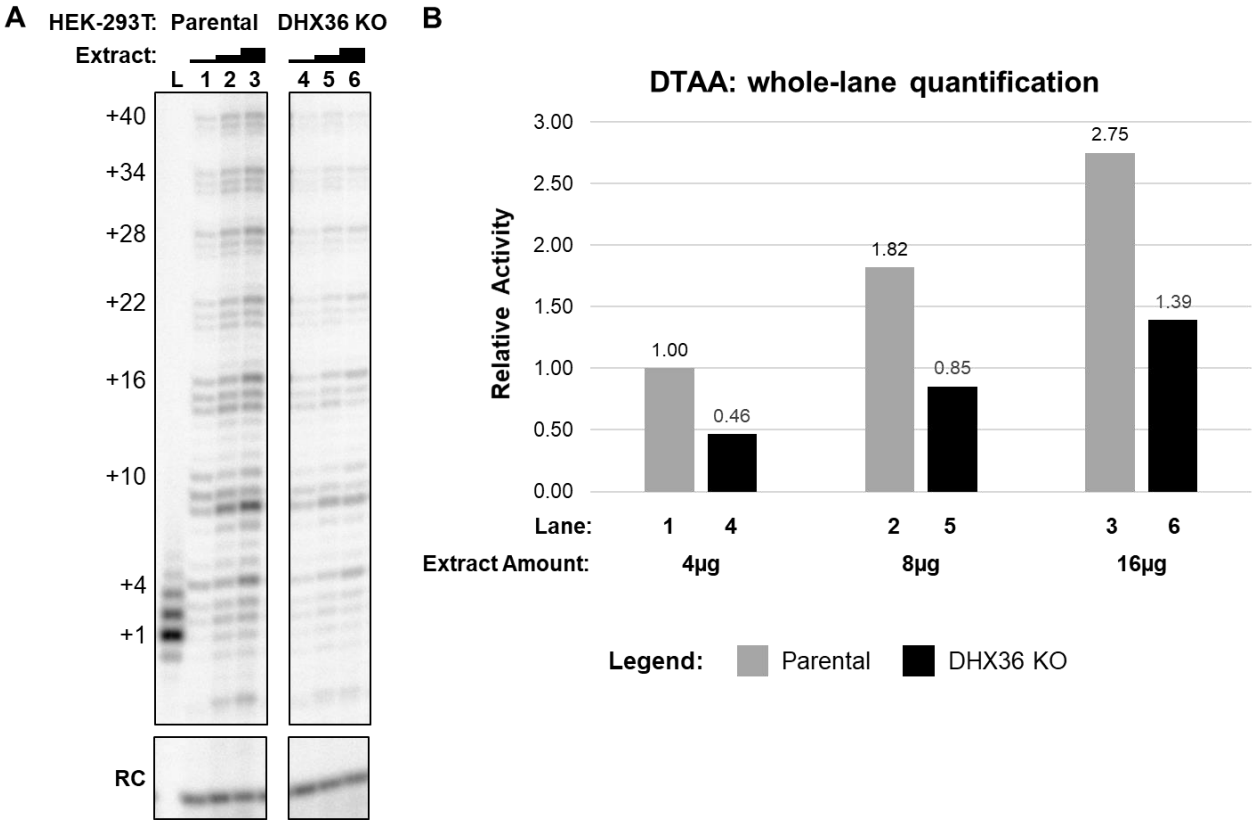

Figure 13: (**A**) Sequencing gel showing the amplification products of increasing amounts of cell extract for HEK-293T cells, either Parental or DHX36 KO. L = Ladder, RC = Recovery Control (**B**) Quantification of the intensity for a whole lane of the gel shown in **A**, normalized over RC signal.

A rescue experiment was done to confirm that the previous result was a direct consequence of DHX36 depletion (Figure 14). Transient overexpression of DHX36 was performed in both HEK-293T cell lines, either parental or DHX36 KO (Figure 14A), together with TERT and hTR. Those cells were used to make the extract utilized in the following DTAAs. Surprisingly, the overexpression of DHX36 did not change the product accumulation detected for both Parental cells (Figure 14B and 14C, compare lanes 3 and 1) and DHX36 KO cells (Figure 14B and 14C, compare lanes 4 and 2). This could suggests that the decrease in telomerase activity observed previously was not a direct consequence of DHX36 depletion. An alternative explanation is that the technical timeframe of the experiment does not allow DHX36 to perform its putative promoting function on telomerase activity. Additionally, the overexpression of hTR and TERT may result in an excess of telomerase complexes that do not associate with DHX36, resulting in no change in detected activity using an *in vitro* system like DTAA.

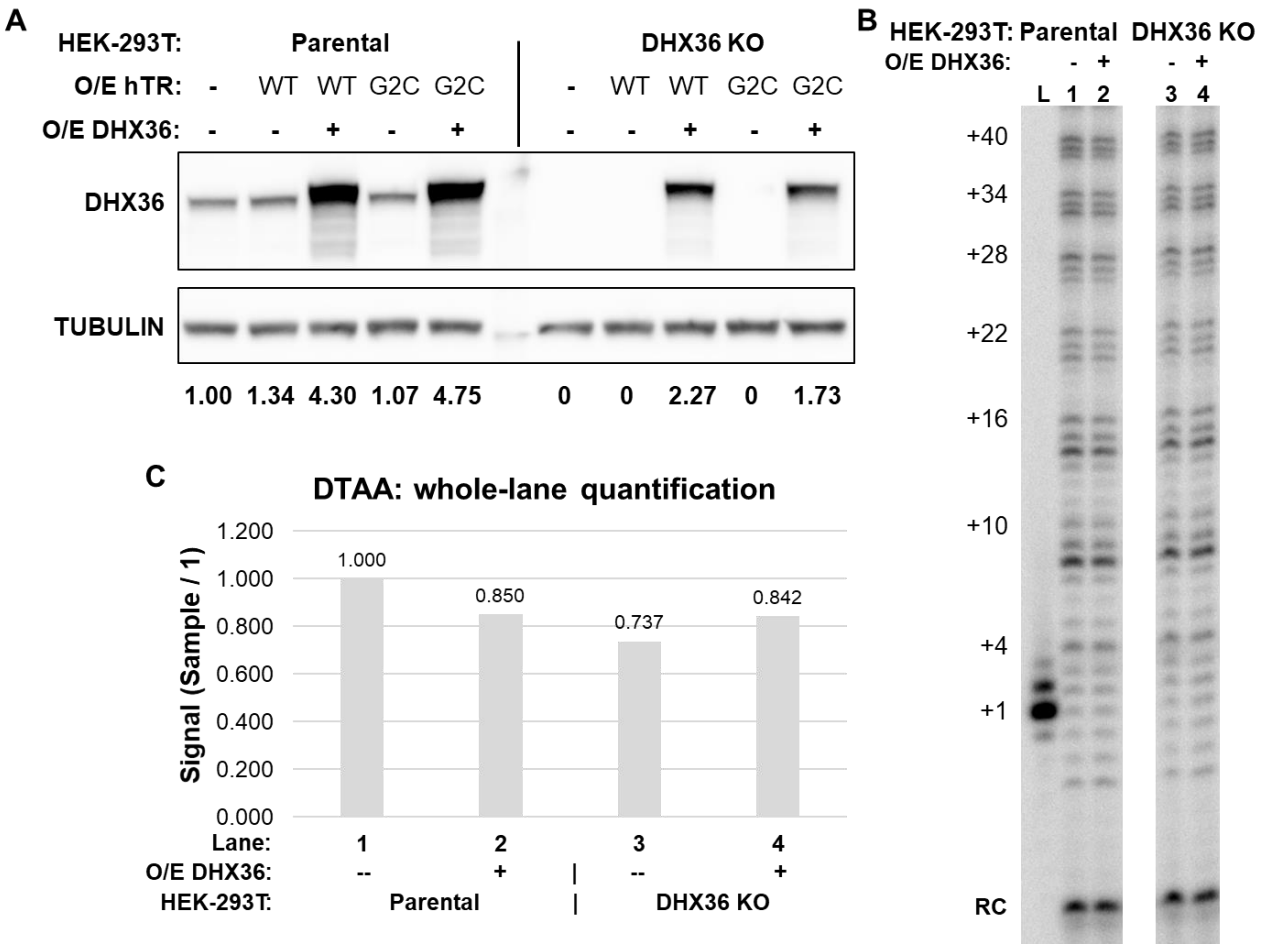

Figure 14: (**A**) Western Blot confirming the overexpression of DHX36. On the bottom, quantification of DHX36 signal compared to un-transfected Parental cells (first lane), normalized over TUBULIN signal. (**B**) Sequencing gel showing the amplification products of cell extract for HEK-293T cells, either Parental or DHX36 KO, subjected to overexpression of DHX36. L = Ladder, RC = Recovery Control (**C**) Quantification of the intensity for a whole lane of the gel shown in **B**, normalized over RC signal.

PF-related mutant G2C-hTR displays reduced telomerase activity

Marrone et al. 2012 reported that a patient affected by Pulmonary Fibrosis was carrying the G2C mutation on the hTR gene [308]. DHX36 is able to bind hTR via the rG4 formed at its 5'-end and unwinds it through its helicase activity [143, 289, 290]. To assess the telomerase activity of the G2C-hTR mutant and the involvement of DHX36, DTAAs were performed. The whole cell extract used for the assay was made from HEK-293T cells, parental or DHX36 KO, where TERT and either WT or G2C-hTR were transiently overexpressed. The rescue condition with overexpression of DHX36 was added to check for possible differences in the effect of DHX36 between WT-hTR and G2C-hTR expressing cells. Similar levels of WT and G2C-hTR were detected in both cell lines by qPCR, suggesting that G2C-hTR does not show major instability compared to WT-hTR (Figure 15A). Successful overexpression of hTR, TERT and DHX36 was confirmed by both qPCR (Figure 15A) and western blot (Figure 15B) before proceeding with DTAAs.

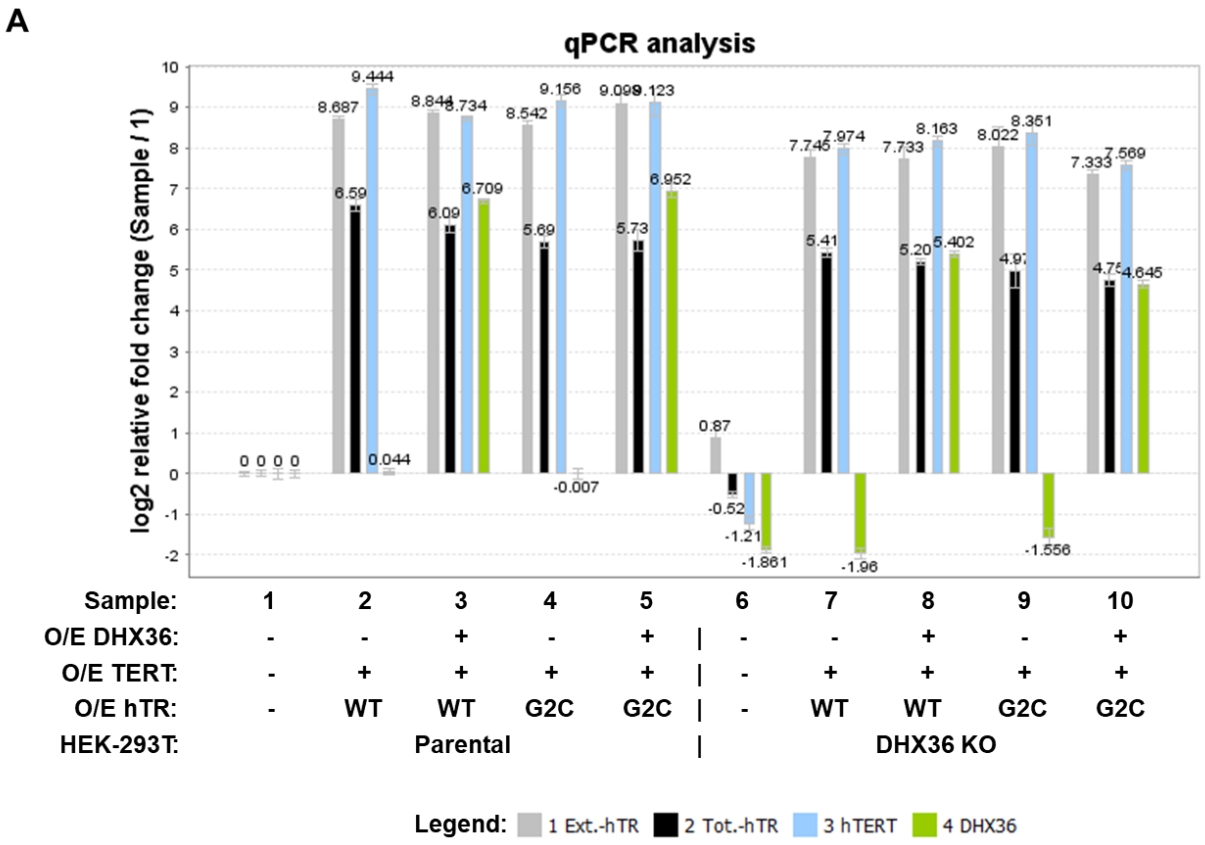

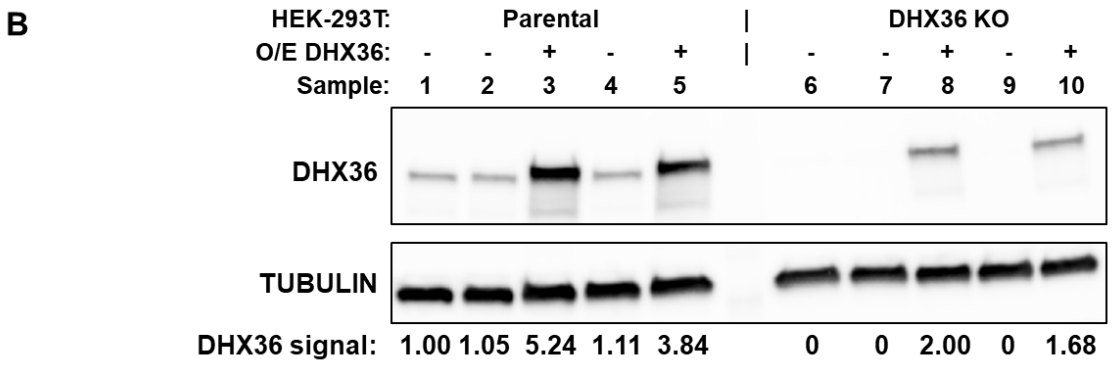

Figure 15: (**A**) qPCR analysis showing the successful overexpression of hTR, TERT mRNA and DHX36 mRNA in both Parental and DHX36 KO cells. Error bars: standard deviation between 3 technical replicates. (**B**) Western Blot confirming the overexpression of DHX36. On the bottom, quantification of DHX36 signal compared to un-transfected Parental cells (first sample), normalized over TUBULIN signal.

G2C-hTR mutant telomerase showed reduced products accumulation comparted to WT telomerase (Figure 16, compare lanes 3 and 1). Furthermore, this mutant of hTR showed an additive effect in reducing telomerase activity in a cellular context where DHX36 is depleted (Figure 16, compare lane 7 with lanes 1, 3 and 5).

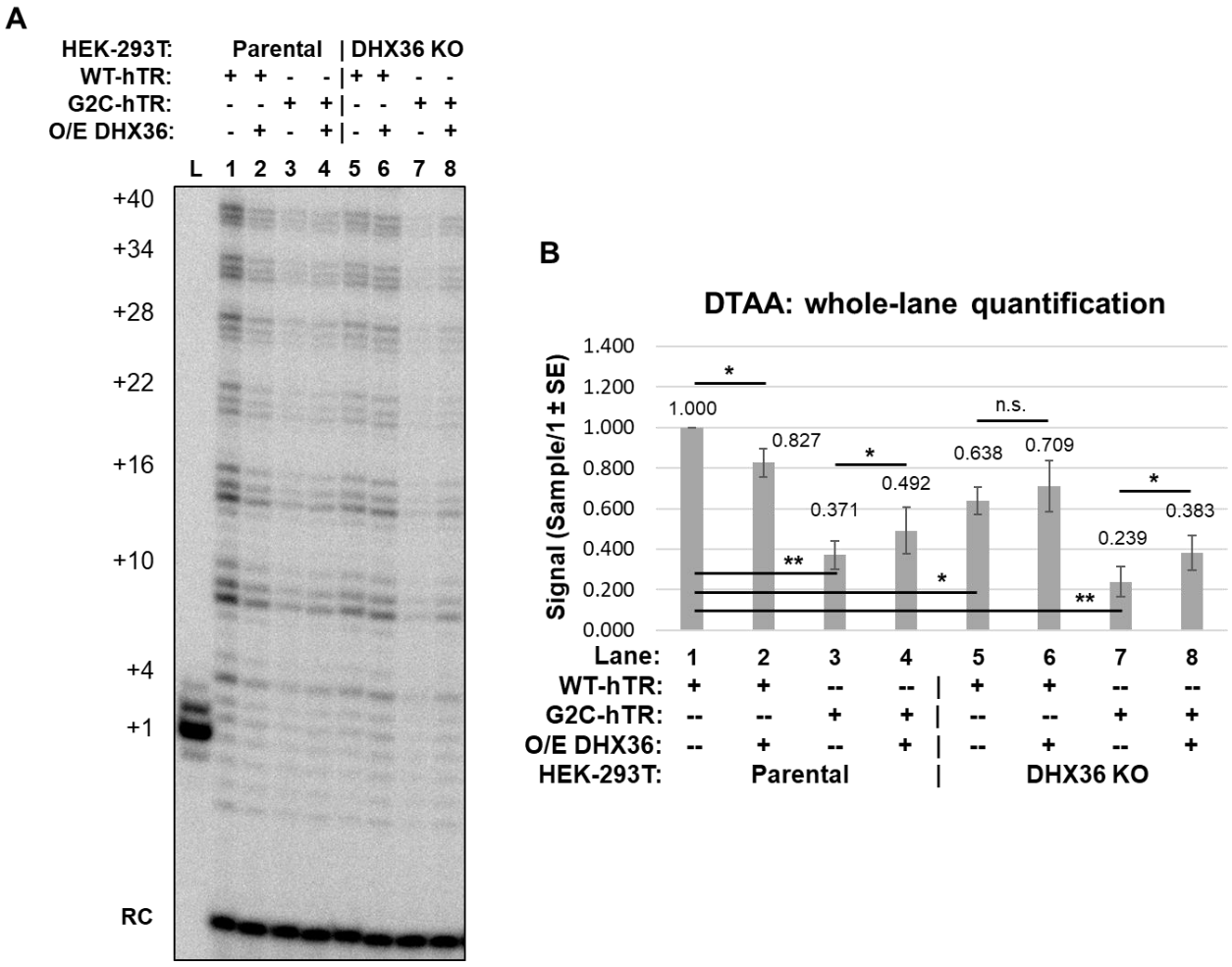

Figure 16: (**A**) Sequencing gel showing the amplification products of cell extract for HEK-293T cells, either Parental or DHX36 KO, subjected to overexpression of DHX36. L = Ladder, RC = Recovery Control (**B**) Quantification of the intensity for a whole lane of three biological replicates like the gel shown in **A**, normalized over RC signal. n = 2 biological replicates, statistical analysis = T.test, * = p.value<0.5, ** = p.value<0.05, n.s.= non significant.

As previously shown in Figure 14, also in this experiment the overexpression of DHX36 is not able to rescue the lower activity observed in the DHX36 KO cell extract (Figure 16, compare lane 6 with lane 5). Additionally, overexpressing DHX36 causes a slight decrease in activity of Parental cell extract (Figure 16, compare lane 2 with lane 1). Conversely, in both Parental and DHX36 KO cells, the overexpression of DHX36 partially rescues the activity observed upon overexpression of the mutant G2C-hTR (Figure 16, compare lane 4 with lane 3, and lane 8 with lane 7 respectively). These data suggest that the structure at the 5'-end of hTR is important for telomerase function. The most likely outcome of the G2C mutation on hTR is an alteration in the rG4 structure at the 5' terminal region of the RNA. One possibility is that such mutation completely abolishes rG4 formation. Alternatively, the loss of the central G in the first stretch of three consecutive Gs could promote the formation of an alternative rG4, utilizing some of the Gs normally involved in the formation of the P1 helix. The inefficient formation of the Template Boundary Element (TBE) could be the cause for the observed reduced telomerase activity compared to WT-hTR. Furthermore, DHX36 plays a role in promoting telomerase activity that becomes more critical when telomerase incorporate the G2C-hTR mutant. It is still unclear why the overexpression of DHX36 is not able to at least partially rescue the activity observed in the DHX36 KO cells. A possibility might be that other G4-interacting proteins or telomerase co-factors involved in the same pathway where DHX36 is required, may act on hTR before it is able to interact with DHX36, preventing the rescue of activity even after its overexpression.

DC-related mutant G11T-hTR displays reduced telomerase activity

Following the previous studies, it was still unclear whether the phenotype of low telomerase activity shown by the G2C-hTR mutant (Figure 16) was a general consequence of altered rG4 formation at the 5'-end of hTR, or a specific feature of the G2C mutation. To address this, a different mutant of hTR, the transversion G11T, was utilized to perform DTAAs under the same conditions as used with G2C. This G11T-hTR mutation is also falling into the rG4 forming region of hTR and is reported to be potentially associated with DC [309]. Once again, successful overexpression of hTR, TERT and DHX36 was confirmed by qPCR and western blot (Figure 17). Like the previous mutant, G11T-hTR shows similar levels after overexpression compared to what was observed for WT-hTR (Figure 17A), suggesting that also this mutant has similar stability to WT-hTR.

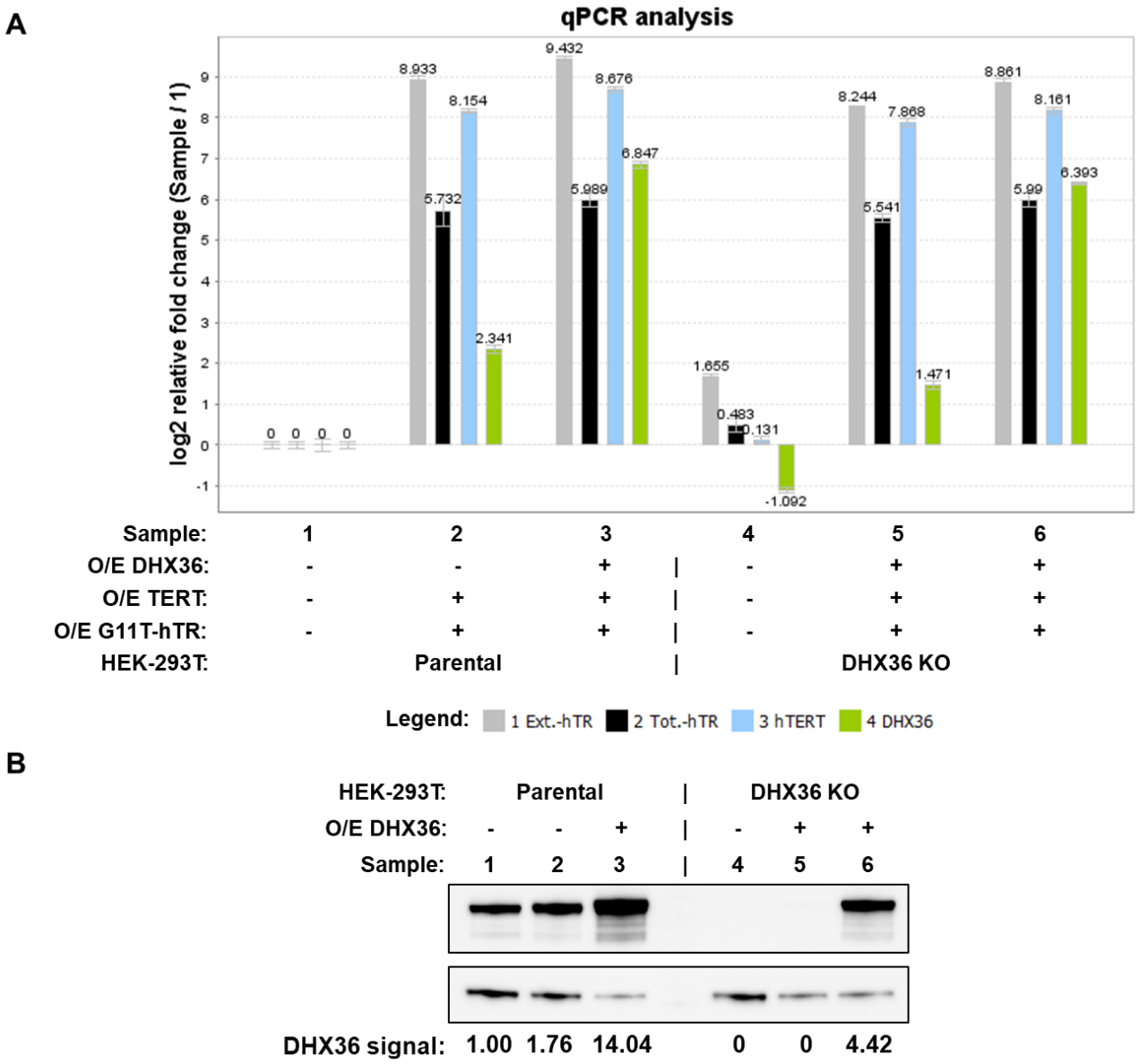

Figure 17: (**A**) qPCR analysis showing the successful overexpression of G11T-hTR, TERT mRNA and DHX36 mRNA in both Parental and DHX36 KO cells. Error bars: standard deviation between 3 technical replicates. (**B**) Western Blot confirming the overexpression of DHX36. On the bottom, quantification of DHX36 signal compared to un-transfected Parental cells (first sample), normalized over TUBULIN signal.

G11T-hTR mutant telomerase showed a reduction in products accumulation similarly to G2C-hTR (Figure 18, compare lanes 3 and 1). Additionally, it was observed that also G11T-hTR has an additive effect in reducing telomerase activity when combined with DHX36 depletion (Figure 18, compare lane 7 with lanes 1, 3 and 5), similarly to the G2C-hTR mutant telomerase.

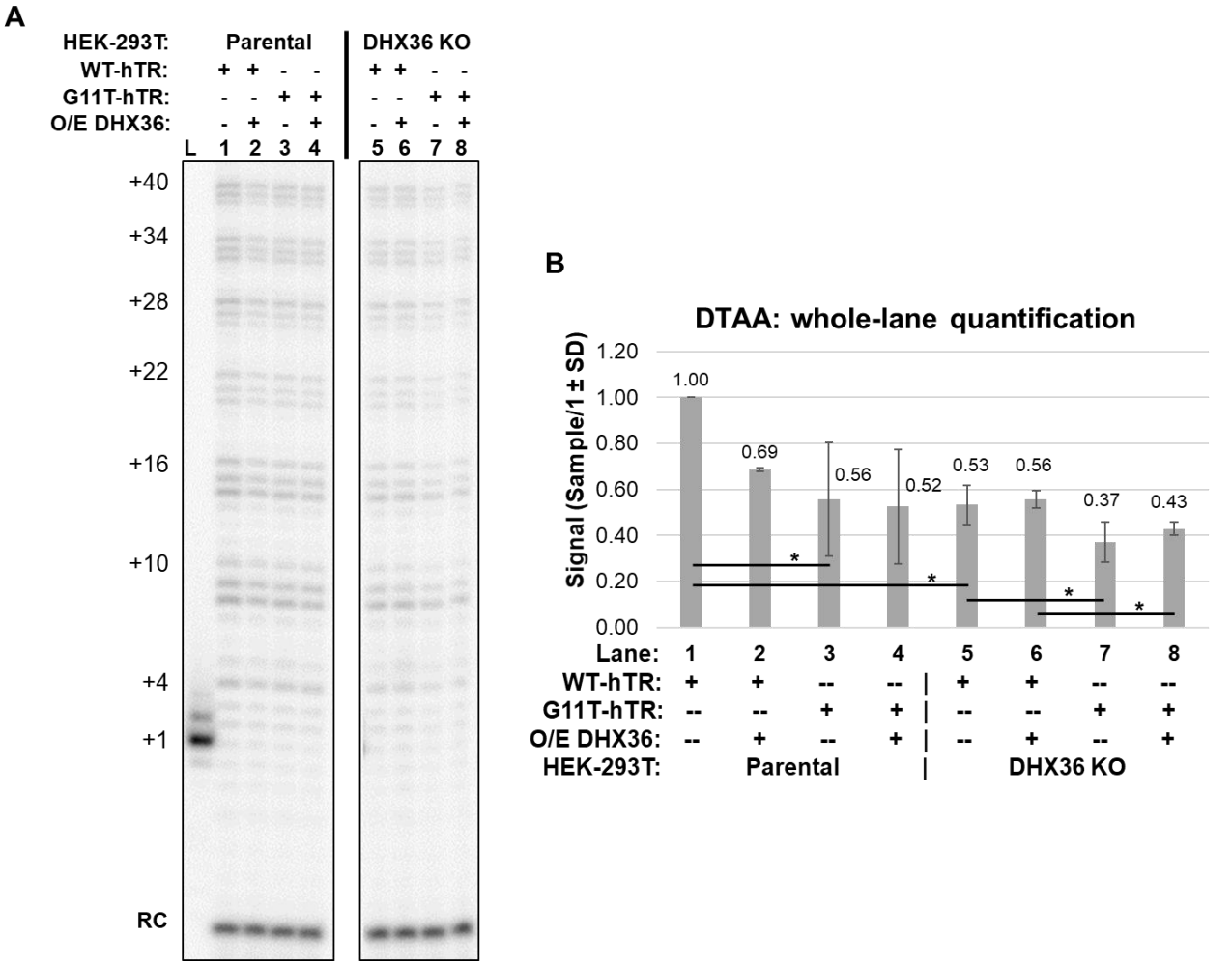

Figure 18: (**A**) Sequencing gel showing the amplification products of cell extract for HEK-293T cells, either Parental or DHX36 KO, subjected to overexpression of DHX36. L = Ladder, RC = Recovery Control (**B**) Quantification of the intensity for a whole lane of two biological replicates like the gel shown in **A**, normalized over RC signal. n = 2 biological replicates, statistical analysis = T.test, * = p.value<0.5

The similar effect on telomerase activity observed with the two mutants G2C-hTR (Figure 16) and G11T-hTR (Figure 18) suggests that this is a general result of altered rG4 formation, rather than the effect of a specific mutation per se in this region of hTR. Nevertheless, the two mutations still possess unique features. For example, while DHX36 overexpression partially rescues telomerase activity in G2C-hTR expressing-cells (Figure16), the presence of DHX36 seems to be completely dispensable in cells expressing G11T-hTR, where DHX36 overexpression shows no significant difference compared to the samples transfected with an empty vector (Figure 18).

hnRNPH1 is a negative regulator of telomerase activity

The same approach of DTAAs utilized to study DHX36, was used to test whether hnRNPH1 plays a role in modulating telomerase activity. For these experiments, the whole cell extract used was made from the two lines of HEK-293T cells, either Parental or DHX36 KO, where knock-down (KD) of hnRNPH1 by siRNA was done at the same time as the transient overexpression of TERT and either WT or G2C-hTR. As shown in Figure 19, hnRNPH1 KD results in an increase in telomerase activity for each of the transfection conditions, suggesting an inhibiting role of hnRNPH1 to telomerase activity.

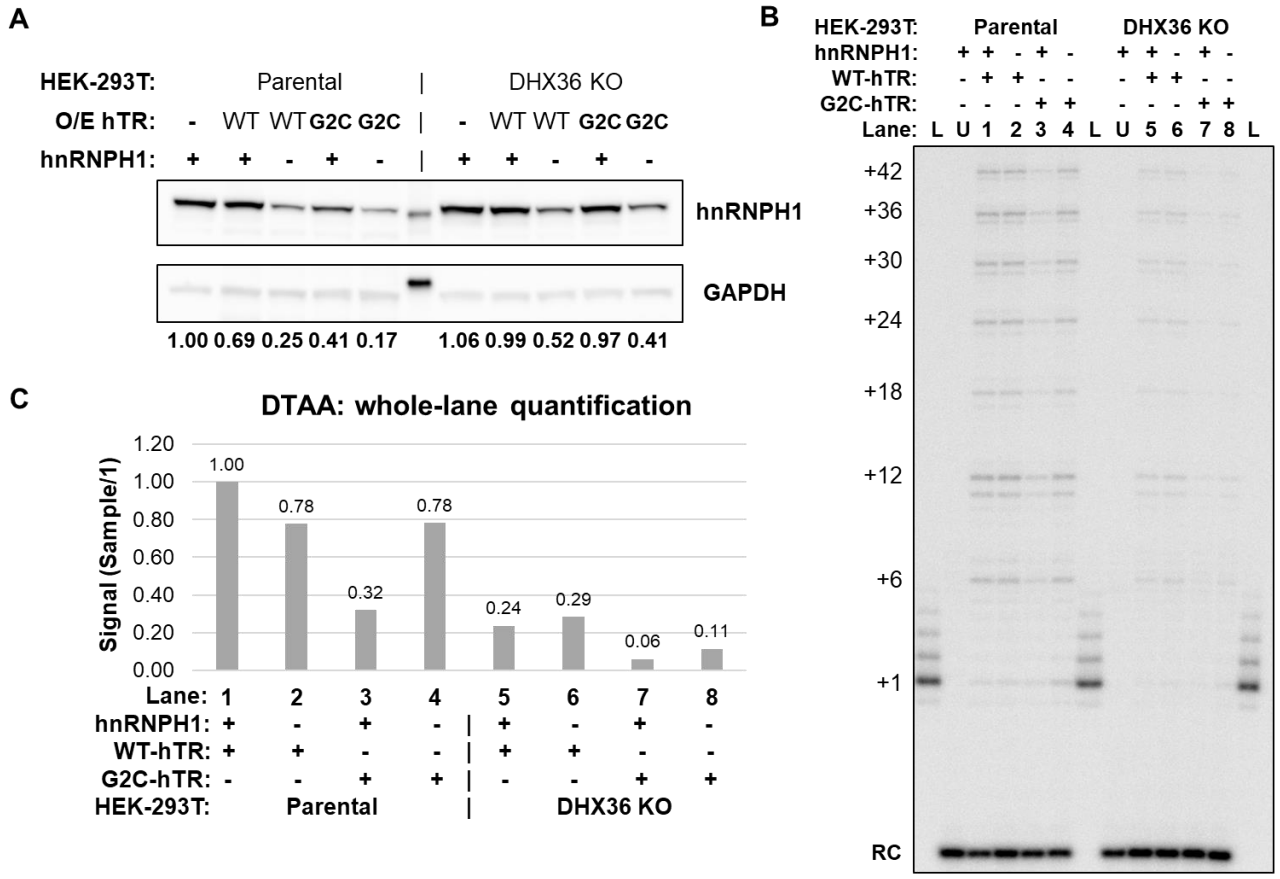

Figure 19: (**A**) Western Blot confirming the knockdown of hnRNPH1. On the bottom, quantification of hnRNPH1 signal compared to un-transfected Parental cells (first lane), normalized over GAPDH signal. (**B**) Sequencing gel showing the amplification products of cell extract for HEK-293T cells, either Parental or DHX36 KO, subjected to knockdown of hnRNPH1. L = Ladder, U = Untreated cells, RC = Recovery Control (**C**) Quantification of the intensity for a whole lane of the gel shown in **B**, normalized over RC signal.

To further explore the modulating activity of hnRNPH1 on telomerase activity, the effect of hnRNPH1 overexpression was tested with the same experimental approach of transient transfection followed by DTAAs. In Figure 20, the confirmation of successful hnRNPH1 manipulation is shown by both qPCR (Figure 20A) and Western blot analysis (Figure 20B). Notably, hnRNPH1 manipulation does not affect the accumulation of hTR after its overexpression, neither for WT, nor for G2C mutant hTR (Figure 20).

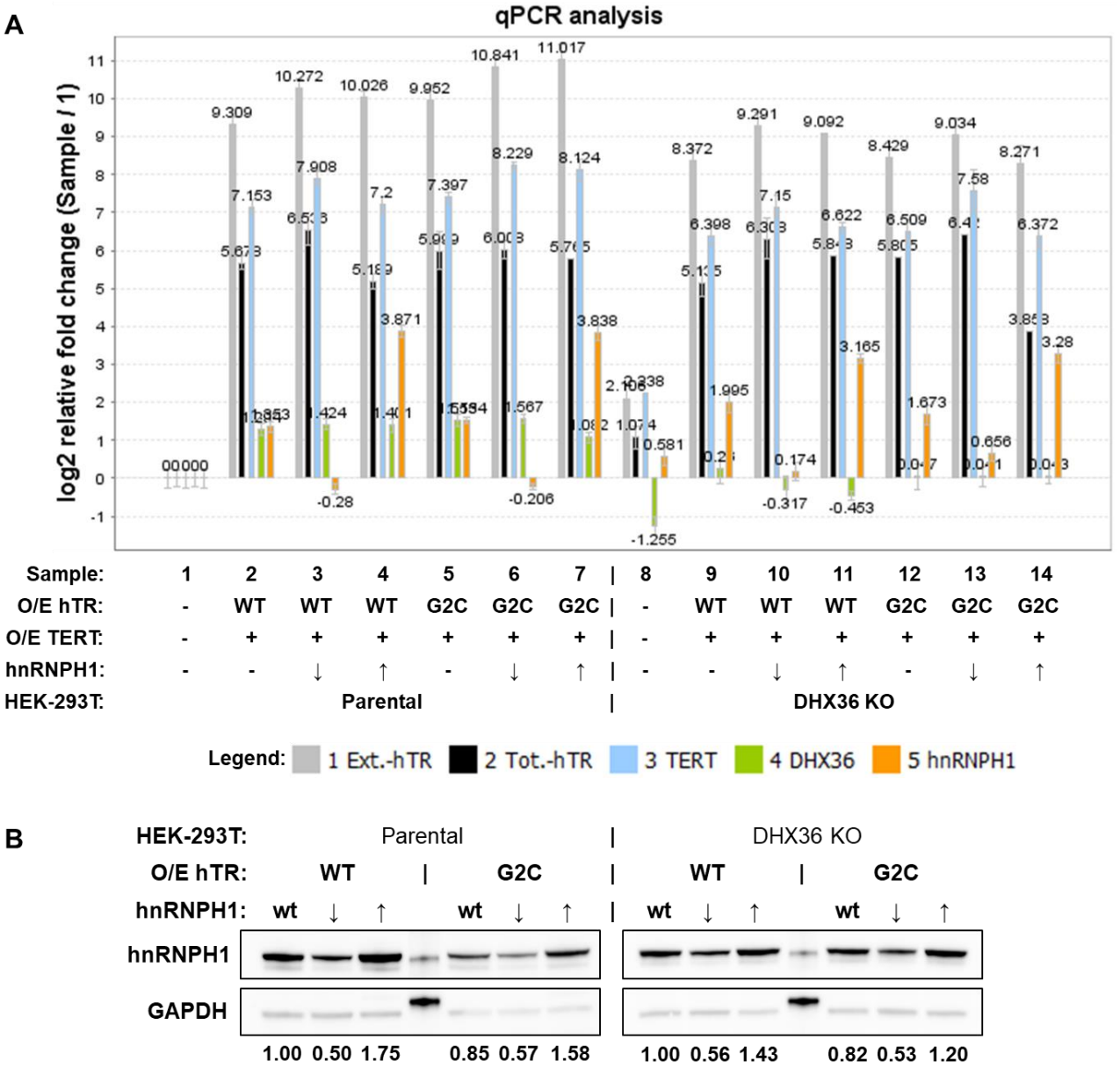

Figure 20: (**A**) qPCR analysis showing the successful overexpression of WT-hTR, G2C-hTR and TERT mRNA in both Parental and DHX36 KO cells. Additionally, DHX36 mRNA and hnRNPH1 mRNA levels are shown, confirming successful manipulation of hnRNPH1 by siRNA knock-down and transient overexpression. Error bars: standard deviation between 3 technical replicates. (**B**) Western Blot confirming the knockdown and the overexpression of hnRNPH1. On the bottom, quantification of hnRNPH1 signal compared to Parental cells with no hnRNPh1 manipulation, normalized over GAPDH signal.

As shown in Figure 21, hnRNPH1 overexpression results in a slight decrease in telomerase activity for each of the transfection conditions. In agreement with the previous hypothesis, this result strengthens the idea of hnRNPH1 as an inhibitory factor of telomerase activity.

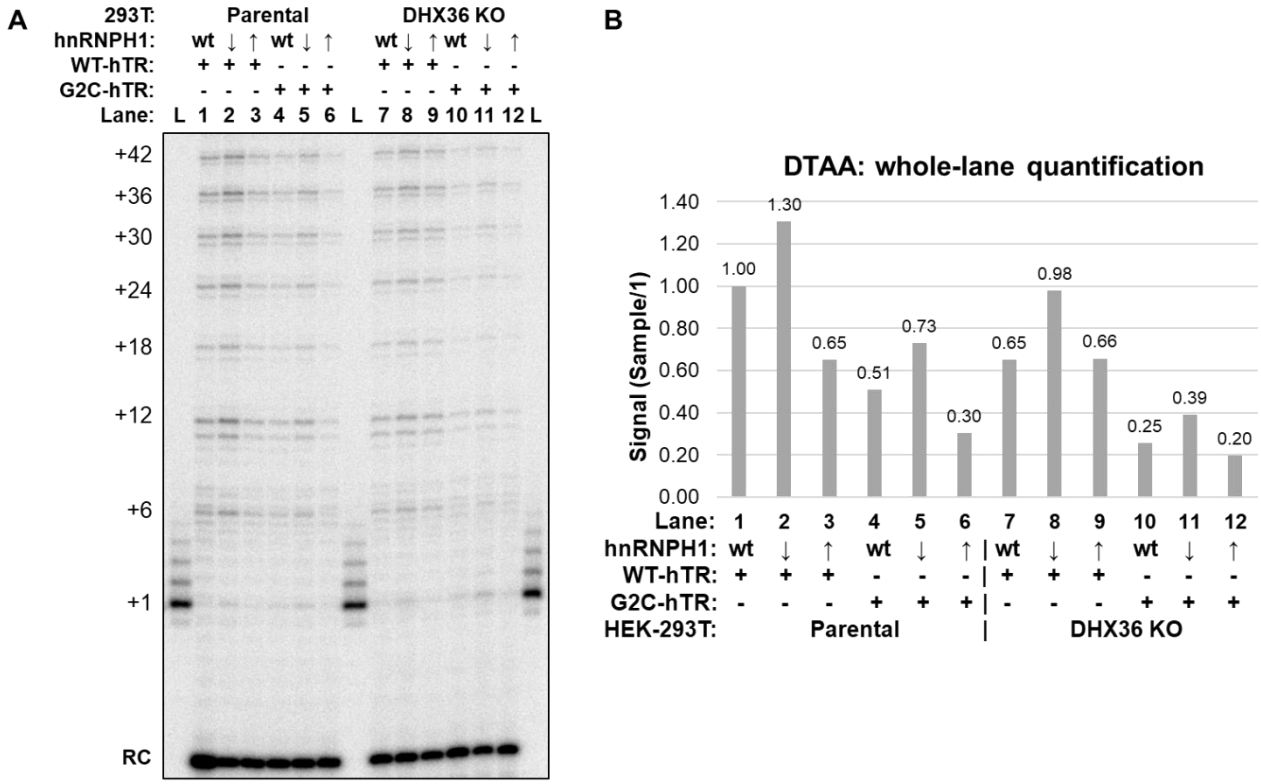

Figure 21: (**A**) Sequencing gel showing the amplification products of cell extract for HEK-293T cells, either Parental or DHX36 KO, subjected to knockdown or overexpression of hnRNPH1. L = Ladder, RC = Recovery Control (**B**) Quantification of the intensity for a whole lane of the gel shown in **B**, normalized over RC signal.

Taken together, the results showed in this section of the thesis suggest that the 5' terminal region of hTR has a less relevant role for its biogenesis, however it plays an important role in modulating telomerase activity. rG4 formation dynamics at the 5' terminal region of hTR influences the affinity of this region to bind DHX36 and hnRNPH1, recruiting two proteins that respectively promote or hinder telomerase activity. This provides a possible mechanism to explain how carrying these mutations results in telomere shortening and development of TBDs.

Mutations within the template region of hTR strongly impair telomerase processivity

The template region of hTR consists of eleven nucleotides between the 46th and the 56th positions, harboring the sequence 5'-CUAACCCUAAC-3'. The first five nucleotides of the template base pair with the end of the telomere, while the last six nucleotides are reverse transcribed into the new telomeric sequence [136]. In human cell lines, when hTR carries a mutation in its template region, telomerase can incorporate such a change in the newly synthetized telomeric repeats [310]. Multiple incorporation of aberrant telomeric repeats into the telomeres may affect the binding of Shelterin components, as well as the formation of the protective terminal structure called T-loop, due to lack of sufficient complementarity between the single stranded 3'-overhang and the double stranded telomeres. All these events may result in telomere de-protection, which in turns can cause the recognition of telomeres as double strand breaks and DDR activation. Besides these possible outcomes resulting from the incorporation of aberrant repeats into the telomeric sequence, my aim concerning template mutants of hTR was to address if these mutations are affecting the telomerase elongation reaction. To answer this question, I applied DTAAs assessing the activity and the repeat addition pattern of two different pathological template mutants of hTR, respectively A48G-hTR and C50A-hTR.

A48G-hTR mutant telomerase is severely unprocessive

Different laboratories reported a collection of hTR variants from patients affected by different TBDs, including the template variant A48G [311, 312]. To assess if this specific mutant had an effect on telomerase elongation, DTAAs were performed using whole cell extract made from VA13 cells, a line of telomerase negative cells that do not express endogenous hTR, where hTERT and either WT or A48G-hTR was overexpressed. Similarly to what was observed with the previous mutants G2C and G11T-hTR, A48G-hTR overexpression resulted in a level of RNA comparable to what is detected for WT-hTR (Figure 22, compare sample 3 with sample 2).

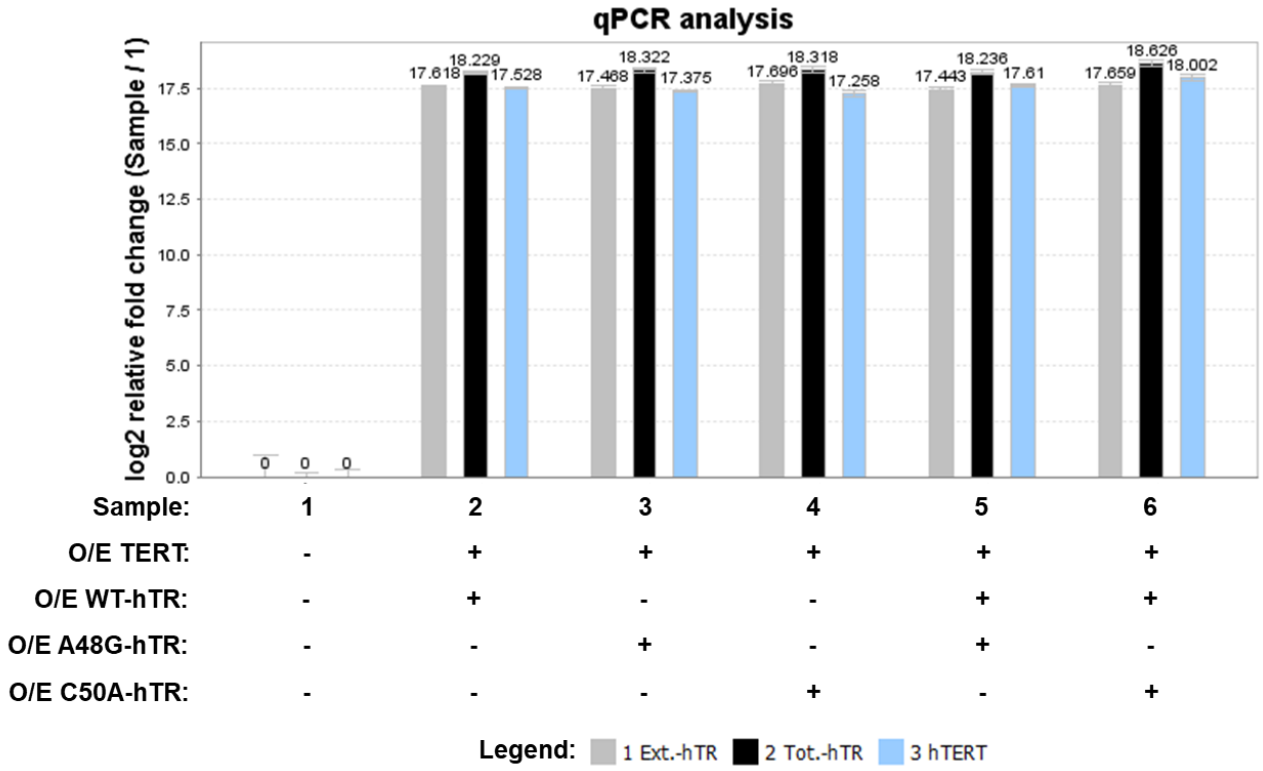

Figure 22: qPCR analysis showing the successful overexpression of TERT mRNA and similar levels of WT, A48G and C50A-hTR in telomerase-negative VA13 cells. Error bars: standard deviation between 3 technical replicates.

To account for possible differences caused by the position of the mismatch within the active site of the telomerase RNP containing A48G-hTR, three of the six possible permutations of the starting primer to extend were used in the assay, consisting of either WT sequence or incorporating the mutation dictated by the A48G-hTR mutant (Figure 23A). When extending an 18 nt primer made of 3 consecutives WT telomeric repeats, a cell extract containing A48G-hTR shows robust addition of only a few repeats, where an extract containing WT-hTR is able to add numerous repeats (Figure 23B, compare lane1 to 3 with lanes 7 to 9). Interestingly, when extending a primer made of 3 consecutives mutant telomeric repeats, the WT telomerase extract shows very low product accumulation (Figure 23B, lanes 4 to 6). The extract containing A48G-hTR mutant telomerase is able to add only a single repeat to the mutant primers used in lane 10 and lane 11, while there is no detectable product for the primer used in lane 12 (Figure 23B). This result suggests that, at least *in vitro*, A48G-hTR possesses very low processivity compared to WT-hTR. Additionally, once the mutation is incorporated into the telomeres, those become a very poor substrate for elongation by both WT and A48G mutant telomerase complexes.

A

Wild Type primer permutations:	**A48G-derived primer permutations:**
Lanes:	Lanes:
(1, 7) AGGGTTAGGGTTAGGGTT	(4, 10) AGGGTCAGGGTCAGGGTC
(2, 8) GGGTTAGGGTTAGGGTTA	(5, 11) GGGTCAGGGTCAGGGTCA
(3, 9) GGTTAGGGTTAGGGTTAG	(6, 12) GGTCAGGGTCAGGGTCAG

B

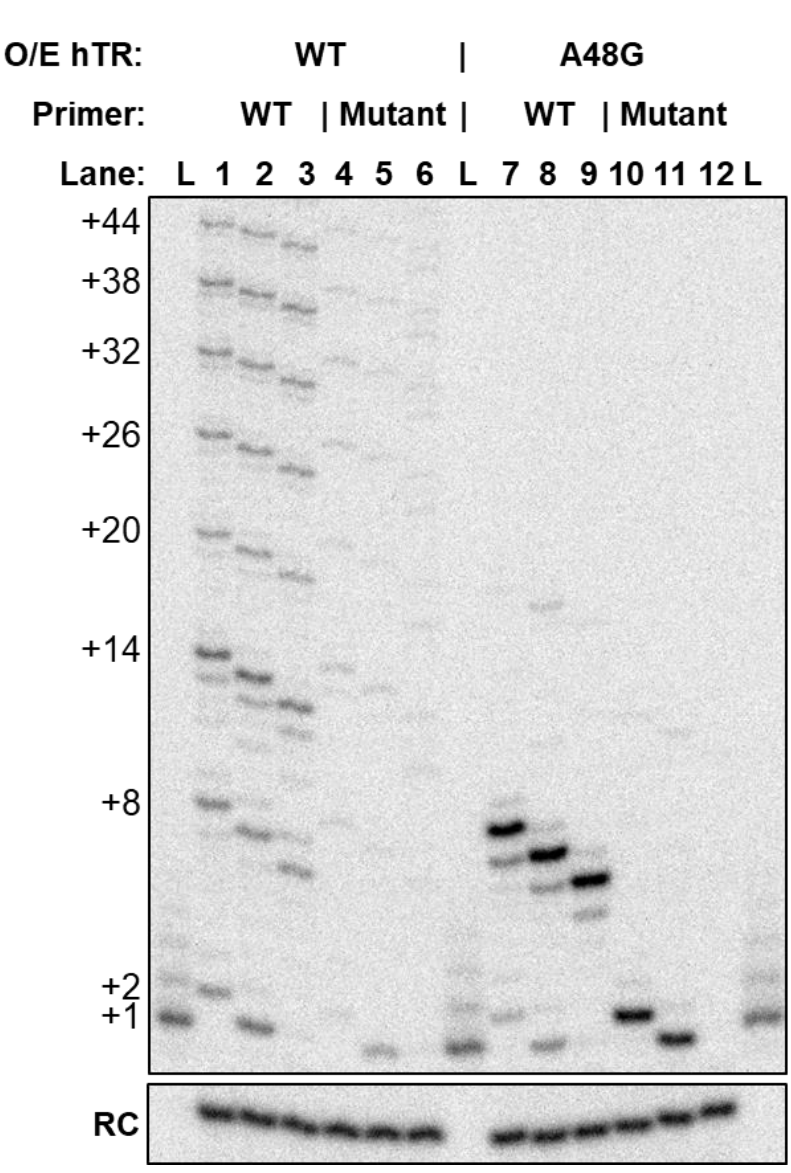

Figure 23: (**A**) Scheme showing the primer permutations utilized in this DTAA. Underlined letters = Nucleotide corresponding to the mutation dictated by the A48G-hTR mutant. (**B**) Sequencing gel showing the amplification products of VA13 cells extract expressing either WT or A48G-hTR. L = Ladder, RC = Recovery Control.

To attempt to mimic the cellular context of an hypothetical patient that carries this hTR mutation in heterozygosis within its genome, telomerase-negative VA13 cells were co-transfected with a 1:1 ratio of two different plasmid expressing either WT or A48G-hTR. The overexpression of A48G-hTR alone or in combination with WT-hTR resulted in a level of RNA comparable to what was detected for WT-hTR alone (Figure 22, compare samples 2, 3 and 5). From such cells, whole cell extract was prepared and subsequently used for DTAAs. Additionally, whole cell extract made from cells expressing exclusively either WT-hTR or A48G-hTR were mixed at 1:1 ration, in order to compare possible differences between distinct telomerase complexes assembled *in vitro* or *in vivo*. Because of the clear difference in processivity observed in Figure 23 between WT-hTR and A48G-hTR containing extracts, exclusively quantifying the signal of the whole-lane, as was done for the previous mutants of hTR, was not sufficient to completely describe these data. Therefore, a different quantification was performed normalizing the signal of each band for the number of radiolabel guanosines added to each extension product, as described in more detail in the section Material and Methods: DTAA quantification. As observed in the gel showed in Figure 24A (compare lane 2 with lane 1) and by the processivity calculation depicted in Figure 24C, the extract expressing A48G-hTR alone is severely unprocessive compared to cells expressing WT-hTR, nonetheless it shows an higher degree of telomerase engagement (Figure 24D). Although A48G-hTR mutant telomerase is less processive than WT telomerase, the excess of primers in the DTAA reaction are contributing to the higher engagement values for the A48G-hTR samples. Due to its high processivity, WT telomerase will elongate the same primer multiple times before dissociating and re-engaging in the elongation of a different primer. Conversely, the A48G-hTR mutant telomerase only adds a few telomeric repeats before rapidly dissociating and re-engaging in elongating another primer in the reaction. In doing so, the A48G-hTR mutant telomerase processes a higher number of primers than WT telomerase in the same reaction time. When comparing the mixed samples with WT-hTR or A48G-hTR alone, some informative differences were observed. First, the product accumulation for the whole-lane of the two mixed samples roughly correspond to the sum of the halves of the WT-hTR and A48G-hTR samples product accumulations (Figure 24B). Second, the telomerase engagement also shows a similar pattern (Figure 24D), where the Total Lane Counts (TLCs) for the mixed samples correspond to half of the sum of the TLCs for the WT-hTR and A48G-hTR samples expressed alone. Third, the processivity of the mixed samples is comparable to that of the WT-hTR sample (Figure 24C). Additionally, no differences between the two mixed samples were detected for all the calculated parameters (Figure 24). Collectively, these results suggest that there is no “poisoning” of WT telomerase by the less processive mutant complex, and that WT and mutant telomerase complexes work independently from each other.

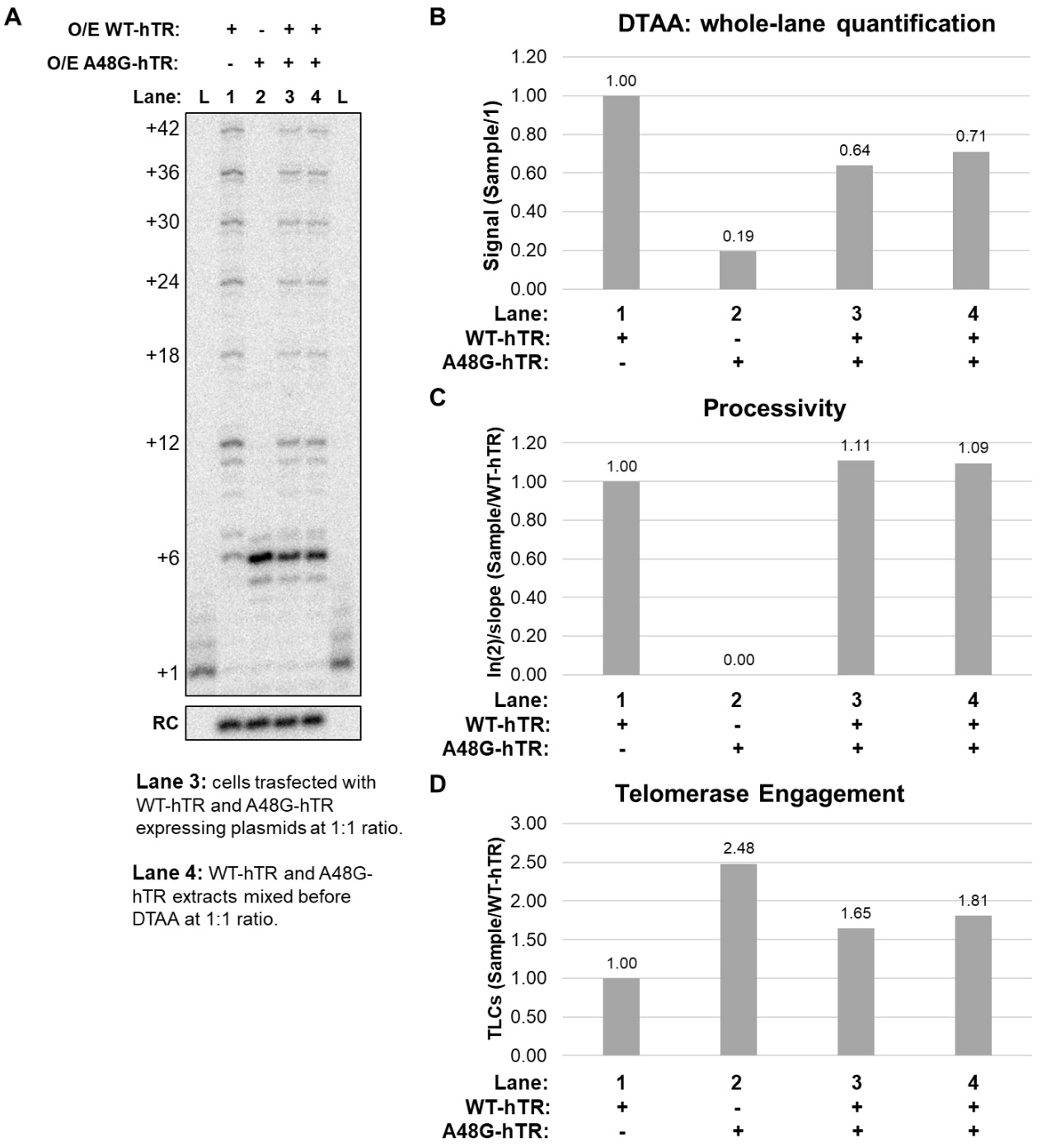

Figure 24: (**A**) Sequencing gel showing the amplification products of VA13 cells extract expressing: WT-hTR, A48G-hTR or both. Starting primer sequence: $(GGTTAG)_3$ L = Ladder, RC = Recovery Control. (**B**) Quantification of the intensity for a whole lane of the gel shown in **A**, normalized over RC signal. (**C**) Processivity quantification of the gel showed in panel (**A**). The processivity of each lane was calculated as described in Materials and methods: DTAA quantification and normalized over WT-hTR expressing sample. (**D**) Telomerase engagement quantification of the gel showed in panel (**A**). The TLCs of each lane was calculated as described in Materials and methods: DTAA quantification and normalized over WT-hTR expressing sample.

C50A-hTR mutant telomerase is unprocessive and impairs telomere maintenance

After sequencing the genome of a patient affected by Dyskeratosis Congenita (DC), the heterozygous template mutation C50A on hTR was identified, as well as the heterozygous nonsense mutation Q1178X in the RTEL1 gene. RTEL1 is a DNA helicase which is involved in the stability, protection and elongation of telomeres, and interacts with proteins of the shelterin complex known to protect telomeres during DNA replication [313]. I decided to primarily characterize the template mutation, in order to unveil the molecular mechanism underlying the development of the disease. Additionally, we were able to isolate fibroblast cells from a skin biopsy of the patient, allowing us to directly analyze cells carrying both mutations in a context as close as possible to the physiological environment within the patient tissues.

In vitro biochemical characterization of C50A-hTR

Once again, DTAAs were executed using whole cell extracts made from telomerase-negative VA13 cells, where TERT and either WT or C50A-hTR alone were transiently overexpressed. A combination of both WT and C50A-hTR expressing plasmids with a ratio of 1:1 was also tested. The C50A mutation in hTR behaved like A48G-hTR, resulting in a level of detected RNA comparable to what was detected for WT-hTR alone (Figure 22, compare sample 4 with sample 2). Testing increasing concentrations of the different extracts showed that C50A-hTR telomerase has lower processivity compared to WT telomerase (Figure 25A). Due to such differences, like for A48G-hTR, the engagement and processivity quantifications were added to the whole-lane quantification. For this purpose, the three increasing concentration of each extract have been treated as independent biological replicates. After quantification, very low processivity was calculated for C50A-hTR containing extracts (Figure 25D), with a slight increase in telomerase engagement (Figure 25C), similarly to what was observed with mutant A48G-hTR and likely for the same reasons. The combination of the two extract at 1:1 ratio shows slightly more than half of the signal compared to WT-hTR alone (Figure 25B, compare purple bars with blue bars). Notably, doubling the amount of extract resulted in increased product accumulation, but no doubling of the signal (Figure 25B). This can be explain by a partial saturation of the system, where the amount of active telomerase present in the less concentrated samples is sufficient to carry out the majority of the repeat additions. These data suggest that this mutant, as well as A48G-hTR, do not affect the stability of the telomerase complex, nor have impaired binding to the telomeric sequence, but strongly affect the processivity of telomerase.

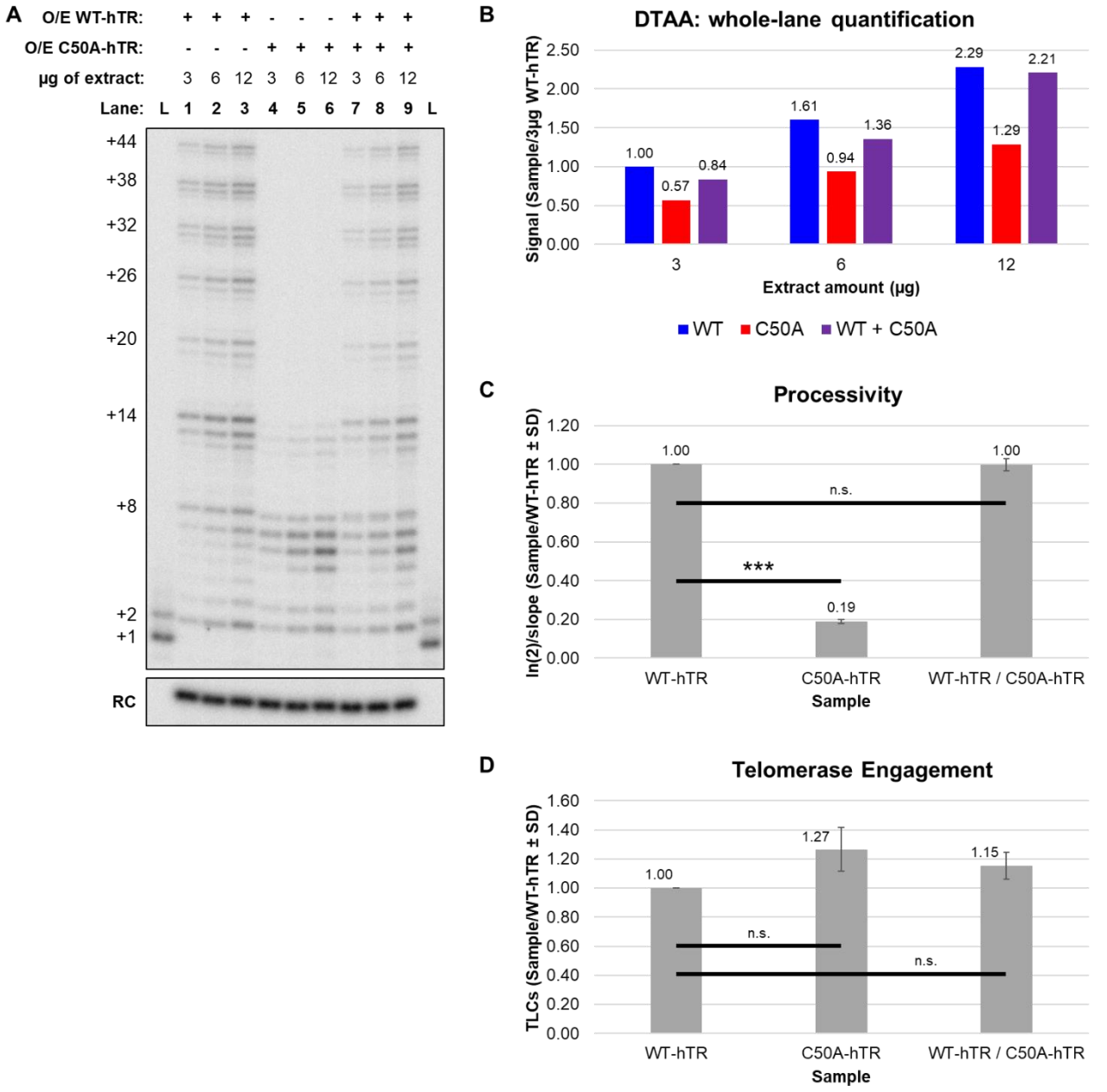

Figure 25: (**A**) Sequencing gel showing the amplification products of increasing amount of VA13 cells extract expressing: WT-hTR, C50A-hTR or both. Starting primer sequence: (AGGGTT)3 L = Ladder, RC = Recovery Control. (**B**) Quantification of the intensity for a whole lane of the gel shown in A, normalized over RC signal. (**C**) Processivity quantification of four biological replicates of DTAAs for different amounts of extract like panel (**A**). The processivity of each lane was calculated as described in Materials and methods and normalized over WT-hTR sample. Error bars equals SD between three biological replicates. The p-value was calculated with T. student statistical analysis. n.s. p>0.05 *** = p<0.001 (**D**) Telomerase engagement quantification of three biological replicates of DTAAs for different amounts of extract like panel (**A**). The TLCs of each lane was calculated as described in Materials and methods and normalized over WT-hTR sample. Error bars equals SD between three biological replicates. The p-value was calculated with T. student statistical analysis. n.s. p>0.05 *** = p<0.001

When testing extracts made from cells co-transfected with plasmids expressing either WT-hTR or C50A-hTR, no difference was observed between this sample and a sample where the two extracts were combined after extract preparation for all the calculated parameters (Figure 26). This suggests that also for C50A-hTR there is no “poisoning” of WT telomerase by the less processive mutant complex.

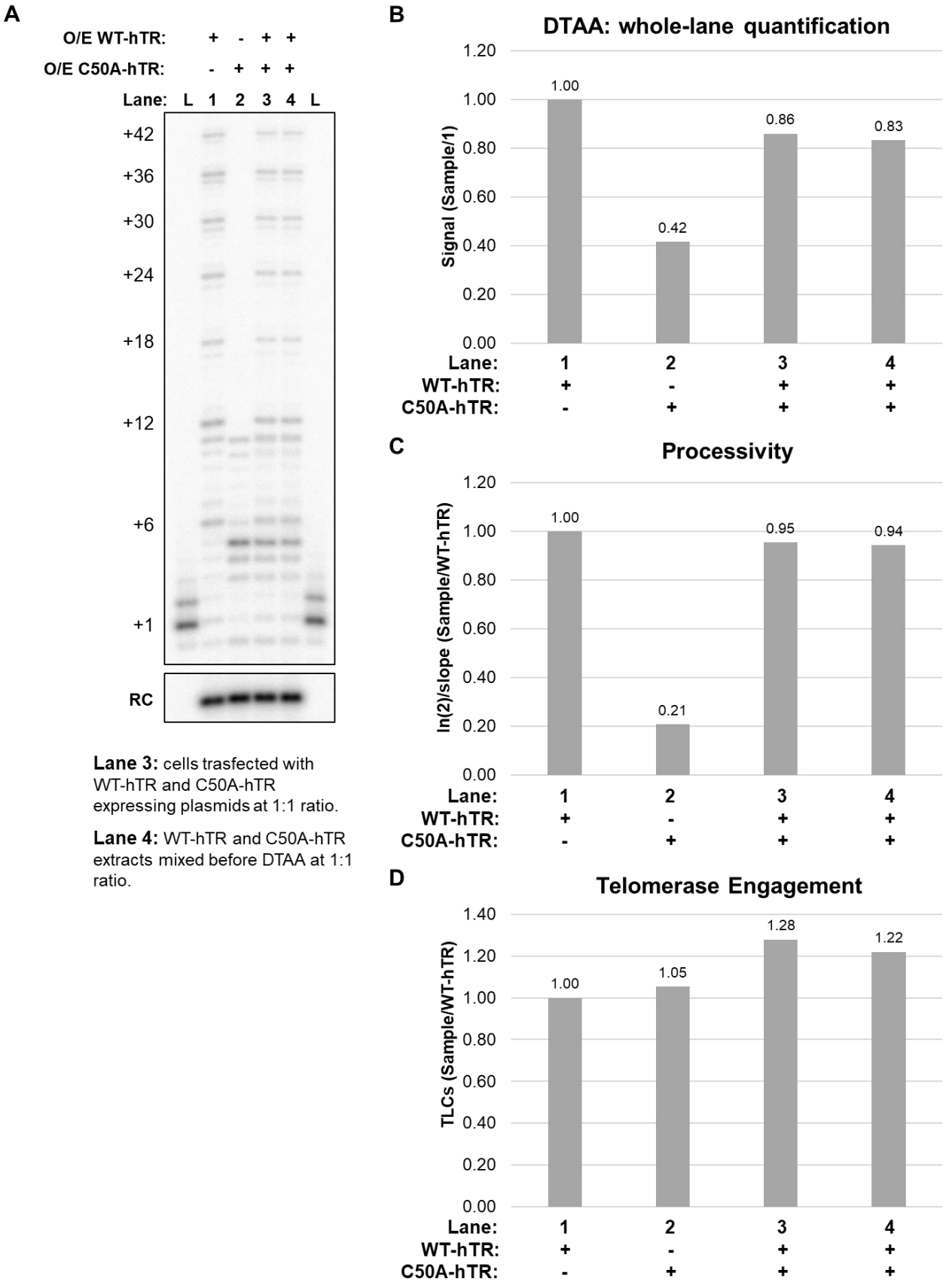

Figure 26: (**A**) Sequencing gel showing the amplification products of VA13 cells extract expressing: WT-hTR, C50A-hTR or both. Starting primer sequence: $(GGTTAG)_3$ L = Ladder, RC = Recovery Control. (**B**) Quantification of the intensity for a whole lane of the gel shown in (**A**), normalized over RC signal. (**C**) Processivity quantification of the gel showed in panel (**A**) normalized over WT-hTR expressing sample. (**D**) Telomerase engagement quantification of the gel showed in panel (**A**) normalized over WT-hTR expressing sample.

After close examination of the bands pattern displayed in the C50A-hTR mutant extracts, a shift to products one nucleotide shorter was observed, when compared to WT-hTR extracts (Figure 25 and 26). To investigate further this phenomenon, additional DTAAs were performed. To account for possible differences caused by the position of the mismatch within the active site of the telomerase RNP containing C50A-hTR, all the six possible permutations of the starting primer to extend were used in the following assay, consisting of either WT sequence or incorporating the mutation dictated by the C50A-hTR mutant (Figure 27A). C50A-hTR has very low processivity for all of the primer permutations tested, including the primers incorporating the mutation (Figure 27B, lanes 7 to 12 and lanes 19 to 24). Conversely, WT-hTR is able to extend efficiently each primer permutation, including the mutated ones (Figure 27B, lanes 1 to 6 and lanes 13 to 18). Analyzing the gel in Figure 27B, we confirmed that C50A-hTR mutant extracts result in products that are one nucleotide shorter compared to WT-hTR extracts for all the WT primer permutations (Figure 27B, compare lanes 7 to 12 with lanes 1 to 6). The same pattern was observed when the mutant primer permutations were used (Figure 27B, compare lanes 19 to 24 with lanes 1 to 6). Interestingly, also when WT telomerase elongated four of the six mutant primer permutations, a shift in the ladder was observed when compared with the elongation of the respective primers consisting of WT sequence (Figure 27B, compare lanes 13 to 16 with lanes 1 to 4). Furthermore, an inconsistent bands pattern of elongation was observed for WT telomerase elongating specifically the primer $(GGTTTA)_3$. Moreover, the overall product accumulation for this primer was reduced, when comparing with the elongation products of the other mutant primer permutations (Figure 27B, compare lane 16 with lanes 13 to 18).

A

Wild Type primer permutations:	**Mutant primer permutations:**
Lanes:	Lanes:
(1, 7) TTAGGGTTAGGGTTAGGG	(13, 19) TTAGGTTTAGGTTTAGGT
(2, 8) TAGGGTTAGGGTTAGGGT	(14, 20) TAGGTTTAGGTTTAGGTT
(3, 9) AGGGTTAGGGTTAGGGTT	(15, 21) AGGTTTAGGTTTAGGTTT
(4, 10) GGGTTAGGGTTAGGGTTA	(16, 22) GGTTTAGGTTTAGGTTTA
(5, 11) GGTTAGGGTTAGGGTTAG	(17, 23) GTTTAGGTTTAGGTTTAG
(6, 12) GTTAGGGTTAGGGTTAGG	(18, 24) TTTAGGTTTAGGTTTAGG

B

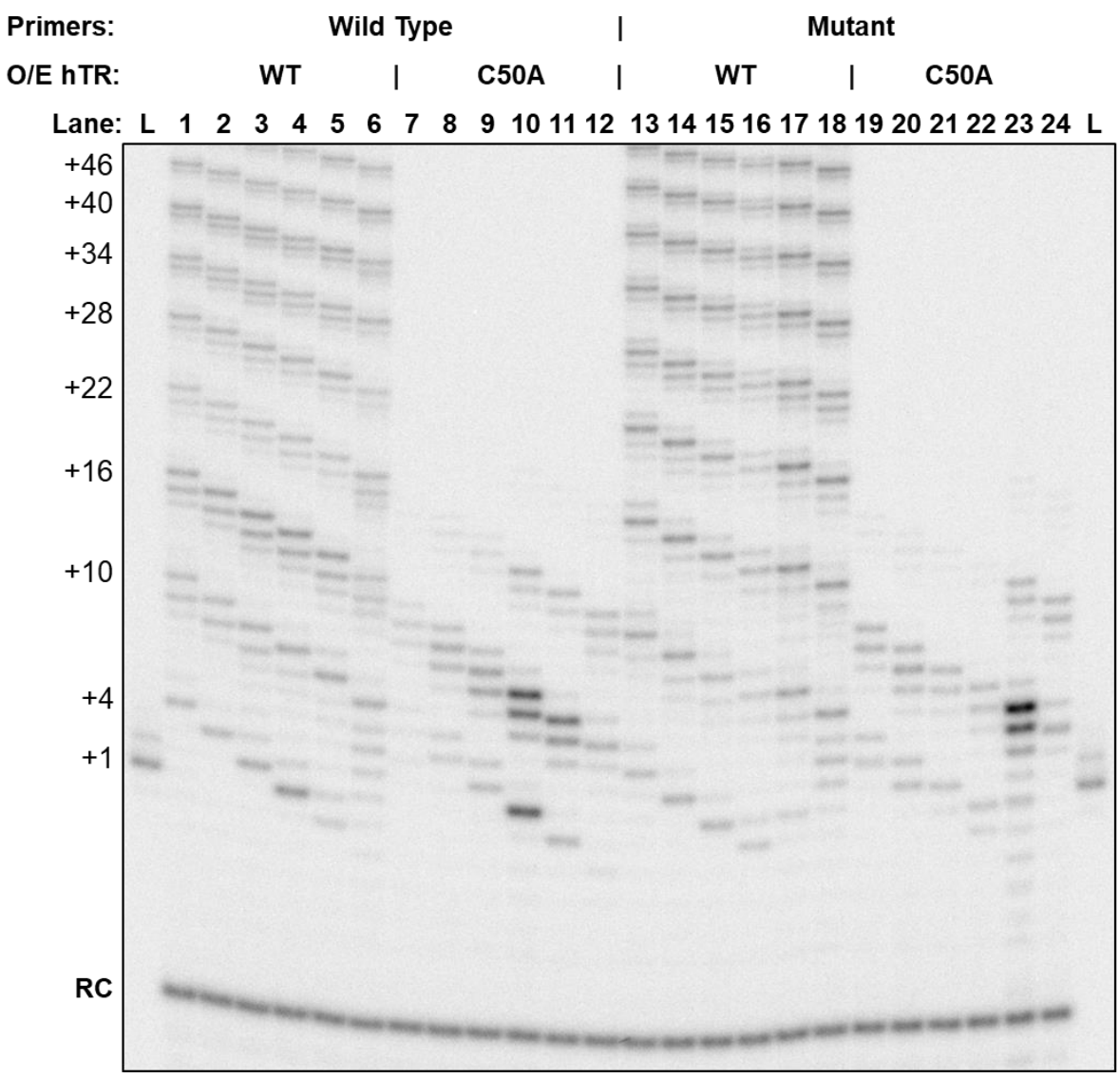

Figure 27: (**A**) Scheme showing the primer permutations utilized in this DTAA. Underlined letters = Nucleotide corresponding to the mutation dictated by the C50A-hTR mutant. (**B**) Sequencing gel showing the amplification products of VA13 cells extract expressing either WT or C50A-hTR. L = Ladder, RC = Recovery Control.

The observed aberrant elongation performed by the C50A-hTR mutant extracts (Figure 27B, lanes 7 to 12) can be explained by the formation of a premature rA-dT base pair 1 nt earlier between hTR and the telomeric primer. This specific base pair within the active site of the enzyme has been shown to act as an intrinsic stop signal of telomerase elongation [136]. In Figure 28A, a schematic depicting the elongation mechanism responsible for the aberrant bands pattern of C50A-hTR mutant telomerase is reported, using the WT telomeric primer $(GGTTAG)_3$ as reference. Notably, only during the first extension the mutant telomerase adds five nucleotides instead of the canonical six. For the following extension reactions, six nucleotides are added, but with a telomeric repeat terminating with a dA instead of a dG (Figure 28A). Regarding the aberrant elongation pattern observed when WT telomerase was extending the $(GGTTTA)_3$ telomeric primer (Figure 27B, lane 16), two alternative and possibly coexisting mechanisms of elongation are shown in Figure 28B. The first model requires the formation of a non-canonical base-pair between the rC/dA nucleotides, resulting in the addition of a six-nucleotide long repeat (Figure 28B). The second model requires the sliding of one nucleotide forward in the alignment between the hTR template region and the DNA primer, resulting in a base-pair of only three nucleotides between them, and producing the addition of a seven-nucleotide long repeat (Figure 28B). In both cases, after the first aberrant elongation the canonical alignment between hTR and the telomeric primer is restored, resulting in the addition of a regular six nucleotide long telomeric repeat (GGTTAG) for the following extension reactions (Figure 28B).

Figure 28: (**A**) Schematics of the elongation mechanism of the WT telomeric primer $(GGTTAG)_3$ by WT telomerase and C50A-hTR mutant telomerase. (**B**) Schematics of the elongation mechanisms of the WT telomeric primer $(GGTTAG)_3$ and the mutant telomeric primer $(GGTTTA)_3$ by WT telomerase.

To confirm these hypotheses regarding the observed patterns of aberrant elongation, DTAAs in the presence of selected ddNTPs were performed. WT telomerase extends the WT primer $(GGGTTA)_3$ (Figure 29, lanes 1 to 3) according to the expected bands pattern depicted in Figure 28B. As shown in Figure 29 (gel on the right), the addition of the first telomeric repeat performed by WT telomerase to the mutated primer $(GGTTTA)_3$ correspond to a product one nucleotide shorter than with a WT primer (Figure 29, compare lanes 7 to 9 with lanes 1 to 3). Interestingly, when the DTAA is done in presence of ddATP (Figure 29, lane 9), two bands of equal intensity appear at positions +5 and +6 of the ladder. This confirms the coexistence of two alternative elongation mechanisms based on the different alignments between the template region of hTR and the starting primer as suggested in Figure 28B. Furthermore, the appearance of a band at position 0 in the right gels, suggests that at least a portion of the primer population is subjected to 3' resection (Figure 29, lanes 7 to 12). The subsequent addition of nucleotides including radioactive dGTP makes this primer detectable on the gel, and at the same time, it renders it a better substrate for elongation. The C50A-hTR mutant telomerase extends both WT and mutant primers with a similar pattern, even if sensibly more efficiently for the WT primer compared to the mutant one (Figure 29, lanes 4 to 6 and lanes 10 to 12). Finally, comparing the extended products of C50A-hTR telomerase versus WT telomerase for the WT primer $(GGGTTA)_3$, we can see how the mutant telomerase adds firstly a repeat that is shifted by one nucleotide and therefore one nucleotide shorter than what WT telomerase adds (Figure 29, compare lanes 4 to 6 with lanes 1 to 3). After this first addition, C50A-hTR telomerase adds up to two 6 nt repeats before dissociating, resulting in a bands pattern coherent with the elongation mechanism illustrated in Figure 28A.

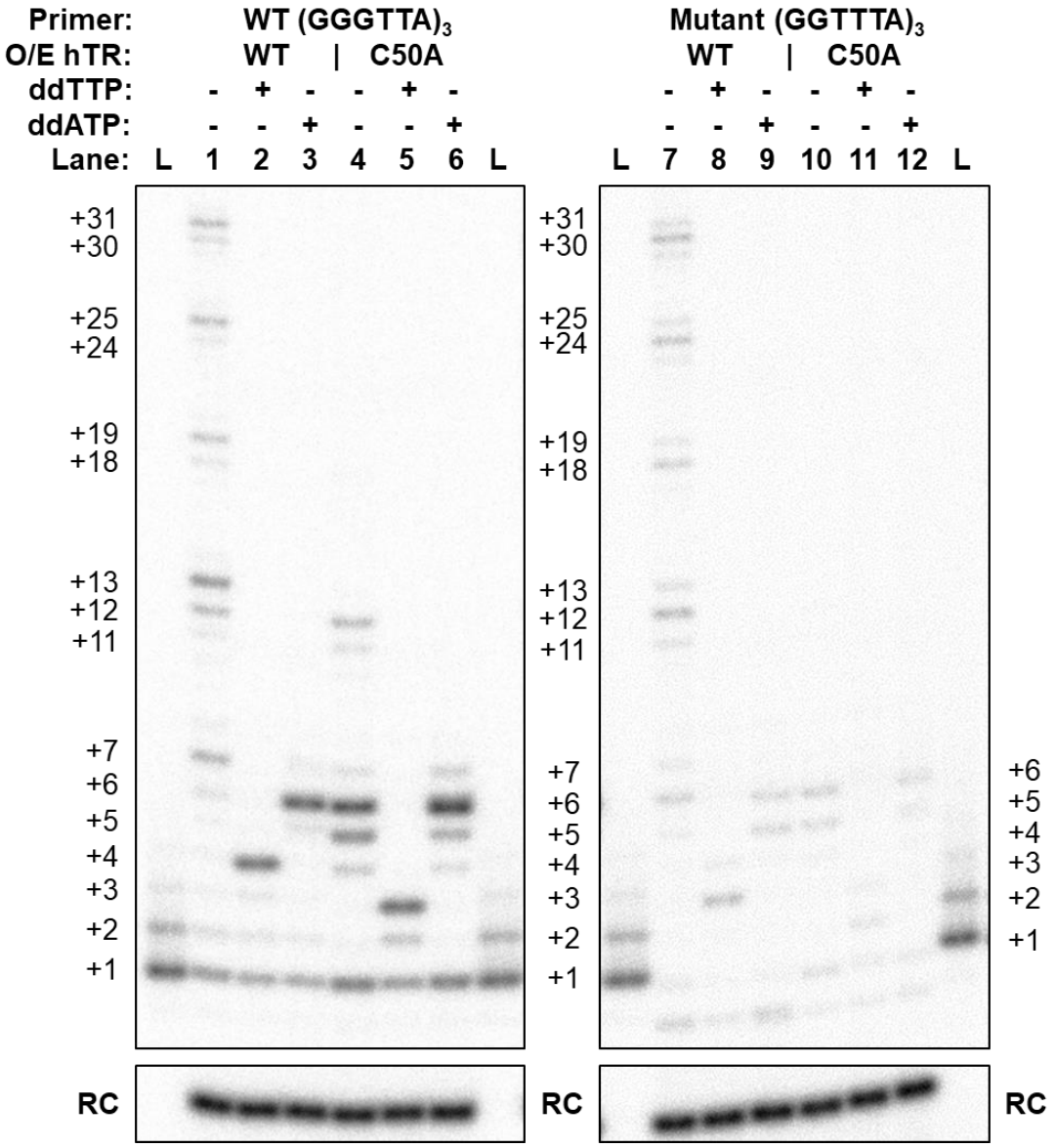

Figure 29: Sequencing gel showing the amplification products of VA13 cells extract, expressing either WT or C50A-hTR, for the indicated starting primers. Reactions were done completely replacing dATP or dTTP with the respective di-deoxy analog where indicated. L = Ladder, RC = Recovery Control.

In the previous DTAAs the reaction time was set to 30 minutes, which is sufficient to allow for telomerase to add numerous repeats to the starting primer. To ensure that no effect in general efficiency of elongation of the mutant primer from WT telomerase was lost due to the reaction reaching completion within the timeframe of the experiment, a time course DTAA was performed. No overall difference was observed between elongation of the WT primer $(GGTTAG)_3$ and the mutant primer $(GTTTAG)_3$ (Figure 30A, lanes 11 to 20, and Figure 30B, bottom graph). Taking into account the alignment and addition scheme (Figure 28) deducted from the previous experiments, we hypothesize that C50A- hTR mutant telomerase would add a telomeric repeats ending with the sequence GGTTTA. To mimic the physiological context where WT telomerase engages into the elongation of a telomeric sequence previously elongated by the C50A-hTR mutant telomerase, the mutated primer $(GGTTTA)_3$ and the respective WT primer $(GGGTTA)_3$ were used in the assay. As shown in Figure 30A, left portion of the gel, WT telomerase accumulates about half of the product when is extending such mutated primers compared to the respective WT primers (Figure 30B, top graph). These data suggest that at least *in vitro*, even if WT telomerase is able to extend a mutated telomeric sequence, not every engagement event corresponds to productive elongation, resulting in an overall slower product accumulation.

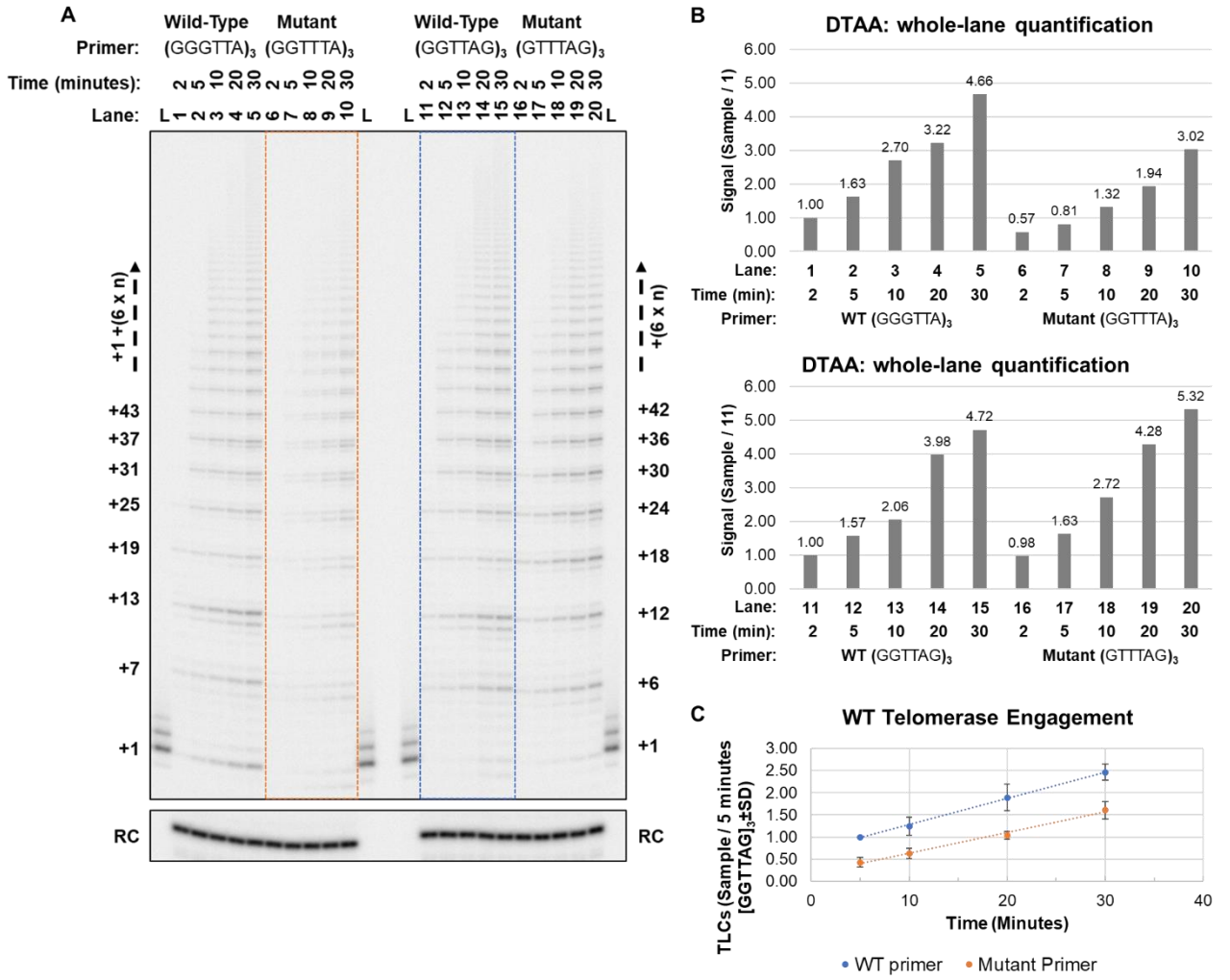

Figure 30: (**A**) Sequencing gel showing the amplification products of VA13 cells extract expressing WT-hTR over a time course. The different starting primer sequences are indicated on the figure. L = Ladder, RC = Recovery Control. (**B**) Quantification of the intensity for a whole lane of the gel shown in (**A**), normalized over RC signal. (**C**) Telomerase engagement quantification over time of the two sets of sample like the one marked in the gel showed in panel (**A**), corresponding to elongation of $(GGTTAG)_3$ WT primer (blue) and $(GGTTTA)_3$ mutant primer (orange). Error bars equals SD between three biological replicates.

Taken together, these results reveal that template mutations alone can directly affect telomerase activity in at least two different ways. Firstly, template-mutant telomerase shows very low processivity, indicating a shift from translocation to dissociation of the complex after few repeat additions. Secondly, once mutant telomeric repeats are present at the terminus of a telomere, the elongation activity of WT telomerase is partially impaired.

In vivo analysis of DC patient-derived cells

To understand how the two heterozygous mutations found in the patient's genome (C50A-hTR and Q1178X-RTEL1) affected cell viability, isolated fibroblasts were cultivated in the laboratory. Measuring cell proliferation rate by cell counting, a faster reduction in cell growth over time was observed in the patient fibroblasts compared to those isolated from healthy individuals of the same age and gender (Figure 31A to C). This is due to an increase in the number of senescent cells, as quantified after senescence staining (Figure 31D to H). To further support that the reduction in cell growth was due to senescence, and not to accelerated cell death, an apoptosis staining with the different lines of fibroblast was performed. After FACS analysis, no significant difference in the percentage of apoptotic cells was observed between the three fibroblast lines examined at earlier cell passages (Figure 31I, cell passages 7 and 11).

At later cell passages, the patient-derived fibroblasts showed a percentage of apoptotic cells similar to what was observed for the Control 2 cell line, while the Control 1 cell line showed a smaller percentage of apoptotic cells (Figure 31I, cell passages 18). This indicated that even at later stages, the percentage of apoptotic cells in the patient's fibroblasts was within the variability detected between healthy individual's fibroblasts.

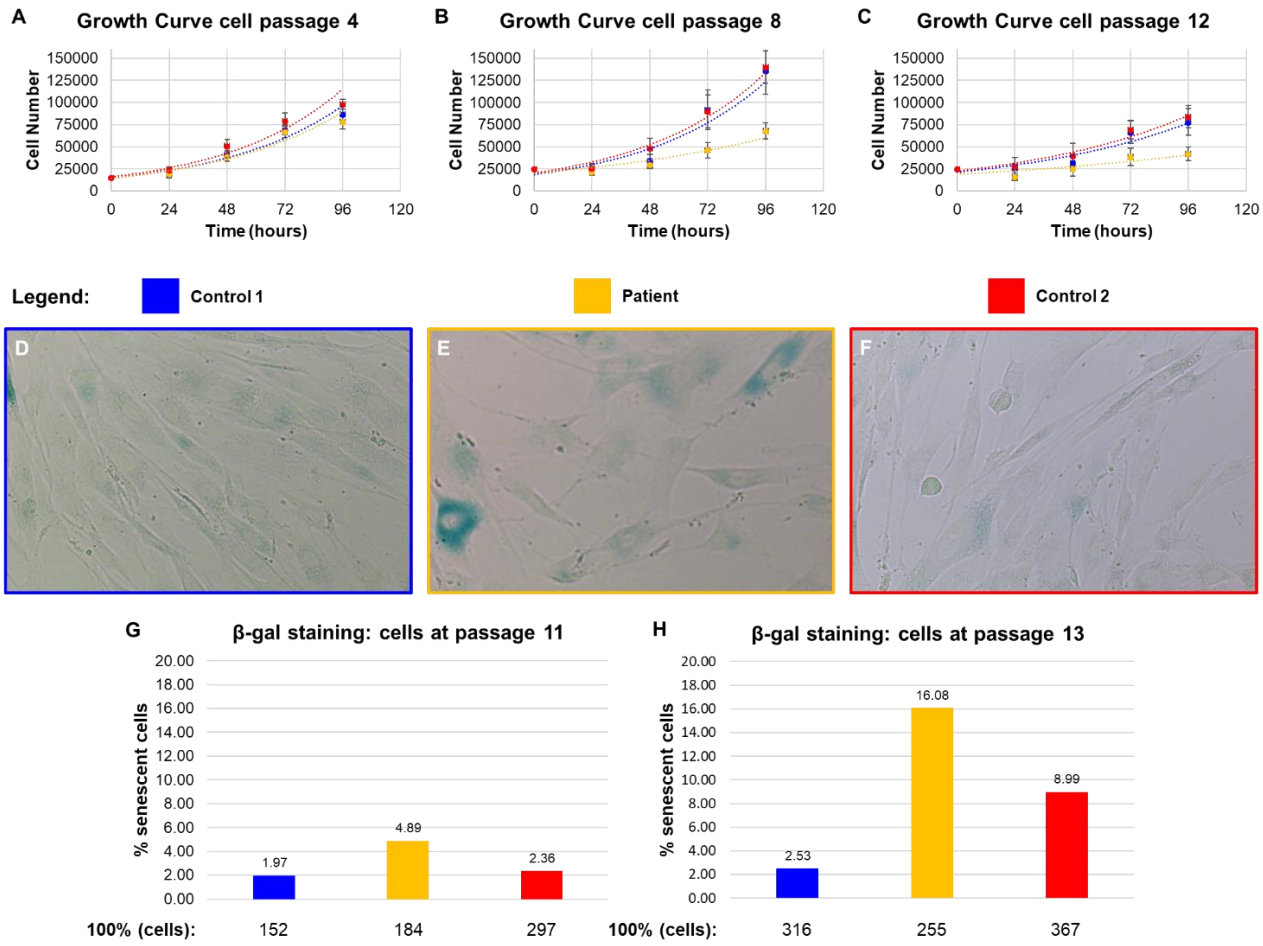

I **Apoptotic cell measurement by Flow-Cytometry**

Fibroblast at cell passage 7			
Individual	**% live cells**	**% necrotic cells**	**% apoptotic cells**
Control 1	94.9	3.6	1.5
Control 2	96.4	2.5	1.1
Patient	95.3	3.1	1.6

Fibroblast at cell passage 11			
Individual	**% live cells**	**% necrotic cells**	**% apoptotic cells**
Control 1	98.0	0.5	1.5
Control 2	96.7	2.5	0.8
Patient	95.6	3.3	1.1

Fibroblast at cell passage 18			
Individual	**% live cells**	**% necrotic cells**	**% apoptotic cells**
Control 1	89.8	6.5	3.7
Control 2	83.0	6.5	10.5
Patient	83.7	5.8	10.5

Figure 31: (**A**, **B**, **C**) Growth curve graphs at different cell passages for three fibroblast lines: one index patient and two healthy controls with matching age and gender. (**D**, **E**, **F**) Representative images after B-gal staining of the three fibroblast lines used in the assay. (**G**, **H**) Graphs showing the quantification of senescent cells after B-gal staining. (**I**) Table showing the percentage of live, necrotic and apoptotic cells for the three fibroblast lines in exam at different cell passages calculated after flow-cytometry analysis.

Discussion

Role of its 5’ terminal region in biogenesis of hTR and telomerase activity

The 5’ terminal region of hTR contains seven guanine tracts that are able to fold into a parallel rG4 and are conserved in a variety of mammalian species [314]. Besides the lack of these ≈40 nt upstream of the template region in the TRs of certain species, such as the murine telomerase RNA, this does not preclude the possibility that when present, this region possesses a regulatory function [315]. In human telomerase RNA, the nucleotides between position +18 and +37 base pair with the nucleotides between positions +187 and +208 to form the P1 helix upstream of the template region [141, 142]. While the P1 helix has been ascribed a critical role in template boundary definition in human, other species appear to use alternative mechanisms [316]. Furthermore, Li et al. [317] demonstrate interactions between the first 17 nt of hTR and two internal regions that appear to modulate activity of the enzyme. The same group also demonstrated that a truncation of hTR at the 5′- end results in an enzyme with increased activity *in vitro*, implicating the region possesses an intrinsic negative regulatory role [317]. In recent years, multiple protein have been found to interact specifically with this region of hTR. The helicase DHX36 recognizes the rG4 structure formed at the 5’ end of hTR and unwinds it [143, 289, 290]. Booy et al. propose that DHX36 promotes the P1-helix formation on hTR by unwinding the rG4 and linearizing the sequence involved in the base pairing forming the P1-helix itself. Additionally, they showed that DHX36 can recognize a rG4 involving exclusively the first 17 nt of hTR, therefore coexisting with the P1-helix and possibly suggesting that DHX36 may play a role in telomerase regulation independent by the P1-helix formation [290]. Xu et al. proved that the heterogeneous nuclear ribonucleoproteins (hnRNP) F, H1, and H2 also interact with the 5’ terminal region of hTR, but contrary to DHX36, these protein bind when this region is linear and not folded into a rG4. They also demonstrated that hnRNP F/H plays an important role in modulating telomerase activity and telomere length. Moreover, hnRNP F/H depletion impairs cell proliferation, and induces stem cell senescence, while hnRNP F/H overexpression delays stem cell senescence [305].

In this thesis, I sought to elucidate the regulatory function of this quadruplex prone region at the 5′ end of hTR by investigating the stability and activity of two disease related mutants of hTR, G2C-hTR and G11T-hTR. Subsequently, to understand if the observed activity phenotype of the hTR mutants was a result of interference with the interaction of binding partners of hTR that specifically recognize this region, we tested the effect in stability of hTR and telomerase activity after depletion and overexpression of DHX36 and hnRNPH1. I showed that both hTR mutants, G2C and G11T, are expressed at a comparable level to WT-hTR, suggesting that they do not affect the stability of this RNA (Figure 15, 17 and 20). Interestingly, both mutants of hTR displayed a strong reduction in elongation products accumulation (parameter used as a proxy to assess telomerase activity) without affecting the processivity of telomerase (Figure 16, 18), suggesting that both mutants of hTR impair the ability of telomerase to engage in successful elongation. Such impairment can be explained by two different mechanisms. On one hand, these specific mutants of hTR can assume an aberrant folding structure that does not interfere with the stability of the RNA, but weakens or disrupts the interaction with the protein components of the telomerase RNP complex. Alternatively, these mutants of hTR can still assemble into telomerase RNP complexes, but they interfere with the binding of telomerase to a telomeric sequence. Ultimately, both mechanisms would result in a reduction in the pool of functional telomerase complexes, which correlates with the reduced elongation product accumulation observed. Nevertheless, when either of these mutant telomerase complexes engages in the binding of the telomeric primers used in the DTAA, it is able to add a number of telomeric repeats comparable to WT telomerase. In turns, once the initial engagement of telomerase happened, either mutation does not affect the elongation capacity of telomerase.

Depletion of DHX36 also resulted in strongly reduced telomerase activity (Figure 13), and when combined with the overexpression of either mutant of hTR, G2C or G11T, an additive effect with further decreased telomerase activity was observed (Figure 16, Figure 18). These results suggest that both DHX36 function and the intrinsic secondary structure of the 5' end of hTR are independent modulators of telomerase activity. Interestingly, the re-expression of DHX36 in the knock-out cells was not able to rescue the telomerase activity detected for cells expressing WT-hTR (Figure 14), but it did so for cells expressing the G2C mutant hTR (Figure 16). The G11T mutant of hTR was unaffected by the overexpression of DHX36 both in Parental and DHX36 knock-out cells (Figure 18). It is possible that the decrease in telomerase activity observed upon DHX36 depletion is an indirect effect, because of the failed rescue after DHX36 re-expression. Nevertheless, the partial increase in telomerase activity detected in cells expressing G2C-hTR, open the possibility for alternative explanations. The timeframe and the conditions of the experiment may not be optimal to allow DHX36 to perform its function on telomerase, making us unable to detect a rescue in activity, unless we are in a sensitized background like in cells expressing the G2C mutant hTR.

In contrast to what was observed by Xu et al. [305], for all tested conditions, namely presence or depletion of DHX36 and expression of WT or G2C mutant hTR, in my hands partial knockdown of hnRNPH1 by siRNA always resulted in an increase of telomerase activity (Figure 19). Conversely, mild overexpression of hnRNPH1 resulted in a decrease of telomerase activity (Figure 21). These results suggest that hnRNPH1 is an inhibitor or telomerase activity. The discrepancy between my data and the work published by Xu et al. [305] may be due to the difference in the used cell line, the different transfection conditions and the assay chosen do detect telomerase activity. Further investigation will be necessary to discern the general role of hnRNPH1 in modulating telomerase activity.

To sum up the discoveries shown in this thesis, concerning the modulation of telomerase activity performed by the structure of the very 5' terminal region of hTR and the association of the proteins DHX36 and hnRNPH1, a model is presented in Figure 32.

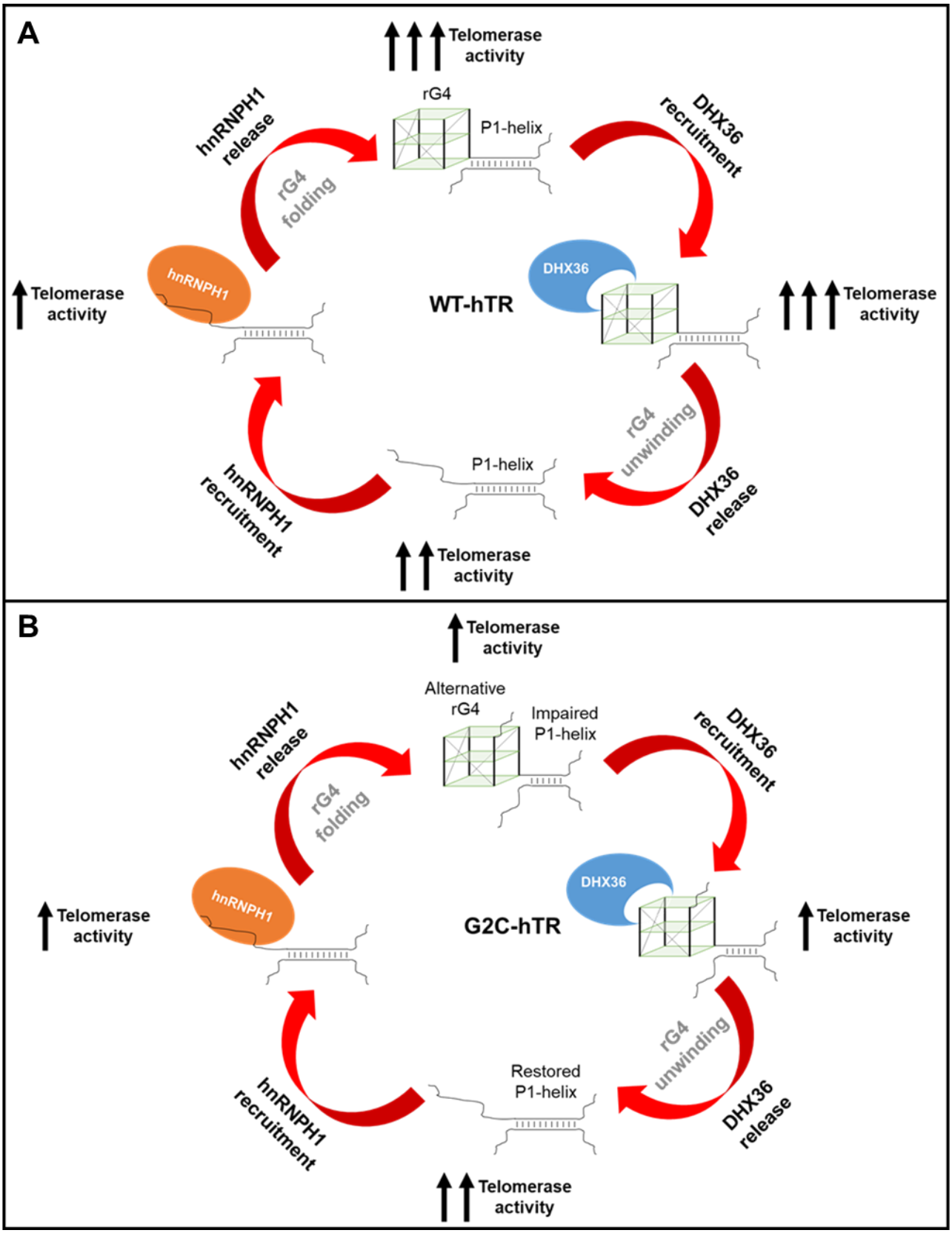

Figure 32: (**A**) Model showing the dynamic cycle of rG4 folding and unwinding at the 5' end of WT-hTR, related to the detected telomerase activity for each structural status of hTR. (**B**) Model showing the dynamic cycle of rG4 folding and unwinding at the 5' end of the G2C-hTR mutant, related to the detected telomerase activity for each structural status of hTR.

Consequences of template mutants of hTR

It has been published that mutations in the template region of hTR may lead to the incorporation of aberrant telomeric repeats into telomeres [310]. This suggests that template mutants of hTR are still able to associate with theirs protein interactors and form functional telomerase RNP complexes. Nevertheless, it remains unclear if mutations within the template region of hTR generally affect its stability and/or telomerase activity.

By overexpressing WT-hTR and the two template mutants A48G-hTR and C50A-hTR in telomerase negative VA13 cells, I showed that all three version of hTR are expressed at similar levels (Figure 22). Additionally, using an RNA sample isolated from blood cells of a patient carrying the C50A-hTR mutation, RNAseq analysis performed by other lab members demonstrated that there is a similar level of both hTR species (data not shown). These data suggest that template mutants of hTR do not have impaired RNA stability and support telomerase RNP assembly. Both template mutants A48G-hTR and C50A-hTR displayed severely impaired telomerase processivity (Figures 23 to 26), suggesting that template mutations on hTR do not affect the initial ability of telomerase to bind telomeric DNA. The general effect of the tested template mutants of hTR is a strong bias towards dissociation between telomerase and the telomeric DNA after few repeat additions, rather than translocation of telomerase to allow for further repeat additions. It is possible that a steric hindrance within the active site of telomerase, caused by the mismatch between the mutated nucleotide in the template region of hTR and the telomeric DNA, is responsible for favoring the dissociation of the telomerase RNP complex.

Besides the general lack of processivity, the two template mutations also show specific phenotypes. A48G-hTR is extremely unprocessive, being able to add only a single mutated full telomeric repeat before dissociating (Figure 23). Possibly the dC – rA mismatch exactly in the middle of five nucleotides base-pairing between the template region of hTR and the telomeric DNA sequence is strongly favoring the dissociation of the RNP complex, not allowing further elongation. Interestingly, WT telomerase displays severely reduced activity when extending a mutated primer that incorporates the A48G-derived mutation (Figure 23 and Figure 24). This is probably due to the presence of the aforementioned dC - rA mismatch within the active site of the enzyme. The addition of a first WT telomeric repeat by WT telomerase to the mutated primer is clearly very inefficient, but once it has happened, further elongation can take place with no further complications.

The C50A-hTR mutant presents an additional issue to telomerase elongation: the establishment of a rA – dT base pair between the template region of hTR and the telomeric DNA, which act as an intrinsic stop signal for nucleotides addition, one position earlier compared to the base pairing alignment of WT-hTR [136]. This leads to the C50A-hTR mutant telomerase adding a first telomeric repeat that is only five nucleotides long and terminates with a dA nucleotide (GTTTA) (Figure 29). After the first repeat is added, the mutant telomerase is able to translocate and add few more telomeric repeats before dissociating, which will be six nucleotides long, but still terminating with a dA nucleotide (GGTTTA) (Figure 29). In Figure 33, a model elucidating the elongation mechanism of WT-telomerase (Figure 33A) and the un-processive elongation performed by C50A-hTR mutant telomerase (Figure 33B) is depicted.

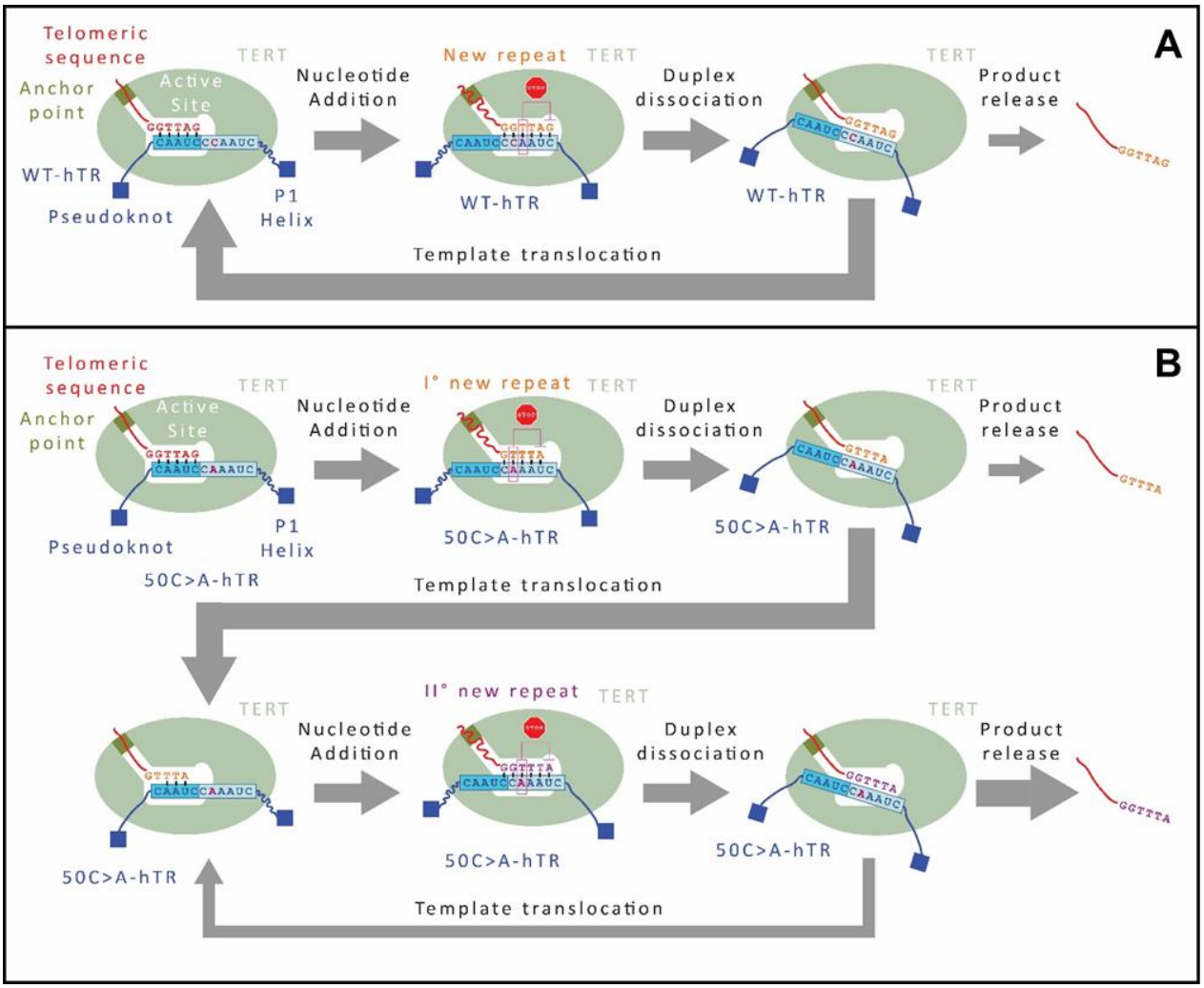

Figure 33: (**A**) Schematic showing the elongation mechanism of WT telomerase. (**B**) Schematic showing the elongation mechanism of mutant C50A-hTR telomerase.

The elongation of a mutated primer incorporating the C50A-hTR derived mutation by WT telomerase depends on sequence permutation of the last six nucleotides that constitute the primer itself. For the mutant permutations (GTTTAG) and (TTTAGG), WT telomerase acts with the same efficiency showed with the respective WT permutations (GGTTAG) and (GTTAGG) (Figure 27). For the following three mutant primer permutations: (TTAGGT), (TAGGTT) and (AGGTTT); WT telomerase acts once again with the same efficiency displayed with the respective WT permutations, respectively (TTAGGG), (TAGGGT) and (AGGGTT), with the difference that the very first repeat added will be one nucleotide shorter than expected (Figure 27). This is due to a necessary sliding of one nucleotide backwards between the alignment of hTR and the mutated telomeric DNA to allow further elongation, in order to obtain a dT – rA base pair with the very last nucleotide of the primer. The elongation of the mutant primer permutation (GGTTTA) by WT telomerase, which interestingly resembles the sequence that would be left after elongation performed by the C50A-hTR mutant telomerase, is the only permutation that shows about half of the products accumulation compared to the respective WT permutation (GGGTTA) (Figure 30). The canonical mechanism would be first, the addition of a single dG to the primer (band +1 on the DTAA gel), followed by repetitive six nucleotides-long repeats addition (bands +7, +13, +19, etc…). Surprisingly, WT telomerase adds very inefficiently the first dG nucleotide to the (GGTTTA) mutant repeat. Furthermore, equally intense bands that differ in length for one nucleotide (+6 and +7, +12 and +13, +18 and +19, etc…) appear on the DTAA gel under these conditions (Figure 30). This suggests that alternative alignments between WT-hTR and this mutant primer must take place, allowing the direct addition of a first 6-nucleotide or 7-nucleotide long repeat (Figure 28).

An additional explanation for this unusual bands pattern is suggested by the appearance of a weak band at position 0 in the DTAA gels (Figure 27 and Figure 30), implying that, at least *in vitro*, a portion of the primer population is subjected to 3' resection. The subsequent addition of nucleotides including radioactive dGTP makes these putative resected primers detectable on the gel. The restoration of a WT-like repeat at the end of the primers could explain the observed bands pattern of +6 and +7, +12 and +13, etc. Collectively, the data presented in this thesis regarding the *in vitro* characterization of C50A-hTR indicate that this mutant of hTR has two negative effect on telomerase activity: 1) C50A-hTR mutant telomerase is severely un-processive compared to WT telomerase; 2) once a mutant telomeric sequence has been added into telomeres, they become a poor substrate for elongation even by WT telomerase.

Lastly, we began to characterize the fibroblasts isolated from a patient diagnosed with DC, who is carrying the C50A-hTR mutation and the Q1178X non-sense mutation in the RTEL1 gene, both in heterozygosis. Our collaborators at the University Medical Center of Mainz are responsible for the clinical phenotyping of the index patient and of other member of its family. Other lab members are analyzing different sequencing data, from the patient and its relatives, to map the hereditability of these mutations within this family tree and the incorporation of mutant telomeric repeats within the telomeres of these individuals. I started with the characterization of cell viability of these patient-derived cells. I showed that the patient fibroblasts have a reduced cell growth compared to two healthy individuals of the same age and gender (Figure 31). I proved that this phenotype is mainly due to premature senescence of these cells, and it is not associated with an increase in cell death by apoptosis (Figure 31). Further analysis, discussed in the next chapter, will be necessary to gain a comprehensive picture of the combinatorial effects that these two mutations have on telomere maintenance.

Future Work

Role of its 5’ terminal region in biogenesis of hTR and telomerase activity

Because of the high number of guanosine within the 5’-terminal region of hTR, substitution of only one of those still supports rG4 formation. Collecting additional information about the secondary structure assumed by the 5’ end of WT-hTR and the mutants examined in this thesis, G2C and G11T-hTR, would help clarifying to which extend rG4 formation may invade the P1-helix forming region and which guanosines are actually involved in rG4 formation. Combining selective mutation of hTR with techniques like Selective 2′ Hydroxyl Acylation analyzed by Primer Extension (SHAPE) [318] can give us the knowledge needed to create a realistic structural model for this region, and predict which guanosines are critical to prevent the rG4 to spreading into the P1-helix forming region. By achieving a same level of overexpression between WT-hTR and the G2C and G11T mutants of hTR, we concluded that these mutants do not have major instability issues. We could check if expressing those mutants at an endogenous level, by mutating all the endogenous loci of hTR within a cell line, is sufficient to support cell viability in a non-overexpressing context.

To understand better the role of DHX36 in modulating telomerase activity, the rescue experiment with re-expression of such protein in the respective KO cell line used in this study, should be performed trying to match a WT protein level of DHX36, rather than an overexpression. This can be achieved by using a construct that expresses DHX36 using its endogenous promoter, or titrating the amount of inducing agent to use with an inducible construct, in order to match the endogenous level of DHX36. Additionally, the re-expression of DHX36 should be done prior to hTR and TERT overexpression, rather than simultaneously, so that once hTR starts being transcribed inside a cell, there is already a DHX36 pool ready to bind it. The binding affinity of DHX36 for G2C and G11T mutants of hTR should also be addressed, and can be tested by RNA-immunoprecipitation.

These mutants are still able to form rG4, but they may exhibit a different affinity for DHX36, due to the competition for the binding of the same region by hnRNP F/H and the contention for the same guanosines between rG4 and P1-helix formation. To further explore the consequences to telomerase activity of hnRNP H/F association with hTR, different approaches can be pursued. A further characterization of the modulator effect of hnRNPH1 on telomerase activity can be done by establishing better knock-down and overexpression conditions. Besides the effect on product accumulation by DTAA being significantly different to WT, I was only able to achieve partial reduction (0.5 fold) and partial increase (1,5 fold) of the hnRNPH1 protein levels(Figure 19 and Figure 20). Once stable knock-down and overexpression conditions for hnRNPH1 are established, the effect on the stability of hTR, either WT or mutant, expressed at endogenous level can be checked with techniques like qPCR and Northern blot. Using a similar set of experiments like the ones showed in this thesis, the effect of hnRNPH2 and hnRNPF on telomerase activity can be tested, to see if the observed phenotype of hnRNPH1 is specific for this protein or a general property of all three hnRNP H/F proteins. Similarly to what was suggested for DHX36, binding affinity for hnRNPH1 can be assayed by RNA-immunoprecipitation. The mutant G2C-hTR is particularly interesting, because of the difficulty in predicting the effect on affinity for hnRNPH1. On one hand, this stretch is likely to be linear and not involved in a rG4, therefore making it more accessible for binding hnRNPH1. On the other hand, this same guanosine stretch is the major binding site on hTR for hnRNPH1, and having the substitution of one G with a C could make the recruitment of the protein less efficient.

Consequences of template mutants of hTR

In this thesis, extensive biochemical characterization of the C50A-hTR template mutant was shown. Following the same experimental outline, the biochemical characterization of the A48G-hTR mutant, as well as for other disease-associated template mutants of hTR, can be achieved. An intriguing follow up would be to genetically modify cell lines, making them express these mutants in homozygosis or heterozygosis at endogenous levels and monitor how this affects hTR stability, cell viability and telomere length over time, using techniques like, qPCR, growth assays, senescence staining, and Southern blot.

We just began the *in vivo* characterization of the patient fibroblasts with the data I showed in this thesis. Taking advantage of the next generation sequencing technologies available to date, we could sequence the telomeres of the index patient, who is carrying the C50A-hTR and the Q1178X-RTEL1 mutations, and of its relatives, whose family tree is depicted in Figure 34, to map the spread of the mutant repeats across the telomeres' sequence itself. This would allow us to identify if the mutant repeats are evenly spread or if they cluster in any specific region of the telomere. Sequencing the telomeres of the cousin of the index patient would be of particular interest, given that she does not have any mutation herself, but her mother, and possibly at least one grandparent, was carrying the C50A template mutant of hTR (Figure 34). With this approach, we could be able to evaluate for how long mutant telomeric repeats within the telomeres sequence are inherited across generations.

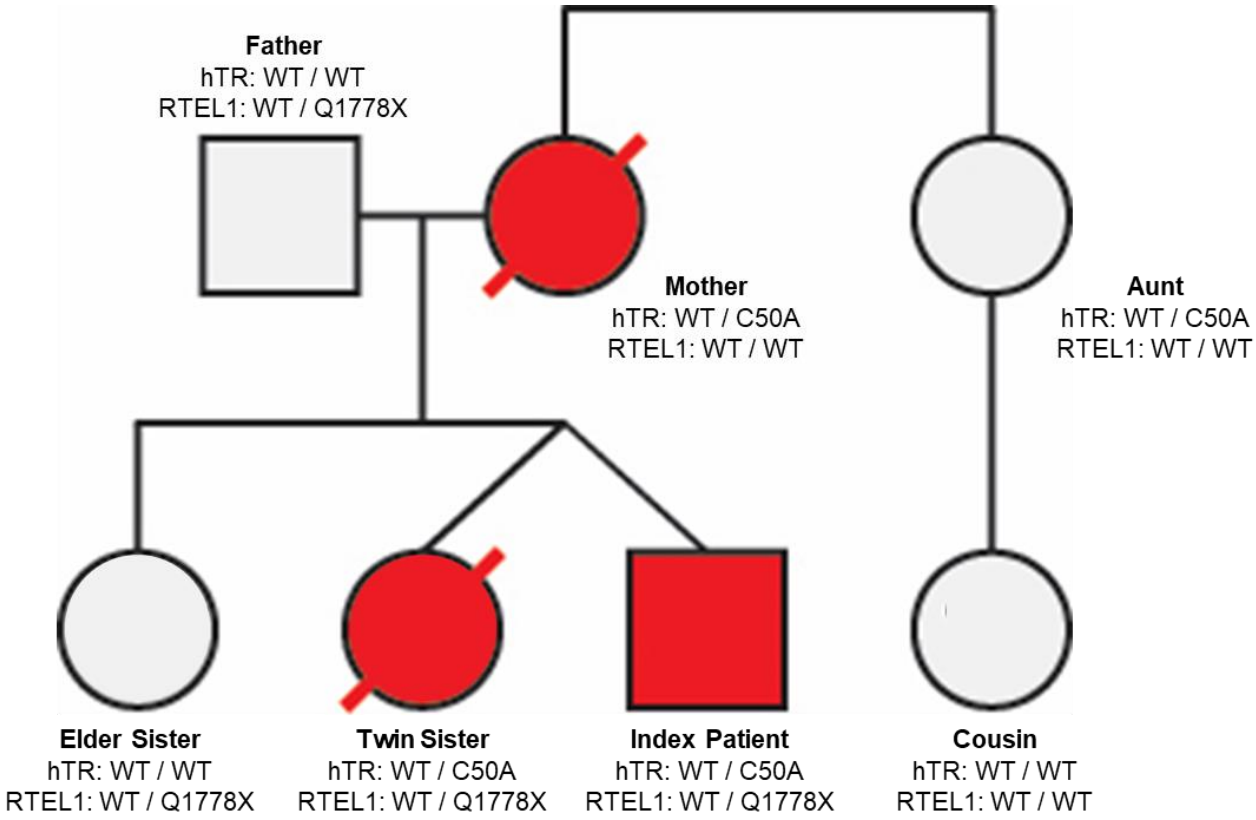

Figure 34: Immediate family tree of our index patient. RTEL1 and hTR genotype are indicated for each family member. Circle = Female; Square = Male; Transversal Bar = Deceased Individual; Red = Index Patient.

Telomere shortening can be the result of different processes, like insufficient telomere elongation after cell division by a sub-functional telomerase RNP complex; massive loss of telomeric sequence in the form of T-circle as consequence of prolonged replication fork stalling; loss of telomere portions as result of DSBs occurring at unprotected telomeres. To understand which of these processes are responsible for the telomere shortening detected in our index patient, I would continue with the *in vivo* characterization of his fibroblasts, as well as characterizing fibroblasts from the other members of this family willing to give samples. I would follow up by checking if their cells present higher levels of DNA damage compared to healthy control cells, and if the association between telomeres and known shelterin components is compromised. I would do so using microscopy techniques, combining telomere FISH, possibly using different probes specific for WT and mutant telomeric repeats, with immunofluorescence, staining for DNA damage associated proteins, like phosphorylated-ATM or the phosphorylated γH2A.X histone, and shelterin proteins like TRF1, TRF2 and POT1. This approach would allow us to detect possible co-localization of DNA damage at telomeres, potential loss of shelterin binding to telomeres, as well as eventual differences in the overall telomere clustering and localization within the nuclear architecture. Collectively, all these newly-gathered information about the telomere status in the cells isolated from the members of our index patient's family tree will help us to clarify the molecular mechanism underlying the telomere shortening detected in these individuals.

Material and Methods

Cell Cultures

HEK293T-Parental and HEK293T-DHX36 KO cells were grown in DMEM (Fisher Scientific, #11500596), 10% fetal bovine serum (FBS; LGC standards, #ATCC-30-2020) and 2mM L-Glutamine (Fisher Scientific, #25030081). VA13 cells were grown in in EMEM (Fisher Scientific, #11440335), 10% fetal bovine serum (LGC standards, #ATCC-30-2020) and 2mM L-Glutamine (Fisher Scientific, #25030081). Fibroblasts were grown in IMDM (Fisher Scientific, #12589059), 15% fetal bovine serum (LGC standards, #ATCC-30-2020) and 100 U/mL Penicillin – 100µg/mL Streptomycin (Fisher Scientific, #11548876). All cells were maintained at 37°C, 5% CO_2 and 20% O_2 and splitted once ≈95% confluence was reached. The cells were detached from the dishes for splitting with TrypLE™ (Fisher Scientific, #12604021), counted with a THOMA chamber (Carl Roth, #T732.1), washed with pre-warmed 1X DPBS (Fisher Scientific, #10444402) and centrifuged at 200 rcf for 5 minutes at RT. Cultures were examined under an inverted microscope to determine confluence and viability.

Viability Assay

2,5 x 10^4 fibroblast cells were seeded into each well of a 12-wells dish with 1 mL of complete medium. Every 24h, for four consecutive days, the cells within three wells were separately collected and counted twice with a THOMA chamber (Carl Roth, #T732.1). A growth curve was constructed by averaging the total number of cells of the three wells.

β-Galactosidase Senescence Staining

5 x 10^4 fibroblast cells were seeded into a cover-slip glass placed into a well of a 6-wells dish with 2 mL of complete medium. After 72h, the growth media was removed, and the cells were rinsed once with 1 mL of 1X DPBS (Fisher Scientific, #10444402). 1 mL of 1X Fixative Solution was added to each well, and the dish was incubated for 10 -15 minutes at RT. The plate was rinsed twice with 1X DPBS and 1 mL of the β-Galactosidase Staining Solution was added to each well. The dish was sealed with parafilm (VWR, #291-1213) and incubated at 37°C at least overnight in a dry incubator without CO_2. Finally, the cover-slip glass was removed from the dish and quickly washed by dipping into ddH_2O, before mounting it on a microscopy glass with mounting media (Agilent, #S302380-2). Pictures of the cells were taken with an upright light microscope (DM2500, Leica) and analyzed with ImageJ software. All the solutions used here were prepared according to the manufacturer protocol of the staining kit (Cell Signalling Technology, #9860S)

Apoptosis Staining

10^6 fibroblast cells were seeded into a 100mm dish with 10 mL of complete medium. After 48h, the cells were collected and washed twice in Hanks Balanced Salt Solution (HBSS, Fisher Scientific, #11530476). Then, the cells were re-suspended to a final concentration of 10^6 cells/mL in HBSS. 1 mL of cell suspension was transferred to a flow cytometry tube (Fisher Scientific, #10186360). 1 µL of Component A and 1 µL of Component B were added to the cell suspension and the tube was incubated at RT for 5 minutes before analysis, protected from light. The sample was analyzed on a BD LSRFORTESSA SORP flow cytometer. All the solutions used here were prepared according to the manufacturer protocol of the staining kit (Fisher Scientific, #10630930).

Super-Telomerase cells preparation

Different amounts of cells were seeded into 100mm dishes: 10^6 cells for VA13, 2 x 10^6 cells for HEK293T-Parental and 2.5 x 10^6 cells for HEK293T-DHX36 KO. After 24h, the media was removed from the dishes and the cells were washed once with pre-warmed Opti-MEM (Fisher Scientific, #15392402). The media was then replaced with 10 mL of pre-warmed Opti-MEM (Fisher Scientific, #15392402) and the cells were left into the incubator during transfection cocktail preparation.

For each dish, 750 µL or transfection cocktail were prepared into a 1.5 mL tube as follows:

- 1 µg of TERT-expressing plasmid (pcDNA6-3HA-hTERT);
- a total of 5 µg of hTR-expressing plasmid (pBS-U1-hTR, either WT, mutant or a combination 1:1 of both);
- 1 µg of either DHX36-expressing plasmid (pcDNA3.1-DHX36) or hnRNPH1-expressing plasmid (pcDNA-hnRNPH1);
- a volume in µL of transfection reagent (Promega, #E2312) equal to 3 times the total amount in µg of added plasmids (independently of what they are expressing, 1 µg → 3 µL);
- Opti-MEM to a final volume of 750µL.

The transfection cocktail was incubated at RT for 20 minutes, before adding it to the cells in a drop-wise manner. After 4h, 2 mL of per-warmed FBS (LGC standards, #ATCC-30-2020) was added to each dish. After 48h, the media was replaced with complete medium and after other 24h the cells were detached with TrypLE™ (Fisher Scientific, #12604021), pelleted at RT by centrifugation at 200 rcf for 5 minutes and whole-cells extract was made.

Transient siRNA knock-down coupled with Super-Telomerase cells preparation

Different amounts of cells were seeded into 100mm dishes: 10^6 cells for VA13, 2 x 10^6 cells for HEK293T-Parental and 2.5 x 10^6 cells for HEK293T-DHX36 KO. After 24h, the media was removed from the dishes and the cells were washed once with pre-warmed Opti-MEM (Fisher Scientific, #15392402). The media was then replaced with 10 mL of pre-warmed Opti-MEM (Fisher Scientific, #15392402) and the cells were left into the incubator during transfection cocktail preparation. For each dish, 750 µL or transfection cocktail were prepared into a 1.5 mL tube as follows:

- 1 µg of TERT-expressing plasmid (pcDNA6-3HA-hTERT);
- a total of 5 µg of hTR-expressing plasmid (pBS-U1-hTR, either WT, mutant or a combination 1:1 of both);
- 1 µg of either DHX36-expressing plasmid (pcDNA3.1-DHX36) or hnRNPH1-expressing plasmid (pcDNA-hnRNPH1);
- a volume in µL of transfection reagent equal to 3 times the total amount in µg of added plasmids (independently of what they are expressing);
- Opti-MEM to a final volume of 750µL.

The transfection cocktail was incubated at RT for 20 minutes, before adding it to the cells in a drop-wise manner. After 4h, 2 mL of per-warmed FBS (LGC standards, #ATCC-30-2020) was added to each dish. After 24h, the media was removed from the cells and replaced with complete medium. Two mixes were prepared: one 2 mL tube per dish containing 970 µL of Opti-MEM (Fisher Scientific, #15392402) and 30 µL of transfection reagent (Thermo Fisher Scientific, #13778150); a second 1.5 mL tube per dish containing 990 µL of Opti-MEM (Fisher Scientific, #15392402) and 10 µL of 20 µM siRNA. The second mix was completely transferred to the 2 mL tube containing the first mix and incubated at RT for 20 minutes. After this time, the 2 mL of transfection cocktail was added to the dishes in a drop-wise manner. After 48h the cells were detached with TrypLE™ (Fisher Scientific, #12604021), pelleted at RT by centrifugation at 200 rcf for 5 minutes and whole-cells extract was made.

CHAPS whole-cells extracts preparation

Cell pellets were thoroughly re-suspended by pipetting with 1:1 V/V of CHAPS buffer [0,5% m/V CHAPS (Merck, #C5070), 50 mM Tris-HCl at pH = 7.5, 50 mM KCl, 1 mM $MgCl_2$, 1 mM EGTA at pH=8, 10% V/V Glycerol, 5 mM DTT, 1 mM PMSF in DMSO] until an homogeneous solution was obtained. The cells were lysed by rotating the suspension at 10 rpm at 4 °C for 1 h. The lysate was cleared by centrifugation at 16'000 rcf at 4 °C for 20 min. The cleared lysate was then transferred to a fresh 1.5 mL tube, snap froze in liquid nitrogen ad stored at -80°C. An aliquot of the lysate was used to measure its protein concentration by Bradford assay.

Bradford Assay

CHAPS extract were diluted 1:5 with CHAPS buffer and 1 µL was transferred to a new 1.5 mL tube. 5 µL of ddH_2O and 994 µL of Bradford reagent (Bio-Rad, #5000205) were added to the extract and incubated at RT for 2 minutes, before measuring the sample absorbance at 595 nm with a UV-Vis spectrophotometer (Amersham Biosciences, Ultrospec 2100 pro). The protein concentration of the sample was extrapolated from a standard curved made with BSA (Bio-Rad, # 5000201), where each standard contained: 5 µL with different concentrations of BSA dissolved in ddH_2O, 1 µL of CHAPS buffer and 994 µL of Bradford reagent (Bio-Rad, #5000205).

Western blotting

5 µL of CHAPS extracts (1 µg/µL) were diluted 1:1 with 5 µL of 2X SDS loading buffer [4X LDS Sample Buffer (Fisher Scientific, #11549166), 100mM DTT (Fisher Scientific, #10386833), 4% SDS (Carl Roth, #8029.3)] and heated at 95°C for 5 minutes before loading them into a gradient 4 - 12% polyacrylamide gel (Fisher Scientific, #10338442). The samples were run on the gel for at least 1h at 150V constant in 1X MOPS buffer (Fisher Scientific, #11589156) at RT. After running, the gel was assembled into a "sandwich" between a sponge and two sheets of Whatman paper (Fisher Scientific, #11330744) per side, in direct contact with a nitrocellulose membrane (Merck, #GE10600012). The sample were transferred to the nitrocellulose membrane for 1h at 100V constant at 4°C in 1X Transfer Buffer [25 mM Tris Base (Fisher Scientific, #10376743), 192 mM Glycine (Fisher Scientific, #10070150), 20% Methanol V/V (Carl Roth, #0082.3), pH = 8.3]. The membrane was then blocked for 1h at RT with gentle shaking in of Blocking solution [5% Milk powder (Carl Roth, #T145.2) in 1X TBST (20 mM Tris-Base (Fisher Scientific, #10376743), 150 mM NaCl (Merck, #S9888), 0.1% V/V Tween™ 20 (Fisher Scientific, #10113103), pH=7,6]. The blocked membrane was next incubated overnight at 4°C with gentle shaking with the indicated primary antibodies diluted in Blocking solution. Subsequently, the membrane was washed three times with 1X TBST at RT for 5 minutes with gentle shaking, before being incubated for 1h at RT with gentle shaking with the indicated secondary antibodies HRP-conjugated diluted in Blocking solution. Finally, the membrane was washed again three times with 1X TBST at RT for 5 minutes with gentle shaking, before developing of the signal with Clarity Max Western ECL Substrate (Bio-Rad, #1705062). The developed membrane was then imaged with ChemiDoc™ MP (Bio-Rad, #17001402) and the resulting images were analyzes with the Image Lab software (Bio-Rad).

RNA isolation from CHAPS extract

250 to 500 µg of protein CHAPS extract (determined by Bradford Assay) were diluted in 100 µL of ddH_2O. 25µL of Stop Buffer [100mM Tris-HCl at pH = 7.5, 200mM EDTA (Fisher Scientific, #10618973), 10 mg/mL proteinase K (Merck, #P2308), 2.5% m/V SDS (Carl Roth, #8029.3)] were added to the sample (1/4 volume). The sample were incubated for 15 minutes at 50°C with gentle shaking. 175µL of ddH_2O were then added to the sample, following by the addition of 300µL (1 volume) of Phenol:Chloroform:Isoamyl Alcohol (25:24:1, pre-equilibrated with 50mM NaOAc pH = 5.2, Merck, #P2069). The sample was thoroughly mixed and then centrifuged at 15'000 rpm for 7 minutes at RT. 270µL of supernatant were transferred to a new 1.5 mL tube and 1µL of Glycogen (5 mg/mL, Fisher Scientific, #AM9510) was added. 675 µL (2.5 volumes) of ice-cold 100% Ethanol and 27µL (1/10 volume) of 3M NaOAc (Merck, #W302406) at pH = 5.2 were added to the sample before overnight precipitation at -20°C. The next day, the sample was centrifuged at 13'500 rpm for 15 min at 4°C and the supernatant was discarded. The obtained RNA pellet was washed with 1 mL of ice-cold 70% EtOH and centrifugation at 13'500 rpm for 3 minutes at 4°C. The surnatant was discarded, the RNA pellet was air-dried and finally dissolved in 168 µL of ddH_2O + 2 µL of RNasin (Promega, #N2615). A DNase treatment was performed by addition of 20 µL of TURBO DNase Buffer 10X and 10 µL of TURBO DNase (2 U/µL, Fisher Scientific, #10722687), incubating the sample at 37°C for 1h. Subsequently, 100 µL of ddH_2O and 300 µL (1 volume) of Phenol:Chloroform:Isoamyl Alcohol (25:24:1, pre-equilibrated with 50mM NaOAc pH = 5.2, Merck, #P2069) were added to the sample. The sample was thoroughly mixed and then centrifuged at 15'000 rpm for 7 minutes at RT. 270µL of supernatant were transferred to a new 1.5 mL tube and 1µL of Glycogen (5 mg/mL, Fisher Scientific, #AM9510) was added. 675 µL (2.5 volumes) of ice-cold 100% Ethanol and 27µL (1/10 volume) of 3M NaOAc (Merck, #W302406) at pH = 5.2 were added to the sample before precipitation at -20°C for 4h. The sample was centrifuged at 13'500 rpm for 15 min at 4°C and the supernatant was discarded. The obtained RNA pellet was washed with 1 mL of ice-cold 70% EtOH and centrifugation at 13'500 rpm for 3 minutes at 4°C. The surnatant was discarded, the RNA pellet was air-dried and finally dissolved in 87 µL of ddH_2O + 1 µL of RNasin (Promega, #N2615). A second DNase treatment was performed by addition of 10 µL of TURBO DNase Buffer 10X and 2 µL of TURBO DNase (2 U/µL, Fisher Scientific, #10722687), incubating the sample at 37°C for 30 minutes. This step is necessary to get reed of all the plasmid DNA in the sample after the cells were subjected to transfection. Subsequently, 200 µL of ddH_2O and 300 µL (1 volume) of Phenol:Chloroform:Isoamyl Alcohol (25:24:1, pre-equilibrated with 50mM NaOAc pH = 5.2, Merck, #P2069) were added to the sample. The sample was thoroughly mixed and then centrifuged at 15'000 rpm for 7 minutes at RT. 270µL of supernatant were transferred to a new 1.5 mL tube and 1µL of Glycogen (5 mg/mL, Fisher Scientific, #AM9510) was added. 675 µL (2.5 volumes) of ice-cold 100% Ethanol and 27µL (1/10 volume) of 3M NaOAc (Merck, #W302406) at pH = 5.2 were added to the sample before overnight precipitation at -20°C. The next day, the sample was centrifuged at 13'500 rpm for 15 min at 4°C and the supernatant was discarded. The obtained RNA pellet was washed with 1 mL of ice-cold 70% EtOH and centrifugation at 13'500 rpm for 3 minutes at 4°C. The surnatant was discarded, the RNA pellet was air-dried and finally dissolved in 16 µL of ddH_2O. 1µL of the sample was used for NanoDrop (Thermo Fisher Scientific, #ND-ONE-W) quantification, before snap-freezing it in liquid nitrogen and storage at -80°C.

qPCR

Between 750 ng and 2 µg of RNA were retrotranscribed in a 20µL using the Invitrogen™ SuperScript™ VILO™ cDNA-Synthesis kit (Fisher Scientific, #11754250). The thermo-cycler settings were as follows: 25°C for 10 minutes; 42°C for 1h; 85°C for 5 minutes; hold at 4°C. After the retrotranscription, 1 µL of RNAse H (NEB, #M0297) was added to the samples and they were incubated at 37°C for 20 minutes. RNase H inactivation was carried out by incubating the samples at 65°C for 20 minutes. The cDNA samples can be stored at -20°C. Quantitative real-time PCR was performed using 2 µL of cDNA sample diluted 1:1 with ddH_2O, 500nM each forward and reverse primers specific to the gene of interest and a FastMix™ with Low-ROX reference dye (VWR, #733-1390). The samples were transferred into a 384-well plate (Fisher Scientific, #10005724) sealed later with an adhesive film (Fisher Scientific, #10299204). The plate was loaded into a ViiA 7 Real-Time PCR System and the results were analyzed with the proprietary ViiA™ 7 Software. The machine settings were as follows: 2 minutes at 50°C, 10 minutes at 95°C, 40 cycles of 95°C for 15 seconds followed by 1 minute at 60°C, then 15 seconds at 95°C, 1 minute at 60°C and 15 seconds at 95°C. The temperature was variated with a speed of 1.6°C/second at all stages except the last change between 60°C and 95°C that was done with a speed of 0.05°C/second. Data collection of the fluorescence signal was done during the 1 minute step at 60°C for the data analysis and during the last temperature ramp at 0.05°C/second for the construction of the melting curve for each primer.

Direct telomerase activity assays (DTAA)

Direct telomerase activity assays were carried out for 30 minutes at 30°C in 20µL reactions. Reaction composition: variable amount of whole-cell CHAPS extracts, 1X reaction buffer [50 mM Tris–HCl (pH 8.0), 50 mM KCl, 1 mM spermidine (Merck, #S0266), 1 mM β-mercaptoethanol (Merck, #M3148), 1 mM $MgCl_2$], 1 mM dATP, 1 mM dTTP, 5.83 µM dGTP, 10 µCi of [a-32P]dGTP at 3000 Ci/mmol (Perkin Elmer, #NEG514H) and 0,7 µM of indicated telomeric primer. Reactions were stopped by the addition of 5 µL of 25 mM EDTA (Fisher Scientific, #10618973) and 5% SDS (Carl Roth, #8029.3). Trace amounts corresponding to 1000 cpm of a ^{32}P-labeled 14-mer DNA oligonucleotide were added as a recovery control. Products were ethanol-precipitated overnight. DNA pellets were re-suspended in 10 µL of 2X RNA Loading Dye (NEB, #B0363S) and heated to 95°C for 5 minutes. 5 µL were then loaded on a pre-warmed (1h at 80W in TBE1X) denaturing gel made with 12% Polyacrylamide 19:1 and 8 M Urea (Merck, #U5378) in 1X TBE [Tris/Borate/EDTA buffer: 0.1 M Tris Base (Fisher Scientific, #10376743), 0.1 M Boric Acid (Merck, #B6768), 2 mM EDTA (Fisher Scientific, #10618973)]. The samples were subjected to electrophoresis at 80W constant for 105 minutes. The gel was then assembled into a “sandwich” between a plastic film (VWR, #LONZ54746) and a sheet of Whatman paper (Fisher Scientific, #11330744) before drying under vacuum at 60°C for 45 minutes. Finally, the gel was incubated with a phosphorscreen in a cassette overnight in the dark. The phosphorscreen was then imaged with a Typhoon Scanner (GE healthcare, #29-187-191) and the image analyzed with the ImageJ software.

DTAA quantification

For G2C and G11T-hTR mutants, where no processivity alteration compared to WT-hTR is observed, the signal of the whole-lane is quantified drawing a rectangle which area completely enclose all the extension products detected for a specific lane. The same rectangle is moved across the gel to quantify the signal of each separate lane, which is first normalized for the recovery control and then further normalized over the wild-type sample.

For A48G and C50A-hTR mutants, in each lane, the counts for each telomerase band were obtained individually, normalized against the recovery control and normalized for the number of radiolabeled guanosines added in that specific extension product and then summed over the entire lane to obtain the total lane counts (TLCs). The data were then further normalized over the wild-type sample and expressed as relative engagement of telomerase between samples.

For processivity calculations, each telomerase band was individually quantitated, normalized against the loading control and normalized for the number of radiolabeled guanosines added in that specific extension product. For a band n, the percentage left behind (%LB) was calculated by adding to the count of band n the sum of counts for the bands underneath band n (corresponding to shorter repeats), all divided by the TLCs and multiplied for 100. Then ln(100 - %LB) was plotted versus the number of nucleotide added to the starting primer. Each lane was fit with a linear regression equation with slope m. The processivity value equals ln(2)/m.

Oligo Sequences

siRNAs	Sequence (5'>3')
siRNA Sense hnRNP H1	GGAGCUGGCUUUGAGAGGA[dT][dT]
siRNA Anti-sense hnRNP H1	UCCUCUCAAAGCCAGCUCC[dT][dT]
Primers	**Sequence (5'>3')**
GAPDH Forward primer for qPCR	ACATCGCTCAGACACCATG
GAPDH Reverse primer for qPCR	TGTAGTTGAGGTCAATGAAGGG
HPRT Forward primer for qPCR	TGCTGAGGATTTGGAAAGGG
HPRT Reverse primer for qPCR	ACAGAGGGCTACAATGTGATG
ATP5β Forward primer for qPCR	GATCCTCTAGACTCCACCTCTC
ATP5β Reverse primer for qPCR	AGAAAGTTCATCCATACCCAGG
TERT Forward primer for qPCR	GCAAGTTGCAAAGCATTGGA
TERT Reverse primer for qPCR	ACCTCTGCTTCCGACAGCTC
Extended-hTR Forward primer for qPCR	CTTTCAGGCCGCAGGAAGAGGAA
Extended-hTR Reverse primer for qPCR	GGTGACGGATGCGCACGAT
Total-hTR Forward primer for qPCR	GCGAAGAGTTGGGCTCTGTCA
Total-hTR Reverse primer for qPCR	TTCCTCTTCCTGCGGCCTGAAA
DHX36 Forward primer for qPCR	CCTTTCCGGTTGTGGAATATCT
DHX36 Reverse primer for qPCR	CCCTCTTAAACTGGGATCTGTG
hnRNP H1 Forward primer for qPCR	GTACACATGCGGGGATTACC
hnRNP H1 Reverse primer for qPCR	CGAACTCGACATCTGCTTCA

Plasmids

Name	Parental	Expressed Gene
pBS-U1-hTR	pBlueScript II SK (+)	U1-hTR
pBS-U1-G2C-hTR	pBlueScript II SK (+)	U1-G2C-hTR
pBS-U1-G11T-hTR	pBlueScript II SK (+)	U1-G11T-hTR
pBS-U1-A48G-hTR	pBlueScript II SK (+)	U1-A48G-hTR
pBS-U1-C50A-hTR	pBlueScript II SK (+)	U1-C50A-hTR
pcDNA6-3xHA-TERT	pcDNA6/His C	3xHA-hTERT
pFRT-FlagHA-DHX36-iso1	pFRT/TO/FLAG/HA-Dest plasmid	DHX36-isoform 1
pKT2-pcDNA3.1-hnRNPH1*	pcDNA3.1(+)	hnRNP H1

* = Gift from J. König's Laboratory

Antibodies

Antibody	Article Number	Supplier
α-GAPDH	G8795	Merck
α-HA-Tag	15337364	Fisher scientific
α-DHX36	sc-398418	Santa Cruz
α-hnRNPH1	-	Gift from J. König's Laboratory
α-TUBULIN	T5168	Merck

Acknowledgments

The following few sentences are definitely not enough to express all the gratitude I have towards everyone who has helped and supported me during these years as a doctoral student. Nevertheless, I would like to mention some people who deserve a special recognition.

I would like to thank my supervisor. Thank you for giving me the opportunity to join your laboratory and for pushing me into a better scientist. You fueled my enthusiasm for science, while teaching me how to be independent and critical. I am grateful for all of our scientific discussions and for how much I learned from you during this time.

A special thanks to all my lab members, present and past. You created an amazing working environment by stimulating intellectual discussion and reciprocal support, both on technical and on a personal level. I am thankful for the fun we had doing science and recreational activities together. I wish all of you all the best for the next steps in your careers.

I would like to thank the IPP as a whole. At the level of management, thank you for putting lot of effort in making us develop our scientific and soft skills, helping us with all the bureaucracy and in general for taking care of us PhD students. At the level of PhD student community, both within and outside the IPP itself, thank you for creating a vibrant environment promoting interdisciplinary collaborations, broadening my scientific knowledge and keeping it up to date.

Thank you, to all my friends. Your friendship and affection has been one of the main reason I was able to keep going through experiment failures and external adversities, like being away from home for the first time and the Covid-19 pandemic we all had to deal with. I am grateful to have met each and everyone of you, both old friends from Italy and new friends here in Mainz, and I hope we will continue to share experiences together and help each other for the years to come.

Finally, last in this section but first within my heart, I would like to thank my family. I could not be the person that I am now, able to work in the field that I love, without the everlasting practical, physical and emotional support of my relatives, specifically my parents, my brother and my partner. I love you all from the bottom of my heart!

Infine, ultimo in questa sezione ma primo nel mio cuore, vorrei ringraziare la mia famiglia. Non potrei essere la persona che sono ora, in grado di lavorare nel campo che amo, senza l'eterno supporto pratico, fisico ed emotivo dei miei parenti, in particolare i miei genitori, mio fratello e il mio compagno. Vi amo tutti dal profondo del mio cuore!

References

1. Casari, E., et al., *To Fix or Not to Fix: Maintenance of Chromosome Ends Versus Repair of DNA Double-Strand Breaks.* Cells, 2022. **11**(20).
2. Muller, H.J., *The remaking of chromosomes.* Collecting Net, 1938. **13**: p. 181-191.
3. McClintock, B., *The Production of Homozygous Deficient Tissues with Mutant Characteristics by Means of the Aberrant Mitotic Behavior of Ring-Shaped Chromosomes.* Genetics, 1938. **23**(4): p. 315-76.
4. Hayflick, L. and P.S. Moorhead, *The serial cultivation of human diploid cell strains.* Exp Cell Res, 1961. **25**: p. 585-621.
5. Hayflick, L., *The Limited in Vitro Lifetime of Human Diploid Cell Strains.* Exp Cell Res, 1965. **37**: p. 614-36.
6. Watson, J.D., *Origin of concatemeric T7 DNA.* Nat New Biol, 1972. **239**(94): p. 197-201.
7. Olovnikov, A.M., *A theory of marginotomy. The incomplete copying of template margin in enzymic synthesis of polynucleotides and biological significance of the phenomenon.* J Theor Biol, 1973. **41**(1): p. 181-90.
8. Blackburn, E.H. and J.G. Gall, *A tandemly repeated sequence at the termini of the extrachromosomal ribosomal RNA genes in Tetrahymena.* J Mol Biol, 1978. **120**(1): p. 33-53.
9. Klobutcher, L.A., et al., *All gene-sized DNA molecules in four species of hypotrichs have the same terminal sequence and an unusual 3' terminus.* Proc Natl Acad Sci U S A, 1981. **78**(5): p. 3015-9.
10. Szostak, J.W. and E.H. Blackburn, *Cloning yeast telomeres on linear plasmid vectors.* Cell, 1982. **29**(1): p. 245-55.
11. Shampay, J., J.W. Szostak, and E.H. Blackburn, *DNA sequences of telomeres maintained in yeast.* Nature, 1984. **310**(5973): p. 154-7.
12. Greider, C.W. and E.H. Blackburn, *Identification of a specific telomere terminal transferase activity in Tetrahymena extracts.* Cell, 1985. **43**(2 Pt 1): p. 405-13.
13. Greider, C.W. and E.H. Blackburn, *The telomere terminal transferase of Tetrahymena is a ribonucleoprotein enzyme with two kinds of primer specificity.* Cell, 1987. **51**(6): p. 887-98.
14. Greider, C.W. and E.H. Blackburn, *A telomeric sequence in the RNA of Tetrahymena telomerase required for telomere repeat synthesis.* Nature, 1989. **337**(6205): p. 331-7.
15. Yu, G.L., et al., *In vivo alteration of telomere sequences and senescence caused by mutated Tetrahymena telomerase RNAs.* Nature, 1990. **344**(6262): p. 126-32.
16. Lundblad, V. and J.W. Szostak, *A mutant with a defect in telomere elongation leads to senescence in yeast.* Cell, 1989. **57**(4): p. 633-43.
17. Lendvay, T.S., et al., *Senescence mutants of Saccharomyces cerevisiae with a defect in telomere replication identify three additional EST genes.* Genetics, 1996. **144**(4): p. 1399-412.
18. Harley, C.B., A.B. Futcher, and C.W. Greider, *Telomeres shorten during ageing of human fibroblasts.* Nature, 1990. **345**(6274): p. 458-60.
19. Sandell, L.L. and V.A. Zakian, *Loss of a yeast telomere: arrest, recovery, and chromosome loss.* Cell, 1993. **75**(4): p. 729-39.
20. Singer, M.S. and D.E. Gottschling, *TLC1: template RNA component of Saccharomyces cerevisiae telomerase.* Science, 1994. **266**(5184): p. 404-9.
21. Lingner, J., et al., *Reverse transcriptase motifs in the catalytic subunit of telomerase.* Science, 1997. **276**(5312): p. 561-7.
22. Feng, J., et al., *The RNA component of human telomerase.* Science, 1995. **269**(5228): p. 1236-41.
23. Harrington, L., et al., *A mammalian telomerase-associated protein.* Science, 1997. **275**(5302): p. 973-7.
24. Lingner, J. and T.R. Cech, *Telomerase and chromosome end maintenance.* Curr Opin Genet Dev, 1998. **8**(2): p. 226-32.
25. McEachern, M.J., A. Krauskopf, and E.H. Blackburn, *Telomeres and their control.* Annu Rev Genet, 2000. **34**: p. 331-358.

26. Prowse, K.R. and C.W. Greider, *Developmental and tissue-specific regulation of mouse telomerase and telomere length.* Proc Natl Acad Sci U S A, 1995. **92**(11): p. 4818-22.
27. Greider, C.W., *Telomere length regulation.* Annu Rev Biochem, 1996. **65**: p. 337-65.
28. Coviello-McLaughlin, G.M. and K.R. Prowse, *Telomere length regulation during postnatal development and ageing in Mus spretus.* Nucleic Acids Res, 1997. **25**(15): p. 3051-8.
29. Kakuo, S., K. Asaoka, and T. Ide, *Human is a unique species among primates in terms of telomere length.* Biochem Biophys Res Commun, 1999. **263**(2): p. 308-14.
30. Campisi, J., *From cells to organisms: can we learn about aging from cells in culture?* Exp Gerontol, 2001. **36**(4-6): p. 607-18.
31. de Lange, T., *Shelterin-Mediated Telomere Protection.* Annu Rev Genet, 2018. **52**: p. 223-247.
32. Takai, K.K., et al., *In vivo stoichiometry of shelterin components.* J Biol Chem, 2010. **285**(2): p. 1457-67.
33. de Lange, T., *Shelterin: the protein complex that shapes and safeguards human telomeres.* Genes Dev, 2005. **19**(18): p. 2100-10.
34. Erdel, F., et al., *Telomere Recognition and Assembly Mechanism of Mammalian Shelterin.* Cell Rep, 2017. **18**(1): p. 41-53.
35. Bianchi, A., et al., *TRF1 is a dimer and bends telomeric DNA.* EMBO J, 1997. **16**(7): p. 1785-94.
36. Bianchi, A., et al., *TRF1 binds a bipartite telomeric site with extreme spatial flexibility.* EMBO J, 1999. **18**(20): p. 5735-44.
37. Nishikawa, T., et al., *Solution structure of a telomeric DNA complex of human TRF1.* Structure, 2001. **9**(12): p. 1237-51.
38. Baumann, P. and T.R. Cech, *Pot1, the putative telomere end-binding protein in fission yeast and humans.* Science, 2001. **292**(5519): p. 1171-5.
39. Lei, M., E.R. Podell, and T.R. Cech, *Structure of human POT1 bound to telomeric single-stranded DNA provides a model for chromosome end-protection.* Nat Struct Mol Biol, 2004. **11**(12): p. 1223-9.
40. Loayza, D., et al., *DNA binding features of human POT1: a nonamer 5'-TAGGGTTAG-3' minimal binding site, sequence specificity, and internal binding to multimeric sites.* J Biol Chem, 2004. **279**(13): p. 13241-8.
41. Hanaoka, S., et al., *NMR structure of the hRap1 Myb motif reveals a canonical three-helix bundle lacking the positive surface charge typical of Myb DNA-binding domains.* J Mol Biol, 2001. **312**(1): p. 167-75.
42. Arat, N.O. and J.D. Griffith, *Human Rap1 interacts directly with telomeric DNA and regulates TRF2 localization at the telomere.* J Biol Chem, 2012. **287**(50): p. 41583-94.
43. Wang, F., et al., *The POT1-TPP1 telomere complex is a telomerase processivity factor.* Nature, 2007. **445**(7127): p. 506-10.
44. Gaullier, G., et al., *A higher-order entity formed by the flexible assembly of RAP1 with TRF2.* Nucleic Acids Res, 2016. **44**(4): p. 1962-76.
45. Necasova, I., et al., *Basic domain of telomere guardian TRF2 reduces D-loop unwinding whereas Rap1 restores it.* Nucleic Acids Res, 2017. **45**(21): p. 12170-12180.
46. Janouskova, E., et al., *Human Rap1 modulates TRF2 attraction to telomeric DNA.* Nucleic Acids Res, 2015. **43**(5): p. 2691-700.
47. Griffith, J.D., et al., *Mammalian telomeres end in a large duplex loop.* Cell, 1999. **97**(4): p. 503-14.
48. Doksani, Y. and T. de Lange, *The role of double-strand break repair pathways at functional and dysfunctional telomeres.* Cold Spring Harb Perspect Biol, 2014. **6**(12): p. a016576.
49. Hockemeyer, D., et al., *Engineered telomere degradation models dyskeratosis congenita.* Genes Dev, 2008. **22**(13): p. 1773-85.
50. Dai, X., et al., *Molecular steps of G-overhang generation at human telomeres and its function in chromosome end protection.* EMBO J, 2010. **29**(16): p. 2788-801.
51. Diotti, R., et al., *DNA-Directed Polymerase Subunits Play a Vital Role in Human Telomeric Overhang Processing.* Mol Cancer Res, 2015. **13**(3): p. 402-10.
52. Freibaum, B.D. and C.M. Counter, *The protein hSnm1B is stabilized when bound to the telomere-binding protein TRF2.* J Biol Chem, 2008. **283**(35): p. 23671-6.

53. Huang, C., X. Dai, and W. Chai, *Human Stn1 protects telomere integrity by promoting efficient lagging-strand synthesis at telomeres and mediating C-strand fill-in.* Cell Res, 2012. **22**(12): p. 1681-95.
54. Lenain, C., et al., *The Apollo 5' exonuclease functions together with TRF2 to protect telomeres from DNA repair.* Curr Biol, 2006. **16**(13): p. 1303-10.
55. van Overbeek, M. and T. de Lange, *Apollo, an Artemis-related nuclease, interacts with TRF2 and protects human telomeres in S phase.* Curr Biol, 2006. **16**(13): p. 1295-302.
56. Wang, F., et al., *Human CST has independent functions during telomere duplex replication and C-strand fill-in.* Cell Rep, 2012. **2**(5): p. 1096-103.
57. Mimitou, E.P. and L.S. Symington, *DNA end resection--unraveling the tail.* DNA Repair (Amst), 2011. **10**(3): p. 344-8.
58. Panier, S. and S.J. Boulton, *Double-strand break repair: 53BP1 comes into focus.* Nat Rev Mol Cell Biol, 2014. **15**(1): p. 7-18.
59. Zimmermann, M. and T. de Lange, *53BP1: pro choice in DNA repair.* Trends Cell Biol, 2014. **24**(2): p. 108-17.
60. Wu, P., H. Takai, and T. de Lange, *Telomeric 3' overhangs derive from resection by Exo1 and Apollo and fill-in by POT1b-associated CST.* Cell, 2012. **150**(1): p. 39-52.
61. Doksani, Y., et al., *Super-resolution fluorescence imaging of telomeres reveals TRF2-dependent T-loop formation.* Cell, 2013. **155**(2): p. 345-356.
62. Stansel, R.M., T. de Lange, and J.D. Griffith, *T-loop assembly in vitro involves binding of TRF2 near the 3' telomeric overhang.* EMBO J, 2001. **20**(19): p. 5532-40.
63. Benarroch-Popivker, D., et al., *TRF2-Mediated Control of Telomere DNA Topology as a Mechanism for Chromosome-End Protection.* Mol Cell, 2016. **61**(2): p. 274-86.
64. Tardat, M. and J. Dejardin, *Telomere chromatin establishment and its maintenance during mammalian development.* Chromosoma, 2018. **127**(1): p. 3-18.
65. Rudenko, G. and L.H. Van der Ploeg, *Transcription of telomere repeats in protozoa.* EMBO J, 1989. **8**(9): p. 2633-8.
66. Azzalin, C.M., et al., *Telomeric repeat containing RNA and RNA surveillance factors at mammalian chromosome ends.* Science, 2007. **318**(5851): p. 798-801.
67. Luke, B., et al., *The Rat1p 5' to 3' exonuclease degrades telomeric repeat-containing RNA and promotes telomere elongation in Saccharomyces cerevisiae.* Mol Cell, 2008. **32**(4): p. 465-77.
68. Schoeftner, S. and M.A. Blasco, *Developmentally regulated transcription of mammalian telomeres by DNA-dependent RNA polymerase II.* Nat Cell Biol, 2008. **10**(2): p. 228-36.
69. Flynn, R.L., et al., *TERRA and hnRNPA1 orchestrate an RPA-to-POT1 switch on telomeric single-stranded DNA.* Nature, 2011. **471**(7339): p. 532-6.
70. Porro, A., et al., *Molecular dissection of telomeric repeat-containing RNA biogenesis unveils the presence of distinct and multiple regulatory pathways.* Mol Cell Biol, 2010. **30**(20): p. 4808-17.
71. Takai, H., A. Smogorzewska, and T. de Lange, *DNA damage foci at dysfunctional telomeres.* Curr Biol, 2003. **13**(17): p. 1549-56.
72. Qian, Y. and X. Chen, *Tumor suppression by p53: making cells senescent.* Histol Histopathol, 2010. **25**(4): p. 515-26.
73. Feretzaki, M. and J. Lingner, *A practical qPCR approach to detect TERRA, the elusive telomeric repeat-containing RNA.* Methods, 2017. **114**: p. 39-45.
74. Farnung, B.O., et al., *Telomerase efficiently elongates highly transcribing telomeres in human cancer cells.* PLoS One, 2012. **7**(4): p. e35714.
75. Lopez de Silanes, I., et al., *Identification of TERRA locus unveils a telomere protection role through association to nearly all chromosomes.* Nat Commun, 2014. **5**: p. 4723.
76. Montero, J.J., et al., *Telomeric RNAs are essential to maintain telomeres.* Nat Commun, 2016. **7**: p. 12534.
77. Diman, A., et al., *Nuclear respiratory factor 1 and endurance exercise promote human telomere transcription.* Sci Adv, 2016. **2**(7): p. e1600031.
78. Deng, Z., et al., *A role for CTCF and cohesin in subtelomere chromatin organization, TERRA transcription, and telomere end protection.* EMBO J, 2012. **31**(21): p. 4165-78.

79. Porro, A., et al., *Functional characterization of the TERRA transcriptome at damaged telomeres.* Nat Commun, 2014. **5**: p. 5379.
80. Beishline, K., et al., *CTCF driven TERRA transcription facilitates completion of telomere DNA replication.* Nat Commun, 2017. **8**(1): p. 2114.
81. Arora, R., et al., *RNaseH1 regulates TERRA-telomeric DNA hybrids and telomere maintenance in ALT tumour cells.* Nat Commun, 2014. **5**: p. 5220.
82. Li, F., et al., *ATRX loss induces telomere dysfunction and necessitates induction of alternative lengthening of telomeres during human cell immortalization.* EMBO J, 2019. **38**(19): p. e96659.
83. Arnoult, N., A. Van Beneden, and A. Decottignies, *Telomere length regulates TERRA levels through increased trimethylation of telomeric H3K9 and HP1alpha.* Nat Struct Mol Biol, 2012. **19**(9): p. 948-56.
84. Chu, H.P., et al., *TERRA RNA Antagonizes ATRX and Protects Telomeres.* Cell, 2017. **170**(1): p. 86-101 e16.
85. Balk, B., et al., *Telomeric RNA-DNA hybrids affect telomere-length dynamics and senescence.* Nat Struct Mol Biol, 2013. **20**(10): p. 1199-205.
86. Skourti-Stathaki, K., K. Kamieniarz-Gdula, and N.J. Proudfoot, *R-loops induce repressive chromatin marks over mammalian gene terminators.* Nature, 2014. **516**(7531): p. 436-9.
87. Grunseich, C., et al., *Senataxin Mutation Reveals How R-Loops Promote Transcription by Blocking DNA Methylation at Gene Promoters.* Mol Cell, 2018. **69**(3): p. 426-437 e7.
88. Lombrana, R., et al., *R-loops and initiation of DNA replication in human cells: a missing link?* Front Genet, 2015. **6**: p. 158.
89. Ohle, C., et al., *Transient RNA-DNA Hybrids Are Required for Efficient Double-Strand Break Repair.* Cell, 2016. **167**(4): p. 1001-1013 e7.
90. Denchi, E.L. and T. de Lange, *Protection of telomeres through independent control of ATM and ATR by TRF2 and POT1.* Nature, 2007. **448**(7157): p. 1068-71.
91. Zou, L. and S.J. Elledge, *Sensing DNA damage through ATRIP recognition of RPA-ssDNA complexes.* Science, 2003. **300**(5625): p. 1542-8.
92. Lopez de Silanes, I., M. Stagno d'Alcontres, and M.A. Blasco, *TERRA transcripts are bound by a complex array of RNA-binding proteins.* Nat Commun, 2010. **1**: p. 33.
93. Deng, Z., et al., *TERRA RNA binding to TRF2 facilitates heterochromatin formation and ORC recruitment at telomeres.* Mol Cell, 2009. **35**(4): p. 403-13.
94. Acharya, S., et al., *Association of BLM and BRCA1 during Telomere Maintenance in ALT Cells.* PLoS One, 2014. **9**(8): p. e103819.
95. Sobinoff, A.P. and H.A. Pickett, *Alternative Lengthening of Telomeres: DNA Repair Pathways Converge.* Trends Genet, 2017. **33**(12): p. 921-932.
96. Episkopou, H., et al., *Alternative Lengthening of Telomeres is characterized by reduced compaction of telomeric chromatin.* Nucleic Acids Res, 2014. **42**(7): p. 4391-405.
97. Sobinoff, A.P., et al., *BLM and SLX4 play opposing roles in recombination-dependent replication at human telomeres.* EMBO J, 2017. **36**(19): p. 2907-2919.
98. Hou, K., et al., *Alternative Lengthening of Telomeres and Mediated Telomere Synthesis.* Cancers (Basel), 2022. **14**(9).
99. Autexier, C. and N.F. Lue, *The structure and function of telomerase reverse transcriptase.* Annu Rev Biochem, 2006. **75**: p. 493-517.
100. Osanai, M., et al., *Identification and characterization of the telomerase reverse transcriptase of Bombyx mori (silkworm) and Tribolium castaneum (flour beetle).* Gene, 2006. **376**(2): p. 281-9.
101. Malik, H.S., W.D. Burke, and T.H. Eickbush, *Putative telomerase catalytic subunits from Giardia lamblia and Caenorhabditis elegans.* Gene, 2000. **251**(2): p. 101-8.
102. Figueiredo, L.M., et al., *The unusually large Plasmodium telomerase reverse-transcriptase localizes in a discrete compartment associated with the nucleolus.* Nucleic Acids Res, 2005. **33**(3): p. 1111-22.
103. Nandakumar, J. and T.R. Cech, *Finding the end: recruitment of telomerase to telomeres.* Nat Rev Mol Cell Biol, 2013. **14**(2): p. 69-82.
104. Wyatt, H.D., S.C. West, and T.L. Beattie, *InTERTpreting telomerase structure and function.* Nucleic Acids Res, 2010. **38**(17): p. 5609-22.

105. Friedman, K.L. and T.R. Cech, *Essential functions of amino-terminal domains in the yeast telomerase catalytic subunit revealed by selection for viable mutants.* Genes Dev, 1999. **13**(21): p. 2863-74.
106. Xia, J., et al., *Identification of functionally important domains in the N-terminal region of telomerase reverse transcriptase.* Mol Cell Biol, 2000. **20**(14): p. 5196-207.
107. Weinrich, S.L., et al., *Reconstitution of human telomerase with the template RNA component hTR and the catalytic protein subunit hTRT.* Nat Genet, 1997. **17**(4): p. 498-502.
108. Miller, M.C., J.K. Liu, and K. Collins, *Template definition by Tetrahymena telomerase reverse transcriptase.* EMBO J, 2000. **19**(16): p. 4412-22.
109. Bosoy, D., et al., *Conserved N-terminal motifs of telomerase reverse transcriptase required for ribonucleoprotein assembly in vivo.* J Biol Chem, 2003. **278**(6): p. 3882-90.
110. Bachand, F. and C. Autexier, *Functional regions of human telomerase reverse transcriptase and human telomerase RNA required for telomerase activity and RNA-protein interactions.* Mol Cell Biol, 2001. **21**(5): p. 1888-97.
111. Beattie, T.L., et al., *Polymerization defects within human telomerase are distinct from telomerase RNA and TEP1 binding.* Mol Biol Cell, 2000. **11**(10): p. 3329-40.
112. Bryan, T.M., K.J. Goodrich, and T.R. Cech, *Telomerase RNA bound by protein motifs specific to telomerase reverse transcriptase.* Mol Cell, 2000. **6**(2): p. 493-9.
113. Lai, C.K., J.R. Mitchell, and K. Collins, *RNA binding domain of telomerase reverse transcriptase.* Mol Cell Biol, 2001. **21**(4): p. 990-1000.
114. Lai, C.K., M.C. Miller, and K. Collins, *Template boundary definition in Tetrahymena telomerase.* Genes Dev, 2002. **16**(4): p. 415-20.
115. Moriarty, T.J., et al., *Functional multimerization of human telomerase requires an RNA interaction domain in the N terminus of the catalytic subunit.* Mol Cell Biol, 2002. **22**(4): p. 1253-65.
116. O'Connor, C.M., C.K. Lai, and K. Collins, *Two purified domains of telomerase reverse transcriptase reconstitute sequence-specific interactions with RNA.* J Biol Chem, 2005. **280**(17): p. 17533-9.
117. Drosopoulos, W.C. and V.R. Prasad, *The telomerase-specific T motif is a restrictive determinant of repetitive reverse transcription by human telomerase.* Mol Cell Biol, 2010. **30**(2): p. 447-59.
118. Beattie, T.L., et al., *Reconstitution of human telomerase activity in vitro.* Curr Biol, 1998. **8**(3): p. 177-80.
119. Nakamura, T.M., et al., *Telomerase catalytic subunit homologs from fission yeast and human.* Science, 1997. **277**(5328): p. 955-9.
120. Harrington, L., et al., *Human telomerase contains evolutionarily conserved catalytic and structural subunits.* Genes Dev, 1997. **11**(23): p. 3109-15.
121. Haering, C.H., et al., *Analysis of telomerase catalytic subunit mutants in vivo and in vitro in Schizosaccharomycespombe.* Proc Natl Acad Sci U S A, 2000. **97**(12): p. 6367-72.
122. Counter, C.M., et al., *The catalytic subunit of yeast telomerase.* Proc Natl Acad Sci U S A, 1997. **94**(17): p. 9202-7.
123. Nakayama, J., et al., *Telomerase activation by hTRT in human normal fibroblasts and hepatocellular carcinomas.* Nat Genet, 1998. **18**(1): p. 65-8.
124. Bryan, T.M., K.J. Goodrich, and T.R. Cech, *A mutant of Tetrahymena telomerase reverse transcriptase with increased processivity.* J Biol Chem, 2000. **275**(31): p. 24199-207.
125. Cote, M.L. and M.J. Roth, *Murine leukemia virus reverse transcriptase: structural comparison with HIV-1 reverse transcriptase.* Virus Res, 2008. **134**(1-2): p. 186-202.
126. Gillis, A.J., A.P. Schuller, and E. Skordalakes, *Structure of the Tribolium castaneum telomerase catalytic subunit TERT.* Nature, 2008. **455**(7213): p. 633-7.
127. Li, Y., J.A. Yates, and J.J. Chen, *Identification and characterization of sea squirt telomerase reverse transcriptase.* Gene, 2007. **400**(1-2): p. 16-24.
128. Xie, M., et al., *A novel motif in telomerase reverse transcriptase regulates telomere repeat addition rate and processivity.* Nucleic Acids Res, 2010. **38**(6): p. 1982-96.
129. Mitchell, M., et al., *Structural basis for telomerase catalytic subunit TERT binding to RNA template and telomeric DNA.* Nat Struct Mol Biol, 2010. **17**(4): p. 513-8.

130. Counter, C.M., et al., *Dissociation among in vitro telomerase activity, telomere maintenance, and cellular immortalization.* Proc Natl Acad Sci U S A, 1998. **95**(25): p. 14723-8.
131. Mason, M., A. Schuller, and E. Skordalakes, *Telomerase structure function.* Curr Opin Struct Biol, 2011. **21**(1): p. 92-100.
132. Stohr, B.A., L. Xu, and E.H. Blackburn, *The terminal telomeric DNA sequence determines the mechanism of dysfunctional telomere fusion.* Mol Cell, 2010. **39**(2): p. 307-14.
133. Guiducci, C., M.A. Cerone, and S. Bacchetti, *Expression of mutant telomerase in immortal telomerase-negative human cells results in cell cycle deregulation, nuclear and chromosomal abnormalities and rapid loss of viability.* Oncogene, 2001. **20**(6): p. 714-25.
134. Li, S., et al., *Rapid inhibition of cancer cell growth induced by lentiviral delivery and expression of mutant-template telomerase RNA and anti-telomerase short-interfering RNA.* Cancer Res, 2004. **64**(14): p. 4833-40.
135. Hanish, J.P., J.L. Yanowitz, and T. de Lange, *Stringent sequence requirements for the formation of human telomeres.* Proc Natl Acad Sci U S A, 1994. **91**(19): p. 8861-5.
136. Brown, A.F., et al., *A self-regulating template in human telomerase.* Proc Natl Acad Sci U S A, 2014. **111**(31): p. 11311-6.
137. Webb, C.J. and V.A. Zakian, *Identification and characterization of the Schizosaccharomyces pombe TER1 telomerase RNA.* Nat Struct Mol Biol, 2008. **15**(1): p. 34-42.
138. Leonardi, J., et al., *TER1, the RNA subunit of fission yeast telomerase.* Nat Struct Mol Biol, 2008. **15**(1): p. 26-33.
139. Seto, A.G., et al., *Saccharomyces cerevisiae telomerase is an Sm small nuclear ribonucleoprotein particle.* Nature, 1999. **401**(6749): p. 177-80.
140. Matera, A.G., R.M. Terns, and M.P. Terns, *Non-coding RNAs: lessons from the small nuclear and small nucleolar RNAs.* Nat Rev Mol Cell Biol, 2007. **8**(3): p. 209-20.
141. Theimer, C.A. and J. Feigon, *Structure and function of telomerase RNA.* Curr Opin Struct Biol, 2006. **16**(3): p. 307-18.
142. Chen, J.L. and C.W. Greider, *An emerging consensus for telomerase RNA structure.* Proc Natl Acad Sci U S A, 2004. **101**(41): p. 14683-4.
143. Sexton, A.N. and K. Collins, *The 5' guanosine tracts of human telomerase RNA are recognized by the G-quadruplex binding domain of the RNA helicase DHX36 and function to increase RNA accumulation.* Mol Cell Biol, 2011. **31**(4): p. 736-43.
144. Mitchell, J.R., J. Cheng, and K. Collins, *A box H/ACA small nucleolar RNA-like domain at the human telomerase RNA 3' end.* Mol Cell Biol, 1999. **19**(1): p. 567-76.
145. Chen, J.L., M.A. Blasco, and C.W. Greider, *Secondary structure of vertebrate telomerase RNA.* Cell, 2000. **100**(5): p. 503-14.
146. Richard, P., et al., *A common sequence motif determines the Cajal body-specific localization of box H/ACA scaRNAs.* EMBO J, 2003. **22**(16): p. 4283-93.
147. Egan, E.D. and K. Collins, *An enhanced H/ACA RNP assembly mechanism for human telomerase RNA.* Mol Cell Biol, 2012. **32**(13): p. 2428-39.
148. Qin, J. and C. Autexier, *Regulation of human telomerase RNA biogenesis and localization.* RNA Biol, 2021. **18**(3): p. 305-315.
149. Fu, D. and K. Collins, *Distinct biogenesis pathways for human telomerase RNA and H/ACA small nucleolar RNAs.* Mol Cell, 2003. **11**(5): p. 1361-72.
150. Soutourina, J., *Transcription regulation by the Mediator complex.* Nat Rev Mol Cell Biol, 2018. **19**(4): p. 262-274.
151. Skaar, J.R., et al., *The Integrator complex controls the termination of transcription at diverse classes of gene targets.* Cell Res, 2015. **25**(3): p. 288-305.
152. Rubtsova, M.P., et al., *Integrator is a key component of human telomerase RNA biogenesis.* Sci Rep, 2019. **9**(1): p. 1701.
153. Darzacq, X., et al., *Stepwise RNP assembly at the site of H/ACA RNA transcription in human cells.* J Cell Biol, 2006. **173**(2): p. 207-18.
154. Boulon, S., et al., *The Hsp90 chaperone controls the biogenesis of L7Ae RNPs through conserved machinery.* J Cell Biol, 2008. **180**(3): p. 579-95.
155. Fu, D. and K. Collins, *Purification of human telomerase complexes identifies factors involved in telomerase biogenesis and telomere length regulation.* Mol Cell, 2007. **28**(5): p. 773-85.

156. Grozdanov, P.N., et al., *SHQ1 is required prior to NAF1 for assembly of H/ACA small nucleolar and telomerase RNPs.* RNA, 2009. **15**(6): p. 1188-97.
157. Hoareau-Aveilla, C., et al., *hNaf1 is required for accumulation of human box H/ACA snoRNPs, scaRNPs, and telomerase.* RNA, 2006. **12**(5): p. 832-40.
158. Venteicher, A.S., et al., *Identification of ATPases pontin and reptin as telomerase components essential for holoenzyme assembly.* Cell, 2008. **132**(6): p. 945-57.
159. Leulliot, N., et al., *The box H/ACA RNP assembly factor Naf1p contains a domain homologous to Gar1p mediating its interaction with Cbf5p.* J Mol Biol, 2007. **371**(5): p. 1338-53.
160. Egan, E.D. and K. Collins, *Specificity and stoichiometry of subunit interactions in the human telomerase holoenzyme assembled in vivo.* Mol Cell Biol, 2010. **30**(11): p. 2775-86.
161. Nguyen, T.H.D., et al., *Cryo-EM structure of substrate-bound human telomerase holoenzyme.* Nature, 2018. **557**(7704): p. 190-195.
162. Tseng, C.K., et al., *The H/ACA complex disrupts triplex in hTR precursor to permit processing by RRP6 and PARN.* Nat Commun, 2018. **9**(1): p. 5430.
163. Tseng, C.K., et al., *Human Telomerase RNA Processing and Quality Control.* Cell Rep, 2015. **13**(10): p. 2232-43.
164. Roake, C.M., et al., *Disruption of Telomerase RNA Maturation Kinetics Precipitates Disease.* Mol Cell, 2019. **74**(4): p. 688-700 e3.
165. Goldfarb, K.C. and T.R. Cech, *3' terminal diversity of MRP RNA and other human noncoding RNAs revealed by deep sequencing.* BMC Mol Biol, 2013. **14**: p. 23.
166. Nguyen, D., et al., *A Polyadenylation-Dependent 3' End Maturation Pathway Is Required for the Synthesis of the Human Telomerase RNA.* Cell Rep, 2015. **13**(10): p. 2244-57.
167. Shukla, S., et al., *Inhibition of telomerase RNA decay rescues telomerase deficiency caused by dyskerin or PARN defects.* Nat Struct Mol Biol, 2016. **23**(4): p. 286-92.
168. Meola, N., et al., *Identification of a Nuclear Exosome Decay Pathway for Processed Transcripts.* Mol Cell, 2016. **64**(3): p. 520-533.
169. Lubas, M., et al., *Interaction profiling identifies the human nuclear exosome targeting complex.* Mol Cell, 2011. **43**(4): p. 624-37.
170. Macias, S., et al., *DGCR8 Acts as an Adaptor for the Exosome Complex to Degrade Double-Stranded Structured RNAs.* Mol Cell, 2015. **60**(6): p. 873-85.
171. Wu, G., et al., *A Two-Layered Targeting Mechanism Underlies Nuclear RNA Sorting by the Human Exosome.* Cell Rep, 2020. **30**(7): p. 2387-2401 e5.
172. Lubas, M., et al., *The human nuclear exosome targeting complex is loaded onto newly synthesized RNA to direct early ribonucleolysis.* Cell Rep, 2015. **10**(2): p. 178-92.
173. Andersson, R., et al., *An atlas of active enhancers across human cell types and tissues.* Nature, 2014. **507**(7493): p. 455-461.
174. Andersen, P.R., et al., *The human cap-binding complex is functionally connected to the nuclear RNA exosome.* Nat Struct Mol Biol, 2013. **20**(12): p. 1367-76.
175. Berndt, H., et al., *Maturation of mammalian H/ACA box snoRNAs: PAPD5-dependent adenylation and PARN-dependent trimming.* RNA, 2012. **18**(5): p. 958-72.
176. Astrom, J., A. Astrom, and A. Virtanen, *In vitro deadenylation of mammalian mRNA by a HeLa cell 3' exonuclease.* EMBO J, 1991. **10**(10): p. 3067-71.
177. Henriksson, N., et al., *Recognition of adenosine residues by the active site of poly(A)-specific ribonuclease.* J Biol Chem, 2010. **285**(1): p. 163-70.
178. Virtanen, A., et al., *Poly(A)-specific ribonuclease (PARN): an allosterically regulated, processive and mRNA cap-interacting deadenylase.* Crit Rev Biochem Mol Biol, 2013. **48**(2): p. 192-209.
179. Schmid, M. and T.H. Jensen, *The Nuclear RNA Exosome and Its Cofactors.* Adv Exp Med Biol, 2019. **1203**: p. 113-132.
180. Zinder, J.C. and C.D. Lima, *Targeting RNA for processing or destruction by the eukaryotic RNA exosome and its cofactors.* Genes Dev, 2017. **31**(2): p. 88-100.
181. Kilchert, C., S. Wittmann, and L. Vasiljeva, *The regulation and functions of the nuclear RNA exosome complex.* Nat Rev Mol Cell Biol, 2016. **17**(4): p. 227-39.
182. Pradet-Balade, B., et al., *CRM1 controls the composition of nucleoplasmic pre-snoRNA complexes to licence them for nucleolar transport.* EMBO J, 2011. **30**(11): p. 2205-18.

183. Deng, T., et al., *TOE1 acts as a 3' exonuclease for telomerase RNA and regulates telomere maintenance.* Nucleic Acids Res, 2019. **47**(1): p. 391-405.
184. Son, A., J.E. Park, and V.N. Kim, *PARN and TOE1 Constitute a 3' End Maturation Module for Nuclear Non-coding RNAs.* Cell Rep, 2018. **23**(3): p. 888-898.
185. Bresson, S.M., et al., *Canonical Poly(A) Polymerase Activity Promotes the Decay of a Wide Variety of Mammalian Nuclear RNAs.* PLoS Genet, 2015. **11**(10): p. e1005610.
186. Bresson, S.M. and N.K. Conrad, *The human nuclear poly(a)-binding protein promotes RNA hyperadenylation and decay.* PLoS Genet, 2013. **9**(10): p. e1003893.
187. Beaulieu, Y.B., et al., *Polyadenylation-dependent control of long noncoding RNA expression by the poly(A)-binding protein nuclear 1.* PLoS Genet, 2012. **8**(11): p. e1003078.
188. Bengoechea, R., et al., *Nuclear speckles are involved in nuclear aggregation of PABPN1 and in the pathophysiology of oculopharyngeal muscular dystrophy.* Neurobiol Dis, 2012. **46**(1): p. 118-29.
189. Zhu, Y., et al., *Telomerase RNA accumulates in Cajal bodies in human cancer cells.* Mol Biol Cell, 2004. **15**(1): p. 81-90.
190. Jady, B.E., E. Bertrand, and T. Kiss, *Human telomerase RNA and box H/ACA scaRNAs share a common Cajal body-specific localization signal.* J Cell Biol, 2004. **164**(5): p. 647-52.
191. Cristofari, G., et al., *Human telomerase RNA accumulation in Cajal bodies facilitates telomerase recruitment to telomeres and telomere elongation.* Mol Cell, 2007. **27**(6): p. 882-9.
192. Jady, B.E., et al., *Cell cycle-dependent recruitment of telomerase RNA and Cajal bodies to human telomeres.* Mol Biol Cell, 2006. **17**(2): p. 944-54.
193. Venteicher, A.S., et al., *A human telomerase holoenzyme protein required for Cajal body localization and telomere synthesis.* Science, 2009. **323**(5914): p. 644-8.
194. Chen, L., et al., *An Activity Switch in Human Telomerase Based on RNA Conformation and Shaped by TCAB1.* Cell, 2018. **174**(1): p. 218-230 e13.
195. Zhong, F., et al., *Disruption of telomerase trafficking by TCAB1 mutation causes dyskeratosis congenita.* Genes Dev, 2011. **25**(1): p. 11-6.
196. Laprade, H., et al., *Single-Molecule Imaging of Telomerase RNA Reveals a Recruitment-Retention Model for Telomere Elongation.* Mol Cell, 2020. **79**(1): p. 115-126 e6.
197. Tomlinson, R.L., et al., *Cell cycle-regulated trafficking of human telomerase to telomeres.* Mol Biol Cell, 2006. **17**(2): p. 955-65.
198. Chen, Y., et al., *Human cells lacking coilin and Cajal bodies are proficient in telomerase assembly, trafficking and telomere maintenance.* Nucleic Acids Res, 2015. **43**(1): p. 385-95.
199. Lee, J.H., et al., *Catalytically active telomerase holoenzyme is assembled in the dense fibrillar component of the nucleolus during S phase.* Histochem Cell Biol, 2014. **141**(2): p. 137-52.
200. Mitchell, J.R. and K. Collins, *Human telomerase activation requires two independent interactions between telomerase RNA and telomerase reverse transcriptase.* Mol Cell, 2000. **6**(2): p. 361-71.
201. Ohno, M., et al., *PHAX, a mediator of U snRNA nuclear export whose activity is regulated by phosphorylation.* Cell, 2000. **101**(2): p. 187-98.
202. Izaurralde, E., et al., *A cap-binding protein complex mediating U snRNA export.* Nature, 1995. **376**(6542): p. 709-12.
203. Fornerod, M., et al., *CRM1 is an export receptor for leucine-rich nuclear export signals.* Cell, 1997. **90**(6): p. 1051-60.
204. Balatsos, N.A., et al., *Inhibition of mRNA deadenylation by the nuclear cap binding complex (CBC).* J Biol Chem, 2006. **281**(7): p. 4517-22.
205. Girard, C., et al., *Characterization of a short isoform of human Tgs1 hypermethylase associating with small nucleolar ribonucleoprotein core proteins and produced by limited proteolytic processing.* J Biol Chem, 2008. **283**(4): p. 2060-9.
206. Boulon, S., et al., *PHAX and CRM1 are required sequentially to transport U3 snoRNA to nucleoli.* Mol Cell, 2004. **16**(5): p. 777-87.
207. Chen, L., et al., *Loss of Human TGS1 Hypermethylase Promotes Increased Telomerase RNA and Telomere Elongation.* Cell Rep, 2020. **30**(5): p. 1358-1372 e5.

208. Liu, J., et al., *Argonaute2 is the catalytic engine of mammalian RNAi.* Science, 2004. **305**(5689): p. 1437-41.
209. Laudadio, I., et al., *AGO2 promotes telomerase activity and interaction between the telomerase components TERT and TERC.* EMBO Rep, 2019. **20**(2).
210. Cheng, Y., et al., *Mitochondrial Trafficking and Processing of Telomerase RNA TERC.* Cell Rep, 2018. **24**(10): p. 2589-2595.
211. Rubtsova, M., et al., *Protein encoded in human telomerase RNA is involved in cell protective pathways.* Nucleic Acids Res, 2018. **46**(17): p. 8966-8977.
212. Gazzaniga, F.S. and E.H. Blackburn, *An antiapoptotic role for telomerase RNA in human immune cells independent of telomere integrity or telomerase enzymatic activity.* Blood, 2014. **124**(25): p. 3675-84.
213. Rossiello, F., et al., *Telomere dysfunction in ageing and age-related diseases.* Nat Cell Biol, 2022. **24**(2): p. 135-147.
214. Alder, J.K. and M. Armanios, *Telomere-mediated lung disease.* Physiol Rev, 2022. **102**(4): p. 1703-1720.
215. Demanelis, K., et al., *Determinants of telomere length across human tissues.* Science, 2020. **369**(6509).
216. Revy, P., C. Kannengiesser, and A.A. Bertuch, *Genetics of human telomere biology disorders.* Nat Rev Genet, 2022.
217. Heiss, N.S., et al., *X-linked dyskeratosis congenita is caused by mutations in a highly conserved gene with putative nucleolar functions.* Nat Genet, 1998. **19**(1): p. 32-8.
218. Alter, B.P., et al., *Very short telomere length by flow fluorescence in situ hybridization identifies patients with dyskeratosis congenita.* Blood, 2007. **110**(5): p. 1439-47.
219. Alder, J.K., et al., *Diagnostic utility of telomere length testing in a hospital-based setting.* Proc Natl Acad Sci U S A, 2018. **115**(10): p. E2358-E2365.
220. Kelich, J., et al., *Telomere dysfunction implicates POT1 in patients with idiopathic pulmonary fibrosis.* J Exp Med, 2022. **219**(5).
221. Vulliamy, T., et al., *Disease anticipation is associated with progressive telomere shortening in families with dyskeratosis congenita due to mutations in TERC.* Nat Genet, 2004. **36**(5): p. 447-9.
222. Armanios, M., et al., *Haploinsufficiency of telomerase reverse transcriptase leads to anticipation in autosomal dominant dyskeratosis congenita.* Proc Natl Acad Sci U S A, 2005. **102**(44): p. 15960-4.
223. Goldman, F., et al., *The effect of TERC haploinsufficiency on the inheritance of telomere length.* Proc Natl Acad Sci U S A, 2005. **102**(47): p. 17119-24.
224. Newton, C.A., et al., *Telomere-related lung fibrosis is diagnostically heterogeneous but uniformly progressive.* Eur Respir J, 2016. **48**(6): p. 1710-1720.
225. Gutierrez-Rodrigues, F., et al., *A novel homozygous RTEL1 variant in a consanguineous Lebanese family: phenotypic heterogeneity and disease anticipation.* Hum Genet, 2019. **138**(11-12): p. 1323-1330.
226. Fernandez, B.A., et al., *A Newfoundland cohort of familial and sporadic idiopathic pulmonary fibrosis patients: clinical and genetic features.* Respir Res, 2012. **13**(1): p. 64.
227. Hao, L.Y., et al., *Short telomeres, even in the presence of telomerase, limit tissue renewal capacity.* Cell, 2005. **123**(6): p. 1121-31.
228. Armanios, M., et al., *Short telomeres are sufficient to cause the degenerative defects associated with aging.* Am J Hum Genet, 2009. **85**(6): p. 823-32.
229. Collopy, L.C., et al., *Triallelic and epigenetic-like inheritance in human disorders of telomerase.* Blood, 2015. **126**(2): p. 176-84.
230. van der Vis, J.J., et al., *Pulmonary fibrosis in non-mutation carriers of families with short telomere syndrome gene mutations.* Respirology, 2021. **26**(12): p. 1160-1170.
231. Alder, J.K., et al., *Ancestral mutation in telomerase causes defects in repeat addition processivity and manifests as familial pulmonary fibrosis.* PLoS Genet, 2011. **7**(3): p. e1001352.
232. Xing, C. and C.K. Garcia, *Epigenetic inheritance of telomere length obscures identification of causative PARN locus.* J Med Genet, 2016. **53**(5): p. 356-8.

233. Mustjoki, S. and N.S. Young, *Somatic Mutations in "Benign" Disease.* N Engl J Med, 2021. **384**(21): p. 2039-2052.
234. Abascal, F., et al., *Somatic mutation landscapes at single-molecule resolution.* Nature, 2021. **593**(7859): p. 405-410.
235. Lee-Six, H., et al., *Population dynamics of normal human blood inferred from somatic mutations.* Nature, 2018. **561**(7724): p. 473-478.
236. Meshkov, I., et al., *Variations in tuberculosis prevalence, Russian Federation: a multivariate approach.* Bull World Health Organ, 2019. **97**(11): p. 737-745A.
237. Benyelles, M., et al., *NHP2 deficiency impairs rRNA biogenesis and causes pulmonary fibrosis and Hoyeraal-Hreidarsson syndrome.* Hum Mol Genet, 2020. **29**(6): p. 907-922.
238. Alder, J.K., et al., *Exome sequencing identifies mutant TINF2 in a family with pulmonary fibrosis.* Chest, 2015. **147**(5): p. 1361-1368.
239. Sharma, R., et al., *Gain-of-function mutations in RPA1 cause a syndrome with short telomeres and somatic genetic rescue.* Blood, 2022. **139**(7): p. 1039-1051.
240. van der Vis, J.J., et al., *Pulmonary Fibrosis and a TERT Founder Mutation With a Latency Period of 300 Years.* Chest, 2020. **158**(2): p. 612-619.
241. Gutierrez-Rodrigues, F., et al., *Pathogenic TERT promoter variants in telomere diseases.* Genet Med, 2019. **21**(7): p. 1594-1602.
242. Maryoung, L., et al., *Somatic mutations in telomerase promoter counterbalance germline loss-of-function mutations.* J Clin Invest, 2017. **127**(3): p. 982-986.
243. Perdigones, N., et al., *Clonal hematopoiesis in patients with dyskeratosis congenita.* Am J Hematol, 2016. **91**(12): p. 1227-1233.
244. Jongmans, M.C., et al., *Revertant somatic mosaicism by mitotic recombination in dyskeratosis congenita.* Am J Hum Genet, 2012. **90**(3): p. 426-33.
245. Schratz, K.E., et al., *Somatic reversion impacts myelodysplastic syndromes and acute myeloid leukemia evolution in the short telomere disorders.* J Clin Invest, 2021. **131**(18).
246. Revy, P., C. Kannengiesser, and A. Fischer, *Somatic genetic rescue in Mendelian haematopoietic diseases.* Nat Rev Genet, 2019. **20**(10): p. 582-598.
247. Kennedy, A.L., et al., *Distinct genetic pathways define pre-malignant versus compensatory clonal hematopoiesis in Shwachman-Diamond syndrome.* Nat Commun, 2021. **12**(1): p. 1334.
248. Tan, S., et al., *Somatic genetic rescue of a germline ribosome assembly defect.* Nat Commun, 2021. **12**(1): p. 5044.
249. Guzman, B.B., et al., *Emerging roles for G-quadruplexes in proteostasis.* FEBS J, 2022.
250. Reddy Sannapureddi, R.K., et al., *Characterization of DNA G-quadruplex Topologies with NMR Chemical Shifts.* J Phys Chem Lett, 2020. **11**(23): p. 10016-10022.
251. Cheng, M., et al., *Loop permutation affects the topology and stability of G-quadruplexes.* Nucleic Acids Res, 2018. **46**(18): p. 9264-9275.
252. Biver, T., *Discriminating between Parallel, Anti-Parallel and Hybrid G-Quadruplexes: Mechanistic Details on Their Binding to Small Molecules.* Molecules, 2022. **27**(13).
253. Bhasikuttan, A.C. and J. Mohanty, *Targeting G-quadruplex structures with extrinsic fluorogenic dyes: promising fluorescence sensors.* Chem Commun (Camb), 2015. **51**(36): p. 7581-97.
254. Chattopadhyay, S., et al., *Protein folding in Escherichia coli: role of 23S ribosomal RNA.* Biochim Biophys Acta, 1999. **1429**(2): p. 293-8.
255. Chiti, F. and C.M. Dobson, *Protein Misfolding, Amyloid Formation, and Human Disease: A Summary of Progress Over the Last Decade.* Annu Rev Biochem, 2017. **86**: p. 27-68.
256. Das, D., et al., *Identical RNA-protein interactions in vivo and in vitro and a scheme of folding the newly synthesized proteins by ribosomes.* J Biol Chem, 2012. **287**(44): p. 37508-21.
257. Pal, D., et al., *Reactivation of denatured proteins by domain V of bacterial 23S rRNA.* Nucleic Acids Res, 1997. **25**(24): p. 5047-51.
258. Pang, Y., et al., *The antiprion compound 6-aminophenanthridine inhibits the protein folding activity of the ribosome by direct competition.* J Biol Chem, 2013. **288**(26): p. 19081-9.
259. Choi, S.I., K. Ryu, and B.L. Seong, *RNA-mediated chaperone type for de novo protein folding.* RNA Biol, 2009. **6**(1): p. 21-4.

260. Varshney, D., et al., *The regulation and functions of DNA and RNA G-quadruplexes.* Nat Rev Mol Cell Biol, 2020. **21**(8): p. 459-474.
261. McRae, E.K.S., et al., *Human DDX21 binds and unwinds RNA guanine quadruplexes.* Nucleic Acids Res, 2017. **45**(11): p. 6656-6668.
262. Chakraborty, P. and F. Grosse, *Human DHX9 helicase preferentially unwinds RNA-containing displacement loops (R-loops) and G-quadruplexes.* DNA Repair (Amst), 2011. **10**(6): p. 654-65.
263. Creacy, S.D., et al., *G4 resolvase 1 binds both DNA and RNA tetramolecular quadruplex with high affinity and is the major source of tetramolecular quadruplex G4-DNA and G4-RNA resolving activity in HeLa cell lysates.* J Biol Chem, 2008. **283**(50): p. 34626-34.
264. Tran, H., et al., *Facilitation of mRNA deadenylation and decay by the exosome-bound, DExH protein RHAU.* Mol Cell, 2004. **13**(1): p. 101-11.
265. Fu, J.J., L.Y. Li, and G.X. Lu, *Molecular cloning and characterization of human DDX36 and mouse Ddx36 genes, new members of the DEAD/H box superfamily.* Sheng Wu Hua Xue Yu Sheng Wu Wu Li Xue Bao (Shanghai), 2002. **34**(5): p. 655-61.
266. Vaughn, J.P., et al., *The DEXH protein product of the DHX36 gene is the major source of tetramolecular quadruplex G4-DNA resolving activity in HeLa cell lysates.* J Biol Chem, 2005. **280**(46): p. 38117-20.
267. Chen, M.C., et al., *Structural basis of G-quadruplex unfolding by the DEAH/RHA helicase DHX36.* Nature, 2018. **558**(7710): p. 465-469.
268. He, Y., G.R. Andersen, and K.H. Nielsen, *Structural basis for the function of DEAH helicases.* EMBO Rep, 2010. **11**(3): p. 180-6.
269. Ye, J., et al., *RecA-like motor ATPases--lessons from structures.* Biochim Biophys Acta, 2004. **1659**(1): p. 1-18.
270. Chang-Gu, B., et al., *The DHX36-specific-motif (DSM) enhances specificity by accelerating recruitment of DNA G-quadruplex structures.* Biol Chem, 2021. **402**(5): p. 593-604.
271. Lattmann, S., et al., *Role of the amino terminal RHAU-specific motif in the recognition and resolution of guanine quadruplex-RNA by the DEAH-box RNA helicase RHAU.* Nucleic Acids Res, 2010. **38**(18): p. 6219-33.
272. Tippana, R., et al., *RNA G-quadruplex is resolved by repetitive and ATP-dependent mechanism of DHX36.* Nat Commun, 2019. **10**(1): p. 1855.
273. Yang, C., et al., *To unwind the biological knots: The DNA/RNA G-quadruplex resolvase RHAU (DHX36) in development and disease.* Animal Model Exp Med, 2022.
274. Huang, W., et al., *Yin Yang 1 contains G-quadruplex structures in its promoter and 5'-UTR and its expression is modulated by G4 resolvase 1.* Nucleic Acids Res, 2012. **40**(3): p. 1033-49.
275. Kumari, S., et al., *An RNA G-quadruplex in the 5' UTR of the NRAS proto-oncogene modulates translation.* Nat Chem Biol, 2007. **3**(4): p. 218-21.
276. Beaudoin, J.D. and J.P. Perreault, *5'-UTR G-quadruplex structures acting as translational repressors.* Nucleic Acids Res, 2010. **38**(20): p. 7022-36.
277. Sauer, M., et al., *DHX36 prevents the accumulation of translationally inactive mRNAs with G4-structures in untranslated regions.* Nat Commun, 2019. **10**(1): p. 2421.
278. Yoo, J.S., et al., *DHX36 enhances RIG-I signaling by facilitating PKR-mediated antiviral stress granule formation.* PLoS Pathog, 2014. **10**(3): p. e1004012.
279. Sun, Y., K. Hamilton, and L. Tong, *Recent molecular insights into canonical pre-mRNA 3'-end processing.* Transcription, 2020. **11**(2): p. 83-96.
280. Newman, M., et al., *The G-Quadruplex-Specific RNA Helicase DHX36 Regulates p53 Pre-mRNA 3'-End Processing Following UV-Induced DNA Damage.* J Mol Biol, 2017. **429**(21): p. 3121-3131.
281. Fatica, A. and I. Bozzoni, *Long non-coding RNAs: new players in cell differentiation and development.* Nat Rev Genet, 2014. **15**(1): p. 7-21.
282. Ulitsky, I. and D.P. Bartel, *lincRNAs: genomics, evolution, and mechanisms.* Cell, 2013. **154**(1): p. 26-46.
283. Matsumura, K., et al., *The novel G-quadruplex-containing long non-coding RNA GSEC antagonizes DHX36 and modulates colon cancer cell migration.* Oncogene, 2017. **36**(9): p. 1191-1199.

284. Tan, N., et al., *Effect of lncRNA-BC200 on proliferation and migration of liver cancer cells in vitro and in vivo.* Oncol Rep, 2020. **43**(2): p. 461-470.
285. Zhao, R., et al., *LncRNA BC200 Promotes Esophageal Squamous Cell Cancer Migration and Invasion and Can Regulate ATF4 Expression.* Front Oncol, 2020. **10**: p. 1392.
286. Booy, E.P., et al., *RNA Helicase Associated with AU-rich Element (RHAU/DHX36) Interacts with the 3'-Tail of the Long Non-coding RNA BC200 (BCYRN1).* J Biol Chem, 2016. **291**(10): p. 5355-72.
287. Zhang, Z., et al., *DDX1, DDX21, and DHX36 helicases form a complex with the adaptor molecule TRIF to sense dsRNA in dendritic cells.* Immunity, 2011. **34**(6): p. 866-78.
288. Ullah, R., et al., *DEAD/H-box helicases:Anti-viral and pro-viral roles during infections.* Virus Res, 2022. **309**: p. 198658.
289. Lattmann, S., et al., *The DEAH-box RNA helicase RHAU binds an intramolecular RNA G-quadruplex in TERC and associates with telomerase holoenzyme.* Nucleic Acids Res, 2011. **39**(21): p. 9390-404.
290. Booy, E.P., et al., *The RNA helicase RHAU (DHX36) unwinds a G4-quadruplex in human telomerase RNA and promotes the formation of the P1 helix template boundary.* Nucleic Acids Res, 2012. **40**(9): p. 4110-24.
291. Krecic, A.M. and M.S. Swanson, *hnRNP complexes: composition, structure, and function.* Curr Opin Cell Biol, 1999. **11**(3): p. 363-71.
292. Biamonti, G. and S. Riva, *New insights into the auxiliary domains of eukaryotic RNA binding proteins.* FEBS Lett, 1994. **340**(1-2): p. 1-8.
293. Matunis, M.J., J. Xing, and G. Dreyfuss, *The hnRNP F protein: unique primary structure, nucleic acid-binding properties, and subcellular localization.* Nucleic Acids Res, 1994. **22**(6): p. 1059-67.
294. Honore, B., et al., *Heterogeneous nuclear ribonucleoproteins H, H', and F are members of a ubiquitously expressed subfamily of related but distinct proteins encoded by genes mapping to different chromosomes.* J Biol Chem, 1995. **270**(48): p. 28780-9.
295. Mahe, D., et al., *Cloning of human 2H9 heterogeneous nuclear ribonucleoproteins. Relation with splicing and early heat shock-induced splicing arrest.* J Biol Chem, 1997. **272**(3): p. 1827-36.
296. Honore, B., *The hnRNP 2H9 gene, which is involved in the splicing reaction, is a multiply spliced gene.* Biochim Biophys Acta, 2000. **1492**(1): p. 108-19.
297. Min, H., R.C. Chan, and D.L. Black, *The generally expressed hnRNP F is involved in a neural-specific pre-mRNA splicing event.* Genes Dev, 1995. **9**(21): p. 2659-71.
298. Chen, C.D., R. Kobayashi, and D.M. Helfman, *Binding of hnRNP H to an exonic splicing silencer is involved in the regulation of alternative splicing of the rat beta-tropomyosin gene.* Genes Dev, 1999. **13**(5): p. 593-606.
299. Hastings, M.L., C.M. Wilson, and S.H. Munroe, *A purine-rich intronic element enhances alternative splicing of thyroid hormone receptor mRNA.* RNA, 2001. **7**(6): p. 859-74.
300. Liu, J., et al., *Heterogeneous nuclear ribonucleoprotein-H plays a suppressive role in visceral myogenesis.* Mech Dev, 2001. **104**(1-2): p. 79-87.
301. Veraldi, K.L., et al., *hnRNP F influences binding of a 64-kilodalton subunit of cleavage stimulation factor to mRNA precursors in mouse B cells.* Mol Cell Biol, 2001. **21**(4): p. 1228-38.
302. Roberts, G.C. and C.W. Smith, *Alternative splicing: combinatorial output from the genome.* Curr Opin Chem Biol, 2002. **6**(3): p. 375-83.
303. Chou, M.Y., et al., *hnRNP H is a component of a splicing enhancer complex that activates a c-src alternative exon in neuronal cells.* Mol Cell Biol, 1999. **19**(1): p. 69-77.
304. Decorsiere, A., et al., *Essential role for the interaction between hnRNP H/F and a G quadruplex in maintaining p53 pre-mRNA 3'-end processing and function during DNA damage.* Genes Dev, 2011. **25**(3): p. 220-5.
305. Xu, C., et al., *HnRNP F/H associate with hTERC and telomerase holoenzyme to modulate telomerase function and promote cell proliferation.* Cell Death Differ, 2020. **27**(6): p. 1998-2013.
306. *Telomerase Database, TERC mutations*. Available from: http://telomerase.asu.edu/diseases.html#tr.

307. Ly, H., E.H. Blackburn, and T.G. Parslow, *Comprehensive structure-function analysis of the core domain of human telomerase RNA.* Mol Cell Biol, 2003. **23**(19): p. 6849-56.
308. Marrone, A., et al., *Functional characterization of novel telomerase RNA (TERC) mutations in patients with diverse clinical and pathological presentations.* Haematologica, 2007. **92**(8): p. 1013-20.
309. *ClinVar Database, NR_001566.1(TERC):n.11G>T*. Available from: https://www.ncbi.nlm.nih.gov/clinvar/variation/534178/?oq=(TERC)[gene]+AND+n.11G%3ET[varname]+&m=NR_001566.1(TERC):n.11G%3ET.
310. Sharaf, R., G.M. Frampton, and L.A. Albacker, *Mutations in the TERC template sequence can be incorporated into the telomeres of human tumors.* PLoS One, 2022. **17**(8): p. e0272707.
311. Vulliamy, T.J., et al., *Mutations in dyskeratosis congenita: their impact on telomere length and the diversity of clinical presentation.* Blood, 2006. **107**(7): p. 2680-5.
312. Xin, Z.T., et al., *Functional characterization of natural telomerase mutations found in patients with hematologic disorders.* Blood, 2007. **109**(2): p. 524-32.
313. Hassani, M.A., J. Murid, and J. Yan, *Regulator of telomere elongation helicase 1 gene and its association with malignancy.* Cancer Rep (Hoboken), 2022: p. e1735.
314. Gros, J., et al., *G-Quadruplex formation interferes with P1 helix formation in the RNA component of telomerase hTERC.* Chembiochem, 2008. **9**(13): p. 2075-9.
315. Hinkley, C.S., et al., *The mouse telomerase RNA 5"-end lies just upstream of the telomerase template sequence.* Nucleic Acids Res, 1998. **26**(2): p. 532-6.
316. Chen, J.L. and C.W. Greider, *Template boundary definition in mammalian telomerase.* Genes Dev, 2003. **17**(22): p. 2747-52.
317. Li, X., et al., *Structure, interactions and effects on activity of the 5'-terminal region of human telomerase RNA.* J Biochem, 2007. **141**(5): p. 755-65.
318. Merino, E.J., et al., *RNA structure analysis at single nucleotide resolution by selective 2'-hydroxyl acylation and primer extension (SHAPE).* J Am Chem Soc, 2005. **127**(12): p. 4223-31.